

**INTERNATIONAL
COUNCIL
FOR SCIENCE**

**INTERGOVERNMENTAL
OCEANOGRAPHIC
COMMISSION**

**WORLD
METEOROLOGICAL
ORGANIZATION**

**COMPARISON OF LARGE SCALE SULPHATE AEROSOL
MODELS (COSAM)
REPORT ON WORKSHOP
19-21 October 1998, Halifax, Canada**

**Organized by:
Dr. Leonard A. Barrie
Meteorological Service of Canada
Toronto, Ontario
Canada**

**Hosted by:
Prof. Ulrike Lohmann
Department of Physics, Dalhousie University
Halifax, Canada**

**Jointly Sponsored by the :
Working Group On Numerical Experimentation (WGNE) of the World
Meteorological Organization**

The International Global Atmospheric Chemistry Program

The Climate Institute of Canada

August 2002

WCRP Informal Report No. 17/2002

Table of Contents

	Page
SUMMARY, CONCLUSIONS AND RECOMMENDATIONS	3
ABSTRACTS OF WORKSHOP PRESENTATIONS	8
Sulfur mass transport and sulfate radiative forcing in the GISS GCM	8
Simulation of global sulfate distribution with a coupled photochemistry-sulfur cycle GCM	12
Sensitivity of the vertical sulfur profiles in the CCCMA GCM to treatment of aqueous phase chemistry	18
Tracer modelling in ECHAM4	23
TOMCAT 3D Chemical Transport Model - COSAM Experiments	26
Global sulfur modeling with the tracer transport model TM3	31
LLNL-IMPACT model	35
Tropospheric Sulfur Simulation with a Global 3D Model (GOCART)	41
Global Modeling of sulfate aerosols at NCAR	43
The Danish Eulerian hemispheric model	45
Field observations used in the COSAM project	49
Sulfate and MSA at Mauna Loa Observatory: How Well can Observations at a Point Represent a Model Grid Box?	54
Vertical S Profiles From Aircraft Used in COSAM	57
Using airborne radon measurements in the development and validation of global 3D atmospheric models	65
A global database of dimethylsulfide emissions	70
Some problem points in atmospheric sulphur modelling	75
Simulation of Size-Segregated Global Sea-salt and Sulphate Aerosol Mixtures Using the Canadian Global Climate Model III (GCMIII)	82
NARCM – LITE Intercomparison Study	83
The 210 Pb data bank : an overview	87
APPENDIX A Workshop participants address list	90
APPENDIX B Agenda of the Halifax workshop	93
APPENDIX C Reports of the working groups	96
APPENDIX D Summary of the models in COSAM	110

Summary, Conclusions and Recommendations

Three-dimensional models of atmospheric trace constituents currently abound since they are important tools in understanding climate, stratospheric ozone depletion, tropospheric oxidants and acidification of ecosystems. Over the years the World Climate Research Programme has sponsored a number of model comparison studies. In 1990, 13 models simulating the atmospheric distribution of CFC-11 were compared (Pyle and Prather, 1996). In 1993, a second comparison of sub-grid scale tracer transport was conducted with 22 models simulating the atmospheric cycle of ^{222}Rn (Jacob et al, 1997). In 1995, the ability of 15 models to simulate the transport and scavenging of sulphur and ^{222}Rn was compared (Rasch et al, 2000b). The Comparison of Large Scale Sulphate Aerosol Models (COSAM) was the next in this series of model comparisons.

The results of the comparison study prior to COSAM (Rasch et al, 2000b) were particularly useful in formulating the experimental design for COSAM. One conclusion was that "models differ dramatically in their simulations of soluble species and observations (particularly at altitude) do not yet provide us with strong constraints on the reality of simulations". Thus, an emphasis in the experimental design of COSAM was on the use of more observations including those in the vertical. A second conclusion was that "transport of SO_x (i.e. SO_4^- plus SO_2) to remote regions was a problem" and that in this respect, "the ability to model the transport, scavenging and transformation of SO_2 and the production, transport and scavenging of SO_4^- is still in its infancy". Thus, the challenge to COSAM was to test, using an expanded remote region sulphur data set, whether the models' performance in simulating transport to remote regions had improved after three years and to understand why variations between models and observations occurred. A third conclusion was that "differences between model results reflect mainly the different treatment of the 'precipitation' scavenging processes as well as differences in the hydrological parameters used to parameterize the scavenging.

The objectives of COSAM were to compare the ability of current models to simulate the spatial/temporal distribution of sulphate aerosols and to use an enhanced set of observations to accomplish this. The latter required a special effort undertaken by the global aerosol data centre (WMO/Global Atmospheric Watch [GAW] programme) in Ispra Italy to assemble all available ground level data on sulphates and its gaseous precursors, the use of a global data base on ^{210}Pb deposition in Grenoble France and the use of an extensive set of aircraft vertical profile measurements of sulphates and related species at regionally representative locations on the periphery of the North American sulphur source region.

The COSAM study from 1998 to 2000 compared the performance of atmospheric models with each other and observations. It involved: (i) design of a standard model experiment for the world wide web, (ii) 10 model simulations of the cycles of sulphur and $^{222}\text{Rn}/^{210}\text{Pb}$ conforming to the experimental design, (iii) assemblage of the best available observations of atmospheric SO_4^- , SO_2 and MSA and (iv) a workshop in Halifax, Canada, on 19-20 October 1998 to analyze model performance and future model development needs. This reports documents details of that workshop.

The community of modelers are divisible roughly into two groups: (i) climate researchers who are attempting to include aerosols as interactive constituents in climate models and (ii) atmospheric chemical transport modelers who are trying to understand the chemical formation, physical transformation and scavenging pathways of these constituents using models driven off-line by climate model generated or observed winds (analyzed winds). Although there are exceptions, the former move in WCRP circles while the latter are generally concentrated in the global integration and modeling (GIM) activity of the International Global Atmospheric Chemistry project (IGAC) of the International Geosphere - Biosphere Programme (IGBP). In both modeling approaches, the processes of trace constituent transport, transformation and removal are parameterized with varying degrees of sophistication. There is a need to bring the two groups together to utilize the expertise of each to the advantage of all.

From 19-20 October 1998, a workshop was held that involved approximately 50 scientists (Appendix A) from four research areas:

1. Atmospheric climate and chemical transport modelers involved in hemispheric to global scale simulations of the trace constituent distribution of aerosols and ozone.
2. Modelers and theoreticians involved in parameterizing the relevant processes.
3. Scientists with a detailed knowledge of the relevant processes.
4. A group of scientists with expertise in observations of large scale distributions of aerosols (e.g. SO_4^-) and their gaseous precursors (e.g. SO_2) as well as in the statistical comparison of model-predictions and observations.

The aim of the workshop was to bring these diverse groups together to: (i) become familiar with each others research, (ii) discuss preliminary results of the model runs and comparisons of the models with observations, and (iii) to assign topics and lead authors to papers that would be published on the results. The agenda of the meeting (Appendix B) involved presentations by individual researchers followed by working group sessions. Appendix C contains reports of three working groups on (i) regional and global sulphur budgets (ii) vertical profiles and remote region ground level distributions. The participants presented papers describing their research (see the next section). Over the two year period following the workshop, three papers were written and accepted for publication in "Tellus":

- i) Barrie, L. A., Y. Yi, W.R. Leitch, U. Lohmann, P. Kasibhatla, G.-J. Roelofs, J. Wilson, F. McGovern, C. Benkovitz, M.A. Melieres, K. Law, J. Prospero, M. Kritz, D. Bergmann, C. Bridgeman, M. Chin, J. Christensen, R. Easter, J. Feichter, C. Land, A. Jeuken, E. Kjellstrom, D. Koch, and P. Rasch, 2001, A comparison of large scale atmospheric sulphate aerosol models (COSAM): overview and highlights, *Tellus* 35B, 615-645.
- ii) Roelofs, G.J., P.Kasibhatla, L. Barrie, D. Bergman, C. Bridgeman, M. Chin, J. Christensen, R. Easter, J. Feichter, A. Jeuken, E. Kjellstrom, D. Koch, C. Land, U. Lohmann, P. Rasch, 2001, Analysis of regional budgets of sulfur species modeled for the COSAM exercise, *Tellus* 35B, 673-694.

- iii) Lohmann, U., R. Leaitch, L. Barrie, K. Law, Y. Yi, D. Bergman, C. Bridgeman, M. Chin, J. Christensen, R. Easter, J. Feichter, A. Jeuken, E.Kjellstrom, D. Koch, C. Land, P. Rasch, and G.-J. Roelofs, 2001, Vertical distributions of sulfur species simulated by large scale atmospheric models in COSAM: Comparison with observations, *Tellus* 35B, 646-672.

Conclusions and Recommendations

The COSAM study involved a design of a model comparison standard and the collection of a new global aerosol chemistry observational data set for validation. It was our intention that the COSAM test could be a standard available to anyone on the world wide web who develops a global sulphate aerosol model and wishes to test its performance (<http://www.msc-smc.ec.gc.ca/armp/COSAM.html>). After initial simulations, a workshop was held in October 1998 in Halifax Canada to review the results and recommend future action in the model improvement.

A systematic comparison of large scale sulphate aerosol models with each other and observations provided us with an estimate of the variance between the population of sulphate aerosol models of the late 1990s and with insights into what causes that variance. This insight is valuable in assigning uncertainty to estimates of the impact of sulphate aerosols on climate that are undertaken by the Inter-governmental Panel on Climate Change (IPCC) as well as in improving models.

Participating in the COSAM study were three general circulation models (GCM's) that generate their own meteorological fields and 6 chemical transport models (CTM's) that are driven by gridded meteorological fields produced from observations (Appendix D). Two of those CTMs were essentially general circulation models nudged to analyzed winds. The following conclusions were drawn:

1. Annual mean global budgets of $^{222}\text{Rn}/^{210}\text{Pb}$ indicate that the GCMs were less efficient in particulate scavenging than CTMs.
2. In most models in all source regions, 40-60% of the sulphate resides above 2.5 km altitude. The greatest export of SO_x from a major source region occurred in Europe and the least from North America and southeast Asia while the greatest variability of SO_x export between models occurred in eastern North America and southeast Asia rather than Europe. The former is in part due to the greater fraction of ocean surface in the regional-budget domain chosen for North America and southeast Asia while the latter is likely related to less intense simulated convection in the European region than in the other two lower latitude regions.
3. Variations between models in the export of SO_x from Europe or North America are not sufficient to explain an order of magnitude variation in spatial distributions of SO_x in the northern hemisphere. The most likely factors underlying such variations are in differences in how the models simulate vertical mixing and subsequent advection. Cloud processes as well as dynamics are involved.

4. On average, models predict surface level seasonal mean SO_4^- aerosol mixing ratios better (most within 20%) than they did those of SO_2 (over-prediction by factors of 2 or more). A higher resolution limited area model performed best by matching both parameters within 20%. In winter, there is a tendency to underpredict SO_4^- close to source regions and overpredict in remote regions.
5. On the basis of global annual sulphur budgets as well as the spatial distributions of biogenic SO_4^- and DMS, it was concluded that the two models with internally-generated-oxidant chemistry (a CTM and a GCM) oxidized DMS quite differently producing a mean annual tropospheric residence time of 2 versus 3.9 days. Thus in marine areas of high DMS emissions, OH concentrations predicted by the two models must differ considerably.
6. Vertical mixing of surface emissions from the planetary boundary layer into the free troposphere in source regions is a major source of uncertainty in predicting the global distribution of SO_4^- aerosols in today climate models.

An outcome of the Halifax workshop and the data analysis is the realization that models are only as good as the data and process parameterizations that goes into them. Model development is currently hindered by a lack of observations with which to test them. An integral part of this study has been the availability of standardized global anthropogenic inventories of sulphur species to the atmosphere and the assemblage of aerosol and related gaseous precursor observations by the World Aerosol Data Center of the World Meteorological Organization's Global Atmosphere Watch (GAW) programme. If aerosol models are to be improved in future, it is essential that globally coordinated research efforts continue to address emissions related to all atmospheric species that ultimately affect the distribution and optical properties of ambient aerosols. Furthermore, systematic atmospheric aerosol and related chemistry observations are required.

Current observational data have great shortcomings. First, there is a lack of a coherent global network of observations that will ultimately produce a world aerosol chemistry climatology. The networks, which currently exist, are principally located in industrially developed regions of Europe and North America. However, even in these areas the data produced from key sites are not always sufficient to address important scientific questions. For instance, data from continental boundary or coastal sites are required to understand long range transport of anthropogenic aerosols. As part of the European EMEP network protocol total sulphate is reported rather than non-sea salt sulphate. Sea salt sulphate is a natural part of the sea salt aerosol, which may dominate at coastal locations. Total sulphate data alone at these locations are thus much less valuable than non-sea salt sulphate data in understanding long range transport of anthropogenic aerosols. It is also very evident from the results that to validate a sulphate aerosol model, simultaneous measurements at a global network of sites are needed, not only the aerosol, but also its gaseous precursors, in this case SO_2 , DMS and key oxidants, H_2O_2 and O_3 .

There are major areas of the globe for which no data are available. In particular, there is sparse coverage in Asia, the Southern Hemisphere, equatorial and Pacific regions. This situation drastically worsened in 1996 when 15 Southern Hemisphere and Pacific sites were closed. There

is now almost a total lack of measurements in these important regions, apart from some individual research sites such as those operated on Antarctica and Cape Grim.

There are very few high altitude measurement sites. Only four sites provided data for the COSAM project and none were in the Southern Hemisphere. Finally, there is a dearth of vertical profile observations of major aerosol constituents and their gaseous precursors. A globally coordinated effort to systematically characterize the spatial and temporal distribution of key aerosols parameters and related gaseous precursors is needed. Vertical profile observations at a few selected sites would be a great step forward.

If the ^{222}Rn and ^{210}Pb natural tracer pair are to be valuable model development tools, more research is needed to improve knowledge of their emissions from continental areas in space and time and to systematically measure both species at aerosol network sites.

References for Summary, Conclusion and Recommendations Section

- Jacob, D.J., M.J. Prather, P.J. Rasch, R.-L. Shia et al, 1997. Evaluation and intercomparison of global transport models using ^{222}Rn and other short lived tracers, *J. Geophys. Res.* 102D, 5953-5970.
- Pyle, J. and M. Prather (Eds.), 1996. Global tracer transport models - report of a scientific symposium (Bermuda, 10-13 December 1990), CAS/JSC Working Group on Numerical Experimentation Report No. 24, WMO/TD-No.770, Geneva, Switzerland.
- Rasch, P.J., J. Feichter, K. Law, N. Mahowald, J. Penner and co-authors, 2000. An assessment of scavenging and deposition processes in global models: results from the WCRP Cambridge workshop of 1995, *Tellus*, 52B, 1025-1056.
- Rasch P.J. (Ed.), 1999. Proceedings of a WCRP workshop on modelling the transport and scavenging of trace constituents by clouds in global atmospheric models (Cambridge, UK, 1-4 August 1995), CAS/JSC Working Group on Numerical Experimentation Report No. 29, WMO/TD-No. 950, Geneva, Switzerland.
- Workshop Organizing Committee (D. Boville, D. Jacob, M. Prather - editors), 1997. Proceedings of a WCRP workshop on parameterization of subgrid-scale tracer transport (Virginia Beach, VA, USA, 30 November - 3 December 1993), CAS/JSC Working Group on Numerical Experimentation Report No. 26, WMO/TD-No. 823, Geneva, Switzerland.

ABSTRACTS OF PRESENTATIONS AT THE HALIFAX WORKSHOP

SULFUR MASS TRANSPORT AND SULFATE RADIATIVE FORCING IN THE GISS GCM

Koch, Rind, Tegen, Del Genio, Tselioudis: GISS/Columbia

Jacob: Harvard

Chin: GSFC/Georgia Tech

Prognostic species run on-line in the GISS GCM (model II-prime) include SO₂, sulfate, H₂O₂, DMS and MSA. Model resolution is 4x5 degrees with 9 vertical layers. The sulfur model, with prognostic in-cloud oxidant H₂O₂, includes a sophisticated in-cloud chemistry scheme, in which the chemistry, transport and deposition are tightly coupled to GCM cloud processes. Dry deposition is determined by a resistance-in-series scheme.

Compared with previous published models, our SO₂ and sulfate concentrations are high in the free troposphere, often by a factor of 2 in the northern hemisphere. Depletion of prognostic H₂O₂ causes an increase in SO₂ of about 30% in the northern hemisphere compared with fixed H₂O₂. In addition, SO₂ in polluted regions is not efficiently oxidized in convective plumes, so that convection deposits large amounts of SO₂ into the free troposphere. Although the SO₂ burden (0.56 Tg S) is considerably higher than previous models, the sulfate burden is within the range of previous model studies.

Because of the efficient transport of anthropogenic SO₂ to the free troposphere, we find a large percentage (77%) of the total burden to be anthropogenic (see Figure 1). Previous estimates of this are lower: Feichter et al. (1997) reported 66% and Chin and Jacob (1996) reported 40%.

At the surface, this model's performance is not remarkably different from published models. SO₂ concentrations are too high, typically by a factor of 2-3 over polluted regions. This is similar to most of the published models [e.g. Feichter et al. (1996); Roelofs et al. (1998); Pham et al. (1996)]. Sulfate magnitude agrees fairly well with surface observations.

We have compared our model with some of the available aircraft campaigns (PEM-West A, B, PEM-tropics and SUCCESS) in order to test the high altitude concentrations in the models. Model SO₂ tends to be lower than observed at high altitudes, in spite of the large model burden. Model sulfate agreement from the Pacific campaigns is variable - too high in some regions, too low in others. Compared with SUCCESS sulfate data over N. America, model sulfate is high by about a factor of 2.

Agreement with high altitude sulfate observations at Mauna Loa is quite good. So far there does not appear to be compelling evidence that this model has excessive SO₂ or sulfate concentrations in the free troposphere.

We also present results for sulfate radiative calculations. Using the relations of Charlson et al. [1984] to account for the dependence of optical thickness on relative humidity, we calculated

the direct radiative forcing of sulfate. It is shown in Figure 2. The annual average forcing is about -0.7 W/m^2 , with strong seasonal variability. For indirect radiative forcing calculations (see Figure 3), we use the relations between cloud droplet number concentrations and sulfate mass of Boucher and Lohmann (1994), and allow the on-line sulfate to affect the radiative properties of the clouds. The indirect annual average radiative forcing is -1.2 W/m^2 . Compared with many previous studies, we find the maximum indirect forcing to be more land-centered, distributed similarly to the direct forcing.

Finally, we consider how changing sources have affected radiative forcing. We use the SO_2 source inventory between 1950 and 1990, as compiled by Lefoen, Husar and Brimblecombe (personal communication). Looking at 10×20 degree blocks in eastern America, central Europe and east Asia, we found the largest 1990 source to be in Europe while the greatest forcing occurs over Asia.

References

- Boucher, O. and U. Lohmann, The sulfate-CCN-cloud albedo effect, *Tellus*, 47B, 280-300, 1995.
- Charlson, R. J., D. S. Covert, and T. V. Larson, Observation of the effect of humidity on light scattering by aerosols. In: *Hygroscopic Aerosols*, ed. L. Ruhnke and A. Deepak, pp 35-44, Hampton, VA, A. Deepak Publ, 1984.
- Chin, M., D. J. Jacob, G. M. Gardner, M. S. Foreman-Fowler, P. A. Spiro, and D. L. Savoie, A global three-dimensional model of tropospheric sulfate, *J. Geophys. Res.*, 101, 18,667-18,690, 1996.
- Chin, M., and D. J. Jacob, Anthropogenic and natural contributions to tropospheric sulfate: A global model analysis, *J. Geophys. Res.*, 101, 18,691-18,699, 1996.
- Feichter, J., E. Kjellstrom, H. Rodhe, F. Dentener, J. Lelieveld, and G.-J. Roelofs, Simulation of the tropospheric sulfur cycle in a global climate model, *Atmos. Env.*, 30, 1693-1707, 1996.
- Feichter, J., U. Lohmann, I. Schult, The atmospheric sulfur cycle in ECHAM-4 and its impact on the shortwave radiation, *Climate Dynamics*, 13, 235-246, 1997.
- Pham, M., J.-F. Muller, G. P. Brasseur, C. Granier, and G. Megie, A three-dimensional study of the tropospheric sulfur cycle, *J. Geophys. Res.*, 100, 26,061-26,092, 1995.
- Roelofs, G.-J., J. Lelieveld, and L. Ganzeveld, Simulation of global sulfate distribution and the influence on effective cloud drop radii with a coupled photochemistry-sulfur cycle model, *Tellus*, 50B, 224-242, 1998.

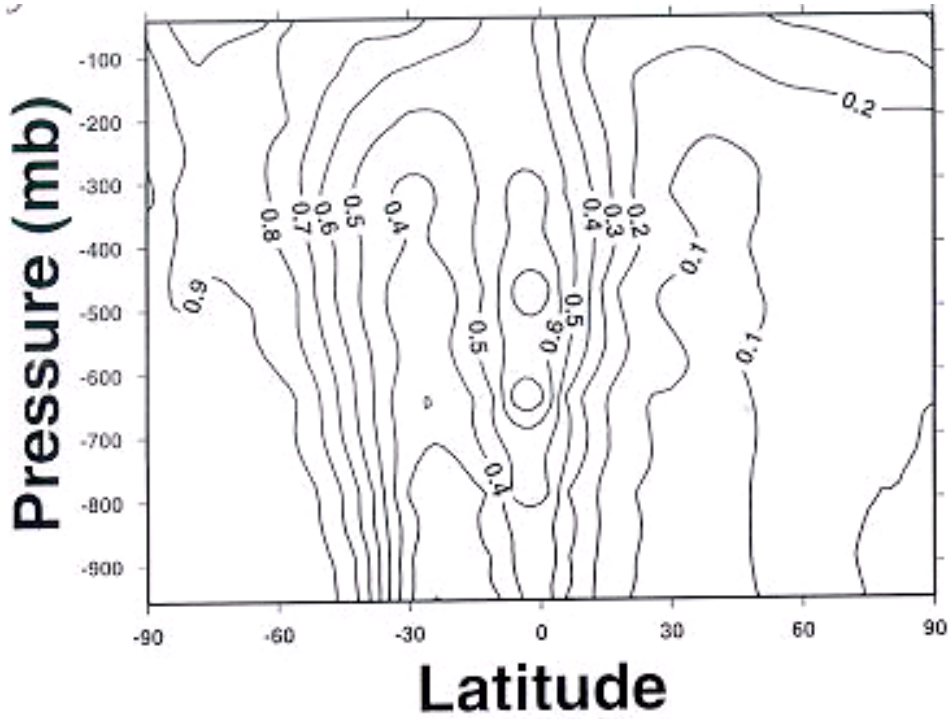


Figure 1 Zonal annual average fraction of natural SO₄.

Figure 2 Direct forcing (-0.68 W/m^2)

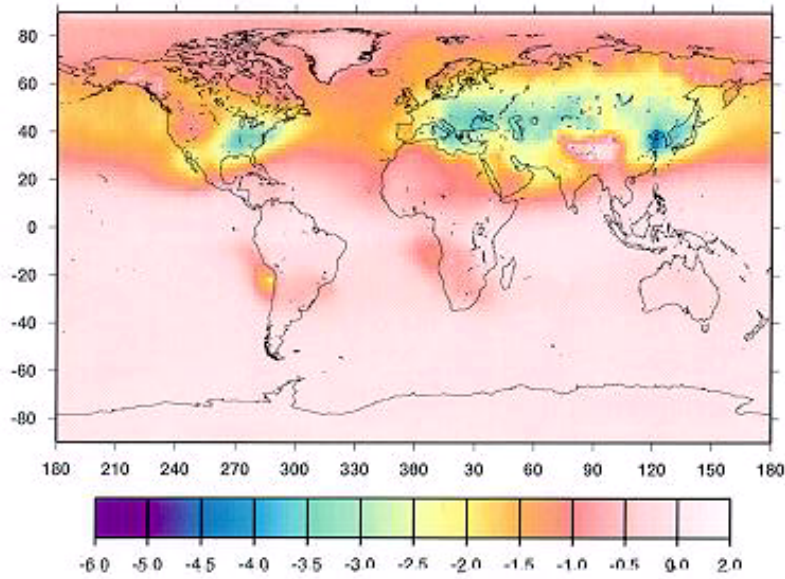
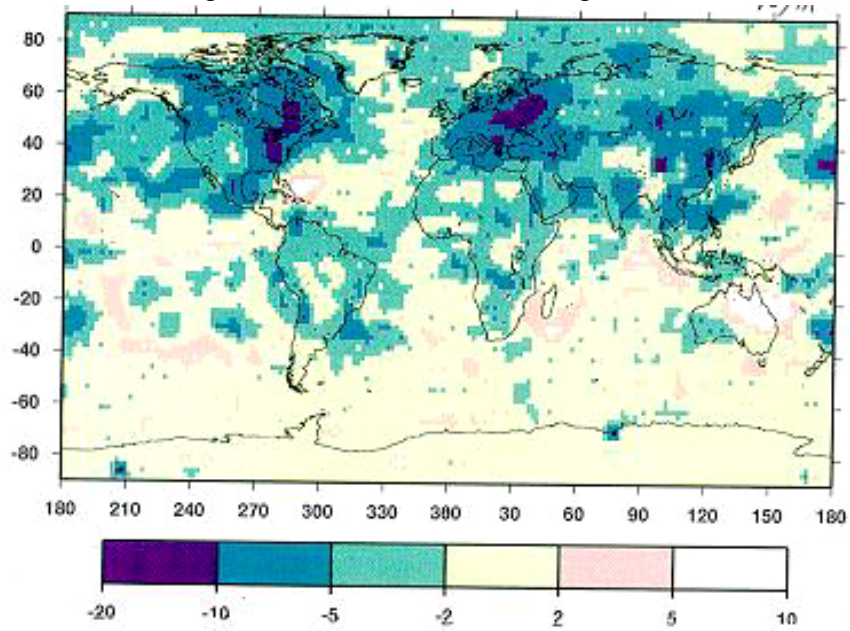


Figure 3 Indirect sulfate forcing (-1.9 W / m^2)



Simulation of global sulfate distribution with a coupled photochemistry-sulfur cycle GCM

Geert-Jan Roelofs and Jos Lelieveld

Institute for Marine and Atmospheric research Utrecht (IMAU), Princetonplein 5, 3584 CC Utrecht, The Netherlands, Phone: (+31) 30 2532821, Fax: (+31) 30 2543163, E-mail: roelofs@phys.uu.nl

1. Introduction

In recent years it has become apparent that the anthropogenic aerosol perturbation of the lower troposphere affects climate with a magnitude that may be comparable, although with opposite sign, to that of the greenhouse gases, at least in the northern hemisphere (IPCC, 1996). Globally, anthropogenic sulfur sources exceed natural sources by a factor of 3 to 4. The atmospheric lifetime of sulfate is of the order of a few days. Compared to the long-lived greenhouse gases, aerosol concentrations are therefore highly variable in space and time. Three-dimensional chemistry/transport models that simulate the sources, transports, transformations, and sinks of sulfur-containing species are important tools for the study of the global distribution of sulfate. In this paper we will discuss the performance of a global sulfur model, earlier described in Roelofs et al. (1998). In the previous study the model has been applied in the T21 resolution (i.e., with a horizontal resolution of $5.8 \times 5.8^\circ$). In this study the T30 resolution, i.e., $3.75 \times 3.75^\circ$, is applied.

2. Model description

The ECHAM spectral general circulation model (version 4) is based on the ECMWF numerical weather prediction model (Roeckner et al., 1996). The model has 19 vertical layers in a hybrid σ - p -coordinate system, from the surface to 10 hPa. ECHAM4 distinguishes between large scale and convective clouds. The large scale cloud scheme is based on the work of Sundqvist (1978) and Roeckner et al. (1991), and convective clouds are represented by the mass flux scheme of Tiedtke (1989). An elaborate description of ECHAM and the simulated climate can be found in, e.g., Roeckner et al. (1996).

The GCM is coupled to a tropospheric chemistry model that considers background CH_4 -CO- NO_x - HO_x chemistry, emissions of NO and CO, dry deposition of O_3 , NO_2 , HNO_3 , and H_2O_2 , and wet deposition of HNO_3 and H_2O_2 . This is coupled to a sulfur cycle scheme, which considers DMS, SO_2 and (particulate) sulfate. In the model, processes that affect concentrations of simulated species are emissions, gas and aqueous phase chemical processes, dry deposition, nucleation scavenging in clouds, impaction scavenging by precipitation, and evaporation of clouds and precipitation. The emissions considered in the model reflect the COSAM requirements. We assume that 5% of

anthropogenic sulfur emissions are released as sulfate. Anthropogenic sulfur emissions from biomass burning release an additional amount of 2.3 Tg S yr⁻¹. For an elaborate discussion of the parameterization of the sulfur chemistry and deposition processes we refer to Roelofs et al. (1998).

3. Results and discussion

3.1 Comparison with surface concentration measurements

The results presented in this section are averaged over two simulation years. Figure 1 shows monthly averaged calculated and observed surface concentrations of sulfate for selected locations. The dotted lines illustrate the horizontal gradients of simulated concentrations. They refer to maximum and minimum concentrations at the grid boundaries, obtained from averaging grid cell concentrations with those in neighboring grid cells. Observed data are compiled by Chin et al. (1996).

The model does not capture the relatively high sulfate concentrations in winter over Europe. The modelled and observed surface sulfate seasonalities agree relatively well for North American sites, although in summer the modelled concentrations appear somewhat low. Monthly averaged surface SO₂ is somewhat overestimated at European sites, as shown in Figure 2, although the SO₂ seasonality is reproduced relatively well. We note that the results of the T30 simulation show an improved agreement with surface observations compared to the results of the T21 simulation, especially for SO₂. Apparently, boundary layer processes such as mixing with the free troposphere, deposition to the surface, and the occurrence of low clouds are represented more realistically with higher resolution. Simulated concentrations are generally within a factor of 2 of the observations, except for polar sites such as Bear Island, where SO₂ is overestimated and sulfate is underestimated in winter. It has been suggested that additional heterogeneous oxidation mechanisms of SO₂ that are not included in the model, e.g., on the surface of atmospheric aerosols, may account for part of the discrepancies (Feichter et al., 1996; Dentener et al., 1996; Kasibhatla et al., 1997). Also, the assumption of a monodisperse drop size distribution (the bulk approach) may underestimate the SO₂ oxidation (Roelofs, 1993).

3.2 Calculated budgets and distributions

Table 1 shows the calculated, yearly integrated, source and sink terms for SO₂ and sulfate and their tropospheric burden and lifetimes. About 35% of the SO₂ is directly deposited, almost exclusively by dry deposition. The calculated wet deposition of SO₂ is negligible. We note that SO₂ that is scavenged by precipitating clouds or precipitation is not deposited as such but is mainly transformed to sulfate in the aqueous phase. In our model this does not contribute to the SO₂ but to the sulfate wet deposition flux. Gas phase oxidation of SO₂ by OH contributes about 14% of the total SO₂ removal. The aqueous phase oxidation pathways by O₃ and H₂O₂ contribute 12 and 42%, respectively. We remark that the coupling between the sulfur cycle and tropospheric background

chemistry enhances the contribution of oxidation by O_3 to the total SO_2 oxidation compared to models that use monthly averaged H_2O_2 distributions. The total simulated source of sulfate (65 Tg S yr^{-1}) consists of sulfate production by SO_2 oxidation and a small contribution by direct sulfate emissions (3.3 Tg S yr^{-1}). We calculate that about 20% of the sulfate is removed by dry deposition and 80% by wet deposition. The calculated sulfate lifetime, 5.2 days, is in the range of previous estimates of 3.9-5.3 days, but our model calculates a larger sulfate burden of 0.94 Tg S compared to previous estimates of 0.55-0.77 Tg S.

Table 1 Simulated contemporary global budgets for SO_2 and sulfate (Tg S yr^{-1})

	SO_2	SO_4^{2-}
total source	92	65
dry deposition	32	12
wet deposition	<1	54
oxidation	62	-
<i>by OH</i>		-
<i>by O₃</i>		-
<i>by H₂O₂</i>		-
burden (Tg S)	0.48	0.94
lifetime (days)	1.9	5.2

Compared to the T21 simulation (Roelofs et al., 1998), the T30 simulation is characterized by a more efficient dry deposition of SO_2 and, consequently, a lower burden and shorter lifetime for SO_2 . The change in deposition probably results from a better description of turbulent transfer and vegetation activity. Also, transport out of the boundary layer into the free troposphere, which enhances the lifetime of chemical species, may be less efficient in the T30 simulation. On the other hand, the sulfate lifetime is larger by about 10% than in the previous simulation.

Acknowledgment

This work has been performed as part of the NOP-II project 951258 (Netherlands organization for scientific research). We thank the Stichting Academisch Rekencentrum Amsterdam for the use of computer facilities.

References

- Chin, M., Jacob, D.J., Gardner, G.M., Foreman-Fowler, M., Spiro, P.A. and Savoie, D.L. 1996. A global three-dimensional model of tropospheric sulfate. *J. Geophys. Res.* **101**, 18667-18690.
- Dentener F.J., Carmichael G.R., Zhang Y., Lelieveld J. and Crutzen P.J. 1996. The role of mineral aerosol as a reactive surface in the global troposphere. *J. Geophys. Res.* **101**, 22869-22889.

- Feichter, J., Kjellström, E., Rodhe, H., Dentener, F., Lelieveld, J. and Roelofs, G.J. 1996. Simulation of the tropospheric sulfur cycle in a global climate model. *Atmos. Environ.* **30**, 1693-1707.
- Intergovernmental Panel on Climate Change IPCC 1996. *Climate Change 1995*, edited by J.T. Houghton, L.G. Meira Filho, B.A. Callander, N. Harris, A. Kattenberg, and K. Maskell, Cambridge University Press, Cambridge, pp. 65-130.
- Kasibhatla, P., Chameides, W.L. and John, J. St. 1997. A three dimensional global model investigation of seasonal variations in the atmospheric burden of anthropogenic sulfate aerosols. *J. Geophys. Res.* **102**, 3737-3760.
- Roeckner, E., Rieland, M. and Keup, E. 1991. Modelling of clouds and radiation in the ECHAM model, in *ECMWF/WCRP Workshop on "Clouds, Radiative Transfer and the Hydrological Cycle"*, ECMWF, 199-222.
- Roeckner, E., Arpe, K., Bengtsson, L., Christoph, M., Claussen, M., Dümenil, L., Esch, M., Giorgetta, M., Schlese, U. and Schulzweida, U. 1996. Simulation of the present-day climate with the ECHAM model: Impact of model physics and resolution. *Report No. 218*. Max-Planck-Institute for Meteorology, Hamburg, Germany.
- Roelofs, G.J. 1993. A cloud chemistry sensitivity study and comparison of explicit and bulk cloud model performance. *Atmos. Environ.* **27A**, 2255-2264.
- Roelofs, G.J., Lelieveld, J. and Ganzeveld, L. 1998. Simulation of global sulfate distribution and the influence on effective cloud drop radii with a coupled photochemistry-sulfur cycle model, *Tellus* **50B**, 224-242.
- Sundqvist, H. 1978. A parameterization scheme for non-convective condensation including prediction of cloud water content. *Quart. J. Roy. Meteor. Soc.* **104**, 677-690.
- Tiedtke, M. 1989. A comprehensive mass flux scheme for cumulus parameterization in large-scale models. *Mon. Wea. Rev.* **117**, 1779-1800.

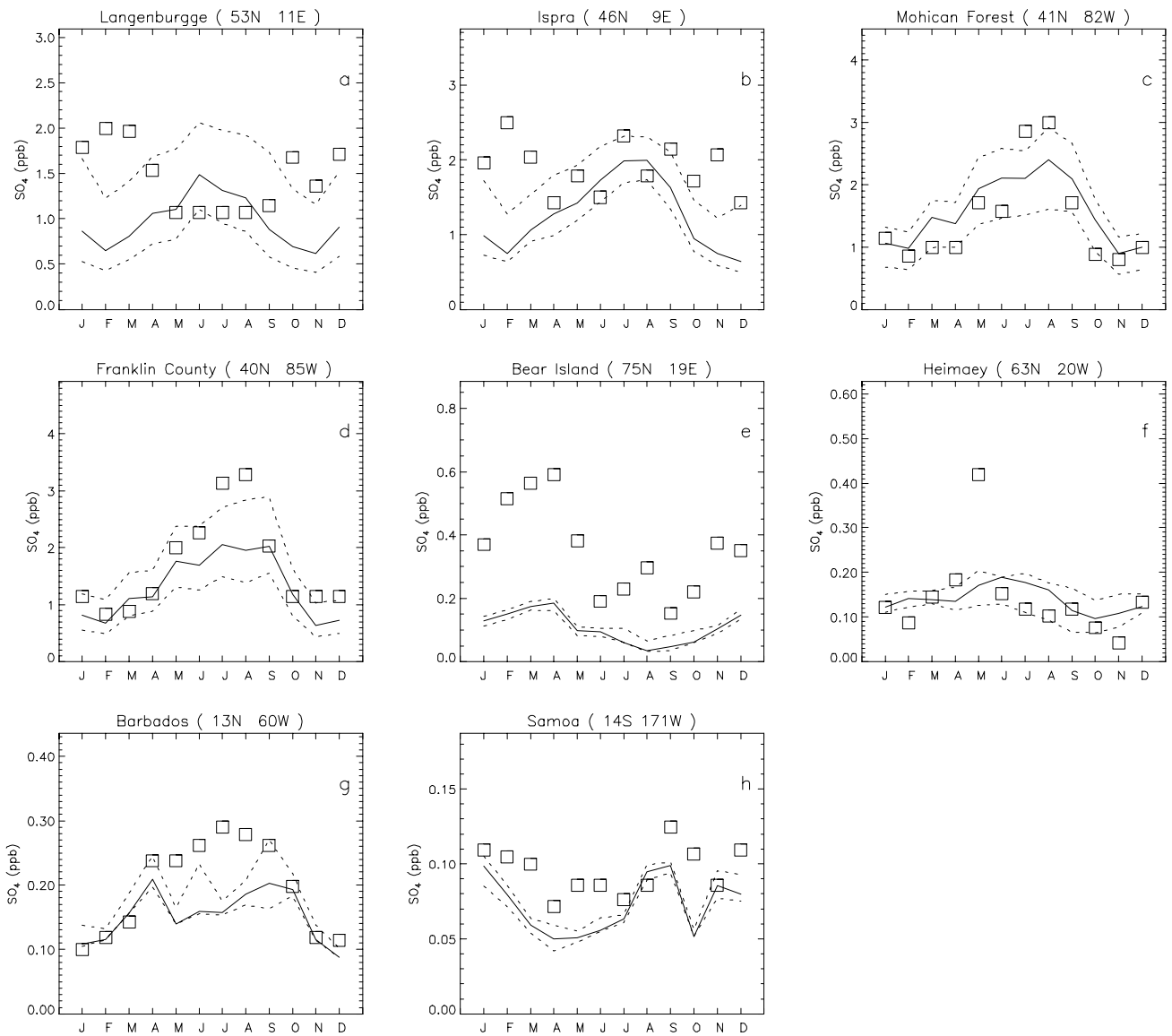


Figure 1. Measured (squares) and model calculated monthly averaged sulfate concentrations (ppbv) at the surface. The dotted lines indicate maximum and minimum concentrations at the grid cell boundaries.

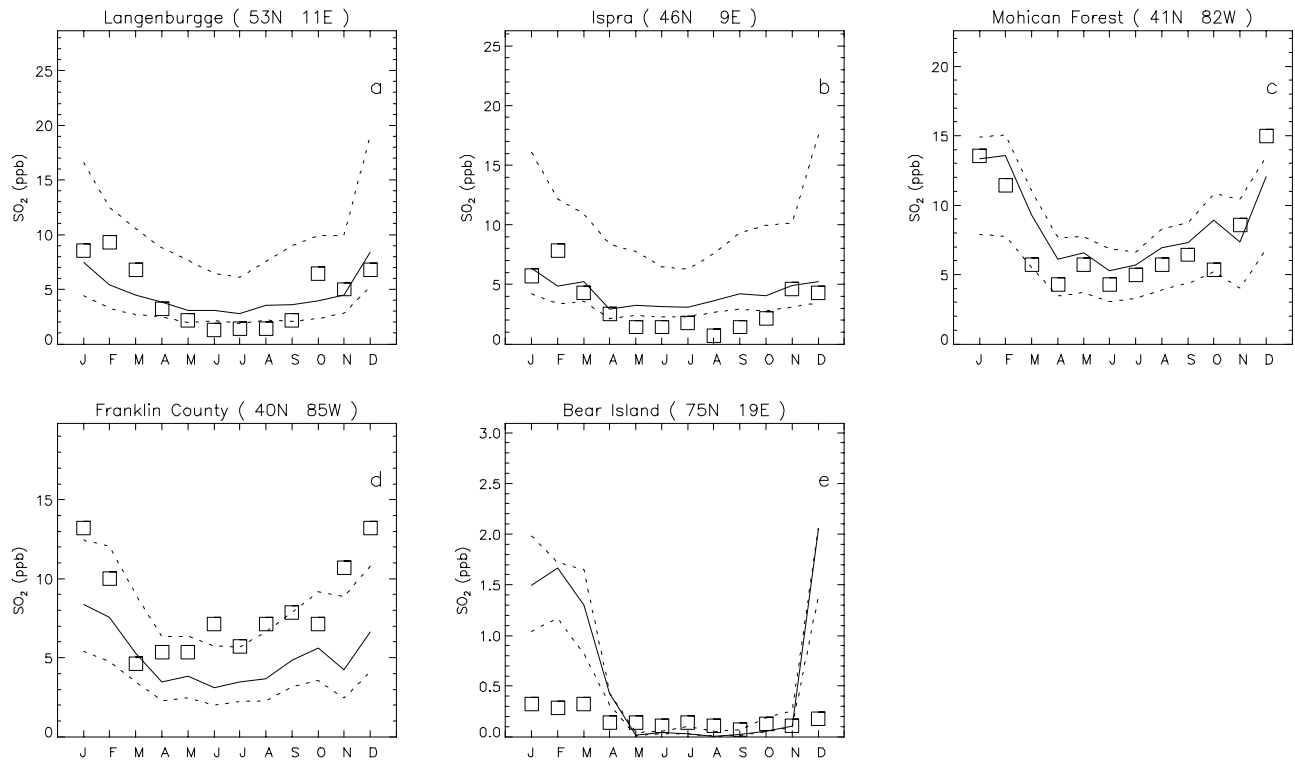


Figure 2. As Figure 1 but for SO₂.

Sensitivity of the vertical sulfur profiles in the CCCMA GCM to treatment of aqueous phase chemistry

Ulrike Lohmann¹, Norman McFarlane²,
Knut von Salzen³, H. G. Leighton³, Johann Feichter⁴

1. Atmospheric Science Program, Department of Physics, Dalhousie University, Halifax, Canada

2. Canadian Centre for Climate Modelling and Analysis, Victoria, Canada

3. McGill University, Montreal, Canada

4. Max Planck Institute for Meteorology, Hamburg, Germany

Introduction

Until now, most GCMs only consider in-cloud oxidation of S(IV) to S(VI) in stratiform clouds including convective cloud water which is detrained into anvils. However, even if the lifetime and areal coverage of convective clouds itself is much shorter than that of stratiform clouds, the time it takes for SO₂ to be oxidized to sulfate is even shorter, so that it is necessary to consider this pathway as well. A new approach to consider in-cloud oxidation in convective clouds has been developed by von Salzen et al. (1998). In this study, it is applied to a climate model for the first time in order to investigate its impact on the global mean sulfur budget and the geographical distribution of sulfur species.

Meteorological model

The CCCma third-generation atmospheric GCM employs a spectral representation with a triangular truncation of 47 waves (T47). Prognostic variables in this model are vorticity, divergence, temperature, (logarithm of) surface pressure, and specific humidity. Advection and physical processes are evaluated at grid points of appropriate "Gaussian grids" with an approximate horizontal resolution of 3.75°. The model employs a hybrid vertical coordinate system with 22 levels. The top level is at 12 hPa. A semi-implicit leap frog time integration scheme with $\Delta t=20$ minutes is used for the experiment at T47.

A semi-Lagrangian technique (Bermejo and Staniforth, 1992) is used for computing the horizontal and vertical advection of water vapor and the sulfur species. Cumulus clouds are represented by a bulk model including the effects of entrainment and detrainment on the updraft and downdraft convective mass fluxes (Zhang and McFarlane, 1995). Vertical fluxes of momentum, heat, and moisture due to turbulent transfer processes are represented using an eddy diffusivity formulations in the free atmosphere, while those at the surface are calculated from Monin - Obukhov similarity theory using the approach of Abdella and McFarlane (1997). The radiation code is based on a two-stream solution of the radiative transfer equation with six spectral intervals in the terrestrial infrared spectrum (Morcrette, 1991) and two in the solar part of the spectrum. The stratiform cloud scheme used is based on Lohmann and Roeckner (1996). Its main characteristic is the separate treatment of cloud water and cloud ice as prognostic variables. For further details see Lohmann et al. (1998)

Sulfur chemistry

The parameterization of the sulfur chemistry used in the reference experiment is described in detail in Feichter et al. (1996). It is linked to the stratiform cloud scheme (Lohmann et al., 1998) in such a way that the sulfate aerosol mass determines the number of cloud droplets. Transport, dry and wet deposition and chemical transformations of the constituents are calculated on-line with the GCM. Prognostic variables are dimethyl sulfide (DMS) and sulfur dioxide (SO_2) as gases and sulfate as an aerosol. The transport of these species due to advection, vertical diffusion and convection is treated in the same way as the transport of water vapor. Biogenic emissions from the oceans and from soils and plants are assumed to occur as DMS, emissions from volcanoes, from biomass burning and from combustion of fossil fuel and from smelting as SO_2 (Lohmann et al., 1998).

The dry deposition flux to the ground is assumed to be proportional to both the concentration in the lowest model layer and to a prescribed dry deposition velocity. For sulfate aerosol the dry deposition velocity is assumed to be 0.025 cm/s over dry surfaces and 0.1 cm/s over wetted surfaces and melting snow or ice. The respective dry deposition velocities for SO_2 are 0.1 cm/s and 0.8 cm/s, respectively (Ganzeveld et al. 1998).

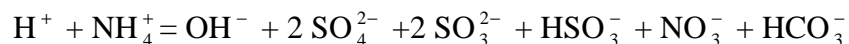
Removal of SO_2 and sulfate by precipitation is calculated explicitly in terms of the model's precipitation formation rate (Feichter et al., 1996). DMS as well as SO_2 in the gaseous phase are oxidized by reaction with hydroxyl (OH) during the day. Additionally, DMS reacts with nitrate radicals (NO_3) at night. We have assumed that the only end product of DMS oxidation is SO_2 .

In the reference experiments, aqueous phase chemistry only takes place in stratiform clouds. Dissolution of SO_2 is calculated according to Henry's law. In the aqueous phase we consider the production of sulfate by oxidation of SO_2 by hydrogen peroxide (H_2O_2) and ozone (O_3). Three-dimensional monthly mean oxidant concentrations are prescribed based on calculations with ECHAM and a more comprehensive chemical model (Roelofs and Lelieveld, 1995). The reaction rates and the effective Henry's law constant for SO_2 are calculated assuming that aqueous phase equilibria and electroneutrality are maintained. Additionally, the simplification $[\text{S(IV)}] = [\text{HSO}_3^-]$, which can be applied if the pH ranges between 3 to 5, and the approximation of the molar ratio of sulfate to ammonium of 1 (Dentener and Crutzen, 1994) are used. For a more detailed description see Feichter et al. (1996).

Experiment with in-cloud oxidation in convection clouds

To simulate in-cloud production of sulfate in convective clouds, the parameterization of von Salzen (1998) is used. In this parameterization, oxidation occurs with hydrogen peroxide and ozone as oxidants. The solubility of SO_2 in convective clouds is changed. To take into account

the dependence of the oxidation rates on the pH, the H^+ concentration is calculated from the ion balance (von Salzen et al., 1998)



which is efficiently solved by an iterative calculation using an adapted version of the approach of Tremblay and Leighton (1986). In this experiment, H_2O_2 in convective clouds is not held constant in order to include hydrogen peroxide limitation effects on sulfate production.

Results

Figure 1 shows vertical profiles of SO_2 , sulfate and liquid water content at two different locations and seasons during which measurements were taken. The NARE experiment took place in August/September 1993 off the coast of Nova Scotia. During these months SO_2 near the surface is 1.5 ± 1.5 nmole/mole, and sulfate 2 ± 2 nmole/mole. The difference between the experiments with in-cloud oxidation in convective clouds or different pH-calculation is smaller than the day to day variability. The same holds for the profile taken at North Bay during February/March.

References:

Abdella, K., and N. McFarlane, A new second order turbulence closure scheme for the planetary boundary layer, *J. Atmos. Sci.*, 54, 1850--1867, 1997.

Bermejo, R., and A. Staniforth, The conversion of semi-lagrangian advection schemes to quasi-monotone schemes, *Mon. Weather Rev.*, 120, 2622--2632, 1992.

Dentener, F., and P. J. Crutzen, A three-dimensional model of the global ammonia cycle, *J. Atmos. Chem.*, 19, 331--369, 1994.

Feichter, J., E. Kjellstrom, H. Rodhe, F. Dentener, J. Lelieveld, and G.-J. Roelofs, Simulation of the tropospheric sulfur cycle in a global climate model, *Atmos. Environ.*, 30, 1693--1707, 1996.

Ganzeveld, L., J. Lelieveld, and G.-J. Roelofs, A dry deposition parameterization for sulfur oxides in a chemistry and general circulation model, *J. Geophys. Res.*, 103, 5679--5694, 1998.

Lohmann, U., and E. Roeckner, Design and performance of a new cloud microphysics scheme developed for the ECHAM general circulation model, *Clim. Dyn.*, 12, 557--572, 1996.

Lohmann, U., K. VonSalzen, N. McFarlane, H. G. Leighton, and J. Feichter, The tropospheric sulfur cycle in the Canadian general circulation model, *J. Geophys. Res.*, 104, D21, 26,833 -- 26,858, 1999.

Morcrette, J. J., Radiation and cloud radiative properties in the {European Centre for Medium Range Weather Forecasts} forecasting system, *J. Geophys. Res.*, 96, 9121--9132, 1991.

Roelofs, G.-J., and J. Lelieveld, Distribution and budget of O₃ in the troposphere calculated with a chemistry general circulation model, *J. Geophys. Res.*, 100, 20983--20998, 1995.

Tremblay, A., and H. G. Leighton, A three-dimensional cloud chemistry model, *J. Clim. Appl. Meteorol.*, 25, 652--671, 1986.

von Salzen, K., H. G. Leighton, S. L. Gong, and U. Lohmann, Simulation of the in-cloud oxidation of {S(IV)} with the northern aerosol regional climate model ({NARCM}), Paper presented at AMS Conference on Cloud Physics, Am. Meteorol. Soc., Everett, Wash., Aug. 17-21, 1998.

Zhang, G. J., and N. A. McFarlane, Sensitivity of climate simulations to the parameterization of cumulus convection in the Canadian Climate Centre General Circulation Model, *Atmos. Ocean*, 33, 407--446, 1995.

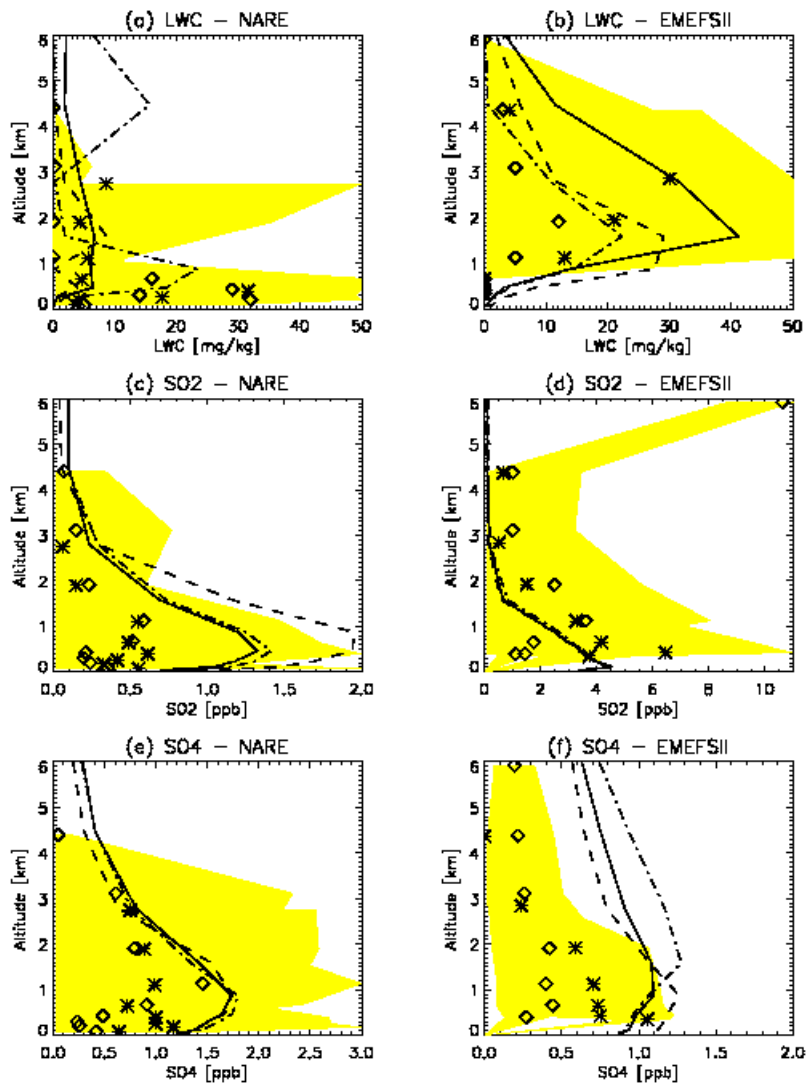


Figure 1: Vertical profiles of SO₂, sulfate and liquid water content at NARE and EMEFS for CCCma (solid), CCCma-pH (dashed-dotted line), and CCCMA-conv (dashed line)

Tracer modelling in ECHAM4

Erik Kjellstrom

Department of Meteorology at Stockholm University

Johann Feichter, Christine Land

Max-Planck-Institute for Meteorology in Hamburg

Abstract

The ECHAM4 model has been run in a simulation of the atmospheric sulfur cycle including DMS, SO₂, SO₄²⁻ and MSA. To put further constraints on the model representation of transport and removal processes also ²²²Rn and ²¹⁰Pb has been included as tracers. In the present experiment the model has been forced to simulate the time period July 1993 to June 1994 with a relaxation technique. In this way a meaningful comparison with observational data from that period has been possible.

Model Description

ECHAM4 is a general circulation model developed at the Max-Planck-Institute for Meteorology in Hamburg; a detailed description can be found in Roeckner et al. (1996). In the present experiment the model is run in T42 resolution which corresponds to a horizontal resolution of 2.8x2.8 degrees. In the vertical there are 19 levels from the surface up to 10 hPa. The sulfur model that is coupled to the meteorological model was first developed by Feichter et al. (1996) for ECHAM3 and has, since then, also been used in ECHAM4 (Feichter et al., 1997). In the following some new characteristics of the model will be described.

Relaxation

In order to force the model to simulate a certain period of time we have applied a Newtonian relaxation technique (Krisnamurti et al., 1991; Jeuken et al., 1996) to the model. The prognostic variables for vorticity, divergence, temperature and surface pressure has been forced to follow observed conditions as analysed by ECMWF. The technique is to add an additional term to the prognostic equations at each time step according to:

$$dX = dX(\text{model}) + Gx (X_{\text{obs}} - X)$$

where X	is any of the prognostic variables listed above,
dX(model)	is the model calculated tendency of the tracer before the relaxation takes place
X _{obs}	is the value of the prognostic quantity from the analyzes fields (ECMWF)
Gx	is the relaxation coefficient

The values of G are taken from Jeuken et al. (1996) - these are: $5E-4$ s⁻¹ for vorticity, $1E-4$ s⁻¹ for divergence and surface pressure, and $1E-5$ s⁻¹ for temperature. The idea of applying the assimilation technique, similar to the one used in numerical weather predictions, is to run the model in periods when there are extensive sets of observations available to put constraints on the model treatment of tracer transport and chemistry.

Transport

Advection of tracers is calculated with a new advection scheme called SPITFIRE (Split Implementation of Transport using Flux Integral REpresentations) which has been developed and tested at NCAR by Rasch and Lawrence (1998). They found the main advantages compared to the semi-Lagrangian scheme previously used in this model (Rasch and Williamson, 1990) to be that it is strictly conservative and that it is easier to treat boundaries with no flux across them.

Sulfur Model

The sulfur model used in this experiment is essentially the same as the one used previously by Feichter et al. (1996 and 1997). The main change is that an additional oxidation pathway of DMS to MSA is included. In the present experiment DMS emissions from the oceans are calculated using sea surface concentrations of DMS (Kettle et al., 1996) and model generated winds according to Liss and Merlivat (1986). The emission is calculated to be 18.6 TgS/yr. Anthropogenic and volcanic emissions add up to 75 TgS/yr.

References

- Feichter, J., Kjellstrom, E., Rodhe, H., Dentener, F., Lelieveld, J. and Roelofs, G.-J., 1996. Simulation of the tropospheric sulfur cycle in a global climate model. *Atmos. Environ.*, 30, 1693-1707.
- Feichter, J., Lohmann, U. and Schult, I., 1997. The atmospheric sulfur cycle in ECHAM-4 and its impact on the shortwave radiation. *Climate Dynamics*, 13, 235-246.
- Jeuken, A., Siegmund, P., Heijboer, L., Feichter, J. and Bengtsson, L., 1996. On the potential of assimilating meteorological analyses in a global climate model for the purpose of model validation. *J. Geophys. Res.*, 101, 16939-16950.
- Kettle, A., Meinrat, M., Amouroux, D., Andreae, T., Bates, T., Berresheim, H., Bingemer, H., Boniforti, R., Hela, G., Leck, C., Maspero, M., Matrai, P., McTaggart, A., Mihalopoulos, N., Nguyen, B.C., Nove, A., Putaud, J.P., Rapsomanikis, S., Roberts, G., Schebeske, G., Sharma, S., Simo, R., Staubes, R., Turner, S. and Uher, G. (1996). A preliminary global database of sea surface dimethylsulfide measurements and a simple model to predict sea surface dimethylsulfide as a function of latitude, longitude and month. *Eos. Trans., AGU*, 77, F417.
- Krisnamurti, T., Xue, J., Bedi, H., Ingle, K., and Oosterhof, D., 1991. Physical initialization for numerical weather prediction over the tropics. *Tellus*, 43AB, 53-81.

Liss, P. and Merlivat, L., 1986. Air-sea gas exchange rates: Introduction and synthesis. In *The Role of Air-sea Exchange in Geochemical Cycling* (edited by P. Buat-Menard), D. Reidel, Hingham, Mass., USA., pp 113-127.

Jeuken, A., Siegmund, P., Heijboer, L., Feichter, J. and Bengtsson, L., 1996. On the potential of assimilating meteorological analyses in a global climate model for the purpose of model validation. *J. Geophys. Res.*, 101. 16939-16950.

Rasch, P. and Williamson, D., 1990. Computational aspects of moisture transport in global models of the atmosphere. *Q.J.R. Meteorol. Soc.*, 116, 1071-1090.

Rasch, P. and Lawrence, M., 1998. Recent development in transport methods at NCAR. In: *MPI Workshop on conservative transport schemes*. B. Machenhauer et al (Eds), 2-3 June 1997, Report No. 265, Max-Planck-Institute for Meteorology in Hamburg, 65-75.

Roeckner, E., Arpe, K., Bengtsson, L., Christoph, M., Claussen, M., Dumenil, L., Esch, M., Giorgetta, M., Schlese, U. and Schulzweida, U., 1996. The atmospheric general circulation model ECHAM-4: Model description and simulation of present-day climate. Report No. 218., Max-Planck-Institute for Meteorology in Hamburg, Germany.

TOMCAT 3D Chemical Transport Model - COSAM Experiments

C.H. Bridgeman, M.P. Chipperfield, C. Giannakopoulos, K.S. Law,
P.-H. Plantevin, J.A. Pyle, D. Shallcross K.-Y. Wang

Department of Chemistry, University of Cambridge, CB2 1EW, U.K.

1. The TOMCAT CTM

1.1 Introduction

TOMCAT is an off-line chemical transport model (CTM) which has been widely used for stratospheric chemistry studies [e.g. Chipperfield et al. 1993, 1994, 1995]. The stratospheric version of the model, which only treats tracer advection, has recently been developed for tropospheric studies by including a scheme for convection and vertical diffusion [Stockwell and Chipperfield 1999] and chemistry [Law et al. 1998].

The model circulation and temperatures are specified from meteorological analyses (e.g. ECMWF or UKMO) or from the output of a general circulation model. These wind fields are generally available 6-hourly or 24-hourly and the fields are linearly interpolated to intermediate model time steps. The model reads in the horizontal winds in the form of vorticity and divergence fields; vertical transport is then diagnosed from the divergence fields. Tracer advection is achieved using the second order moments scheme of Prather [1986]. This scheme, although costly in terms of storage, is non-diffusive and is able to maintain sharp gradients in the tracer distributions. Because of the storage cost with a large number of tracers or at high resolution, the model can also be run with conservation of first order moments, equivalent to the slopes scheme of Russell and Lerner [1981].

The vertical domain and resolution of the TOMCAT CTM is defined by the levels of the meteorological analyses or GCM output. For example, with ECMWF analyses TOMCAT uses the same hybrid sigma/pressure levels as the ECMWF model giving a top level at 10hPa. The horizontal resolution of TOMCAT is independent of the resolution of the forcing winds and is completely variable.

1.2. Physical parameterization schemes

Turbulent vertical diffusion was previously parameterised using the scheme of Louis [1979] based on code provided by M. Heimann. This is a local scheme, and as such has two limitations: it is unable to account for large eddy transports that can occur throughout the planetary boundary layer (PBL) even when part of the depth of the PBL is dry statically stable [Deardorff, 1972, Holtslag and Boville, 1993] and it does not account for entrainment at the top of the PBL. As a

result, mixing is underestimated in the PBL and between the PBL and the lowermost free troposphere [Stockwell et al., 1998]. A non-local vertical diffusion scheme, based on Holtslag and Boville and taken from the NCAR CCM2, has recently been implemented into TOMCAT [K. Wang, 1998] and is used in the COSAM experiments.

The model used the Tiedtke [1989] convection scheme based on code provided by M. Heimann.

1.3. Wet and Dry Deposition

The wet deposition scheme is divided into two types of precipitation, convective and dynamic. The convective part is calculated according to the method of Balkanski et al. [1993] by applying a scavenging efficiency to all wet convective events. An efficiency of 100% was used for soluble species in deep wet convection and 50% in shallow wet convection. For SO₂ scavenging efficiencies of 3% and 1.5% were used for deep and shallow wet convection respectively. The large scale precipitation was calculated according to the scheme of Walton et al. [1988], which deals with the problem of sub-gridscale patchiness of precipitation by defining an equivalent precipitation rate, assuming that precipitation occurs over a fraction of the cell and that the species mixing ratio is uniform across the grid cell at the beginning and the end of the cycle. The coefficients used to calculate large-scale precipitation were those of Lee and Feichter [1995].

For the dry deposition a parameterization with prescribed deposition velocities was used and applied in the model layer the nearest to the ground [Giannakopoulos, 1998]. Deposition velocities were allowed to vary for SO₂ and SO₄ according to different vegetation categories. The global archive of Wilson [1985] was employed for this reason. Deposition velocities from the literature at 1m were extrapolated to the middle of the lowest model level using the Monin-Obukhov similarity theory. Thus the rate of dry deposition varied with the lowest model level height, according to the meteorological conditions near the surface. For SO₂ we used 0.6 cm/s over land, 0.8 cm/s over water and 0.1 cm/s over snow; for SO₄ 0.2 cm/s everywhere. For Pb-210 a global we used 0.05 cm/s over snow, 0.5 cm/s over water, 0.2 cm/s over grass and forests and 0.1 cm/s everywhere else. No seasonal variation in the deposition velocities was employed.

2. Experiments

We performed the COSAM experiments by running TOMCAT for a 3 month spin up period from April to June 1993 and then for 12 months, during which time output was saved every 1.25 days. The model was run at a 5.6° × 5.6° (T21) horizontal resolution and with 31 vertical levels, and a 30 minute time step for the dynamics and chemistry. Meteorological input data was taken from ECMWF-ERA analyses. The non-local vertical diffusion scheme was used in order to improve mixing in the boundary layer and lowermost free troposphere. The effect of the non-local scheme can be seen in Figure 1, which shows observed [Kritz et al., 1998] and calculated average radon vertical profiles.

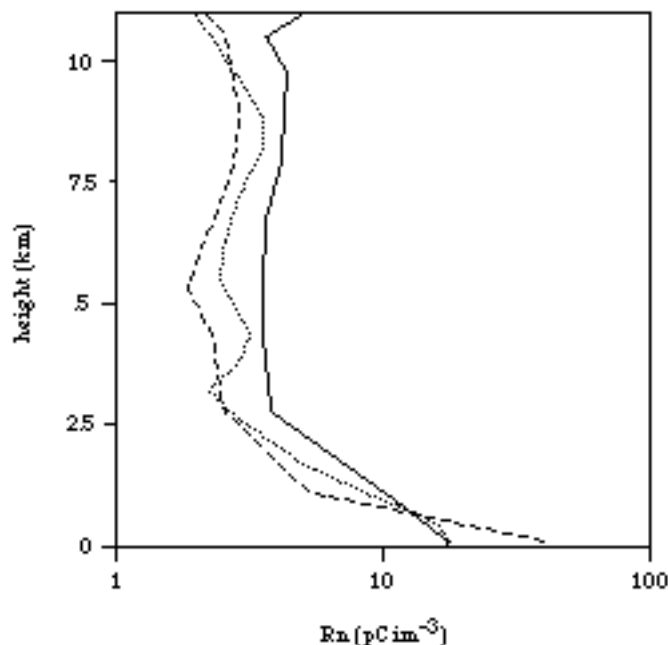


Figure 1. Radon profiles calculated using TOMCAT with non-local vertical diffusion (dotted line) local vertical diffusion (dashed line), and observed profile (solid line).

Table 1. Comparison of budget terms for 3 TOMCAT experiments

Model details		Annual mean tropospheric mass (10^9 moles S)			
DMS oxidation	aqueous chemistry	SO ₄	SO ₂	DMS	MSA
OH	no	14.5	24.5	10.2	3.3
OH	yes	24.8	13.1	10.0	3.1
OH, NO ₃	yes	24.5	12.9	1.5	1.4

A previous TOMCAT experiment using a local vertical diffusion scheme tended to underestimate vertical mixing out of the PBL leading to radon concentrations which were too high close to the surface and too low in the lower troposphere [Stockwell et al., 1998]. The improved boundary-layer scheme causes more radon to be mixed higher up, thus reducing the amount in the lower boundary layer, in better agreement with the experimental results near to the surface.

Our preliminary results which we presented at the workshop were obtained by running the model with no in-cloud chemistry, resulting in unusually low SO₄ and high SO₂ values compared with other models. Aqueous-phase chemistry has since been included and the

experiment rerun to provide our final results. We have also run the model with DMS oxidation by OH only and by OH and NO₃. In both cases DMS is converted to SO₂ and MSA in a ratio dependent on the temperature and ozone concentration. SO₂ is oxidized by OH in the gas phase to produce SO₄.

The aqueous phase chemistry considers the dissolution of SO₂ in cloud water and the subsequent oxidation of S(IV) to sulphate by dissolved O₃ and H₂O₂. Aqueous phase chemical reaction rates and Henry's law coefficients are from Seinfeld, 1986.

OH, O₃, H₂O₂ and NO₃ concentrations for the original experiment are 5 day averages from an annual integration of the 3D TOMCAT model, and those for the subsequent two experiments are 10 day averages from the same integration. Details of and budget terms from the three experiments are compared in Table 1.

References

Balkanski, Y.J., D.J. Jacob, G.M. Gardner, W.C. Graustein, and K.K. Turekian, Transport and residence times of tropospheric aerosols inferred from a three-dimensional simulation of ²¹⁰Pb, *Geophys. Res.*, *98*, 20573-20586, 1993.

Chipperfield, M.P., D. Cariolle, P. Simon, R. Ramarosan, and D.J. Lary, A three-dimensional modeling study of trace species in the Arctic lower stratosphere during winter 1989-1990, *J. Geophys. Res.*, *98*, 7199-7218, 1993.

Chipperfield, M.P., D. Cariolle, and P. Simon, A 3D chemical transport model study of chlorine activation during EASOE, *Geophys. Res. Lett.*, *21*, 1467-1470, 1994.

Deardorff, J.W., Theoretical expression for the counter-gradient vertical heat flux, *Geophys. Res.*, *77*, 5900-5904, 1972.

Chipperfield, M.P., J.A. Pyle, C.E. Blom, N. Glatthor, M. Höpfner, T. Gulde, Ch. Piesch, and P. Simon, The Variability of ClONO₂ in the Arctic Polar Vortex: Comparison of Transall MIPAS Measurements and 3D Model Results, *J. Geophys. Res.*, *100*, 9115-9129, 1995.

Giannakopoulos, C., Modelling the impact of physical and removal processes on tropospheric chemistry, Ph.D. Thesis, University of Cambridge, Cambridge, 1998.

Holtslag, A.A.M., and B.A. Boville, Local Versus Nonlocal Boundary Layer Diffusion in a Global Climate Model, *J. Climate*, *6*, 1825-1842, 1993.

Kritz, A.M., Rosner, S.W., and D.Z. Stockwell, Validation of an off-line three-dimensional chemical transport model using observed radon profiles 1. Observations, *J. Geophys. Res.*, *103*, 8425-8432, 1998.

Law, K.S., P.-H. Plantevin, D.E. Shallcross, H. Rogers, C. Grouhel, V. Thouret, A. Marengo and J.A. Pyle, Evaluation of modelled O₃ using MOZAIC data, *J. Geophys. Res.*, *103*, 25721-25740, 1998.

Lee, H.N., and J. Feichter, An intercomparison of wet precipitation scavenging schemes and the emission rates of ²²²Rn for the simulation of global transport and deposition of ²¹⁰Pb, *J. Geophys. Res.*, *100*, 23253-23270, 1995.

Louis, J.-F., A parametric model of vertical eddy fluxes in the atmosphere, *Boundary Layer Meteorology*, *17*, 187-202, 1979.

Prather, M.J., Numerical advection by conservation of second order moments, *J. Geophys. Res.*, *91*, 6671-6681, 1986.

Russell, G.L., and J.A. Lerner, A new finite differencing scheme for the tracer transport equation, *J. Appl. Meteorol.*, *20*, 1483-1498, 1981.

Seinfeld, J.H. 1986. *Atmospheric chemistry and physics of air pollution*, John Wiley. New York, pp 195-227.

Stockwell, D.Z., and M.P. Chipperfield, A tropospheric chemical transport model: Development and validation of the model transport schemes, *Q. J. Roy. Met. Soc.*, Vol. 125, No. 557, 1747-1783, 1999

Stockwell, D.Z., M.A. Kritz, M.P. Chipperfield, and J.A. Pyle, Validation of an off-line three-dimensional chemical transport model using observed radon profiles 2. Model results, *J. Geophys. Res.*, *103*, 8433-8445, 1998.

Tiedtke, M., A comprehensive mass flux scheme for cumulus parameterization in large-scale models, *Mon. Wea. Rev.*, *117*, 1779-1800, 1989.

Walton, J.J., M.C. MacCracken, and S.J. Ghan, A global-scale lagrangian trace species model of transport, transformation, and removal processes, *J. Geophys. Res.*, *93*, 8339-8354, 1988.

Wang, K.-Y., Development of a three-dimensional tropospheric chemistry model, Ph.D. Thesis, University of Cambridge, Cambridge, 1998.

Wilson, M.F., and A. Henderson-Sellers, A global archive of land cover and soils data for use in general circulation model, *J. Climatol.*, *5*, 119-143, 1985.

GLOBAL SULFUR MODELING WITH THE TRACER TRANSPORT MODEL TM3

Ad Jeuken (KNMI)
Frank Dentener (IMAU)

The transport model

The tracer transport model (TM3) used in this study has been adapted from the global tracer transport model TM2 (*Heimann, 1995, Rehfeld, 1997*). The present model calculates the horizontal and vertical transport of tracer mass using meteorological fields from the ECMWF. These input fields are updated every 6 hours. In a pre-processing step they are interpolated from an original resolution of 2.5° times 2.5° onto the TM3 model grid.

Global fields of wind, surface pressure, temperature, humidity, cloud cover, cloud liquid/ice water, surface precipitation and several other surface parameters are in this way made available. Different resolutions can be chosen: $7.5^\circ \times 10^\circ$, $3.75^\circ \times 5^\circ$ and $2.5^\circ \times 2.5^\circ$. At the latter resolution also a Hemispheric version of the model is available. The model has 19 hybrid sigma-pressure layers between the surface and 10 hPa. For the COSAM model inter comparison the $3.75^\circ \times 5^\circ$ resolution has been used.

Three-dimensional tracer transport in the model is accounted for by advection for the resolved motions and by convection and vertical diffusion for the unresolved motions (the sub-grid scale). The advection of tracers is calculated with the slopes scheme described by *Russell and Lerner, 1981*.

The sub-grid scale convection fluxes are calculated using the parametrization of *Tiedke, 1989*. Vertical diffusion is parametrized using the *Louis (1979)* formulation. In a recent paper by *Dentener et al. (1998)*, the model transport is evaluated. Model simulations of ^{222}Rn are compared with observations. Results show that the model is well capable to simulate the transport of Radon from its land source to remote measurement stations. In another recent paper, by *Jeuken et al. (1999)*, modelled ozone columns are compared with TOMS and TOVS measurements. Results suggest that the model transport is little diffusive and that it preserves dynamical structures (in ozone) very well.

The chemical model

The model contains 18 tracers that are transported and an additional 16 intermediate species. The sulfur species in the model are SO_2 , SO_4^- , DMS and, MSA. In addition it contains ammonia and ammonium. The Sulfur cycle is coupled to a tropospheric background chemistry scheme, which solves the $\text{CH}_4\text{-CO-NO}_x\text{-HO}_x$ chemistry (see also *Roelofs and Lelieveld 1995*). In comparison with models that prescribe the oxidant fields for SO_2 and DMS this approach is more realistic, yet much more demanding in computing time.

For DMS we use the compilation of ocean surface concentrations of Kettle and Andreae in combination with the *Liss and Merlivat (1986)* piston velocity parametrization to calculate DMS emissions. This results in an annual DMS emission of 17 Tg S. DMS is oxidized in the gas phase by OH, leading to SO₂ and MSA, and by the NO₃ radical, leading also to SO₂.

Emissions of SO₂ are taken from the GEIA data base. We use the two level seasonal emission distributions. Volcanic emissions are derived from the work of *Andres and Kasgnoc (1998)*. The total global SO₂ emission is about 75 Tg per year.

The main removal mechanism of SO₂ is dry deposition at the surface. Dry deposition of all tracers in the model is calculated with the extensive scheme of *Ganzeveld et al.1998*. In this scheme the deposition velocity of SO₂ depends on the aerodynamic resistance and surface characteristics like for example snow cover, soil pH or soil wetness. Tests of this deposition scheme in the ECHAM model show that the SO₂ concentrations near the surface have increased considerably compared to an old scheme which used constant deposition velocities. For the sulfate an integrated sulfate deposition velocity is calculated, applying a unimodal mass size distribution over land and a bimodal mass size distribution over sea. The deposition over sea, in addition, is dependent on the surface roughness which varies with wind speed.

Both gas phase as well as reactions of SO₂ are considered. About 36% is oxidized by OH in the gas phase the rest by H₂O₂ and O₃ in the cloud. The removal path via ozone is strongly pH dependent. The pH is calculated from all bases, weak and strong acids that are available in the model (so also ammonium). To determine the amount of dissolved SO₂ in the cloud droplet, the effective Henry equilibrium coefficient is calculated.

The main removal mechanism of Sulfate is wet scavenging either by rain drops or cloud drops. In a previous model version a simple parameterization for this process was applied. In this parameterization, the precipitation at the surface is scaled with a normalized zonally and seasonally averaged climatology of the vertical distribution of precipitation formation. The climatology was taken from a GCM. The resulting vertical distribution of precipitation formation rates is directly related to the amount of tracer being scavenged inside the cloud (*See also Langner and Rodhe, 1991*). Only an additional solubility factor depending on the Henry's Law constants. has to be applied. No distinction has been made between convective and large scale precipitation and between in- and below cloud scavenging.

In a new approach we explicitly calculate the three dimensional precipitation formation rates in large scale clouds every six hours from ECMWF fields of cloud liquid and ice water content. The formulation we use for this purpose are the same as in the ECHAM model (*Roeckner et al,1992*).

In cloud scavenging of gases and aerosols depends on the transfer time between gas and cloud droplet and on the rate of precipitation formation. Only at low cloud water contents the first process can be rate determining. For the below cloud scavenging we calculate an effective raindrop radius and rain fall speed. Together with the transfer time from gases to the rain droplet

and the before mentioned solubility factor, this gives the rate of below cloud scavenging (Roelofs and Lelieveld, 1995). The below cloud scavenging of aerosols is somewhat reduced to account for the effect that particles in the 1 micron range are less effectively scavenged by falling droplets.

For convective scavenging we follow the approach of Balkanski *et al.* (1993), in which the amount of tracer mass scavenged is proportional to the updraft mass flux in convective clouds. For low level convection an efficiency of 50 % is assumed and for deep convection an efficiency of 100 %.

Some results

Lead 210 simulations with the new scavenging scheme show that in comparison with the old scheme more tracer mass is scavenged at higher altitudes. Comparison with measurements of the PEM-west campaign (Dibb *et al.*) show that the vertical distribution of aerosol is much more realistic with the new scheme. SO₂ concentrations near the surface over Europe are found to be extremely high both in comparison with other models as well as measurements.

References

Andres, R. J. And A. D. Kasgnoc, A time-averaged inventory of subaerial volcanic sulfur emissions, *J. Geophys. Res.* 103, 19, 25,251-25,261,1998.

Balkanski, Y. J., D. J. Jacob, G. M. Gardner, W. C. Graustein and K. K. Turekian, Transport and residence times of tropospheric aerosols inferred from a global three-dimensional simulation of 210 Pb, *J. Geophys. Res.* 98, 20,573-20,586, 1993.

Dentener, F., J. Feichter and, A. Jeuken, Simulations of Rn²²² using on-line and off-line global models at different horizontal resolutions; a detailed comparison with measurements, *Tellus*, 51B, 573-602, 1999.

Dibb, J, R. Talbot, K. Klemm, G. Gregory, H. Singh, J Bradshaw and S. Sandholm, Asian influence over the western North Pacific during the fall season: Inferences from lead 210, soluble ionic species and ozone, *J. Geophys. Res.*, 101, 1779-1792, 1996.

Ganzeveld, L., J. Lelieveld and G.-J. Roelofs, Dry deposition parametrization of sulfur oxides in a chemistry and general circulation model, *J. Geophys. Res.* 103, 5679-5694, 1998.

Houweling, S., F. Dentener and J. Lelieveld, The impact of nonmethane hydrocarbon compounds on tropospheric chemistry, *J. Geophys. Res.* 103, 10,673-10,696, 1998.

Jeuken, A., H. Eskes, E. Holm, F.J.P. van Velthoven, H. Kelder and E. Holm. Assimilation of total ozone satellite measurements in a three-dimensional tracer transport model, *J. Geophys. Res.*, Vol 104, D5, 5551-5563, 1999.

Kettle, A. J., T. S. Rhee, M. von Hobe, A. Poulton, J. Aiken, and M. O. Andreae. 2001. Assessing the flux of different volatile sulfur gases to the atmosphere. *J. Geophys. Res.* 106 (D11): 12193-12209.

Langner, J. and H. Rodhe, A global three-dimensional model of the tropospheric sulfur cycle, *J. Atm. Chem.* 13, 225-263, 1991.

Liss P. And L. Merlivat, Air-sea gas exchange rates: introduction and synthesis, in: Buat-Menard, P. (editor), the role of sea-air exchange in geochemical cycling, Reidel, Dordrecht, pp. 113-127, 1986.

Louis, J. F., A parametric model of vertical eddy fluxes in the atmosphere, *Boundary Layer Meteorol.* 17, 187-202, 1979.

Roelofs, G.-J. and J. Lelieveld, Distribution and Budget of O₃ in the troposphere calculated with a chemistry general circulation model, *J. Geophys. Res.* 100, 20,983-20,998, 1995.

Russell and Lerner, A finite difference scheme for the tracer transport equation, *J. Appl. Meteorol.*, 20, 1483, 1981.

Tiedke, M., Representation of clouds in large-scale models, *Month. Wea. Rev.* 121, 3040-3061, 1993.

LLNL-IMPACT model

Dan Bergmann, Cyndi Atherton, Jane Dignon, Doug Rotman, and John Tannahill

The LLNL (Lawrence Livermore National Laboratory) IMPACT (Integrated Massively Parallel Atmospheric Chemical Transport) model is a global, three-dimensional chemistry-transport-deposition model that contains both a prognostic troposphere and stratosphere. It uses as input meteorological fields from either a General Circulation model (GCM) or data assimilated meteorological fields (Rotman et al., 1993) (Penner et al. 1998). The data assimilated meteorological fields are currently those from the Data Assimilation Program at NASA-Goddard. This data is assimilated output from the DAO based GEOS system that covers the time period of the ongoing NASA STRAT measurement campaign from May 1995 to present (and should continue for some time into the future). The meteorological data is provided on a 2 degree by 2.5 degree horizontal resolution with 46 levels in the vertical, from ground to 0.1 mb. This data contains a more highly defined boundary layer than previous tropospheric models and the resolution allows for analysis of either regional to global scale and tropospheric to stratospheric issues. The advantage of using assimilated data is that the model can simulate specific historic events, allowing direct model-observation comparisons and thus model validation.

IMPACT is based on an operator splitting method for advection, diffusion, convection, photolysis and chemistry. The chemistry equations are solved using SMVGEAR II (Jacobson, 1995), a technique capable of highly accurate solutions to both stiff and non-stiff sets of ordinary differential equations. SMVGEAR II is a version of the original predictor/corrector, backward differentiation code of Gear (1971) and uses a variable time step, variable order, implicit technique for solving stiff numerical systems with strict error control. Jacobson's formulation gives the identical answers as the original GEAR code, but is 120 times faster than the Gear code. The chemical continuity equation is solved for *each individual species* (i.e., no lumping of species into chemical families are made). The chemical reaction mechanism and applicable parameters are incorporated in files that are generated external to the IMPACT model.

The photochemistry within IMPACT has included reaction mechanisms appropriate for both the stratosphere and troposphere. Reactions in the stratospheric mechanism include those comprising the families O_x , NO_y , ClO_y , HO_y , BrO_y , and CH_4 and its oxidation (46 transported species, 116 thermal reactions, and 38 photolytic reactions). A full tropospheric reaction mechanism in IMPACT is based on the mechanism of Lurmann et al., 1986. The mechanism has been updated to account for isoprene reactions (Paulson and Seinfeld, 1992), reactions in the remote atmosphere (Jacob and Wofsy, 1988) and peroxy radical reactions (Kirchner and Stockwell, 1996). Species treated include O_3 , OH, PAN, NO, NO_2 , CO, CH_4 , HNO_3 , isoprene, ethane, propane, C4-5 alkanes, C6-8 alkanes, ethene, propene, and aromatic hydrocarbons, ketones (including acetone), and formaldehyde, acetaldehyde, and higher aldehydes. Where applicable, absorption cross sections and reaction rate coefficients were taken from DeMore et al. (1997). A simplified tropospheric reaction mechanism has also been implemented within IMPACT and is now being tested. It includes 28 species, 58 thermal reactions, 17 photolysis reactions, and both anthropogenic and natural source terms for CO, CH_4 , and NO_2 .

Advection in all three directions uses a variable order multidimensional flux form of the semi-Lagrangian method, an up-stream-biased monotonic grid point scheme (Lin and Rood, 1996). The upstream nature of this method reduces phase errors to a minimum and the monotonicity control eliminates the need for a filling algorithm and the severe problems that would arise with negative values of chemical species concentrations. This scheme also avoids the

strict Courant stability problem at the poles, thus allowing large time steps to be used, resulting in a highly efficient advection operation. Vertical diffusion is done implicitly following the algorithm of Walton et al. (1988). Convective transport uses the scheme of Lin (DAO, NASA Goddard, private communication), which for infinitely thin layers is essentially the apparent momentum transport of clouds (Schneider and Lindzen, 1976).

IMPACT uses the dry deposition algorithm of Wang et al. (1998a-c). This is an improved version of that published in Jacob et al. (1993). This algorithm internally computes the local deposition velocity for a tracer species based on aerodynamic resistance and surface resistance, (Wesely et al., 1985). For this COSAM Rn/Pb exercise, both species were dry deposited, Rn as a gas and Pb as an aerosol. Wet scavenging has five separate components:

- *convective wet deposition* (Balkanski et al. 1993) - treats the deposition due to convective updrafts. This uses the values of convective mass flux in the GEOS-STRAT data.
- *large scale (stratiform) scavenging* (Giorgi and Chameides 1986) - requires separate condensation rates for large scale and convective precipitation, yet our GEOS-STRAT meteorological data files contain a single condensation rate. The GEOS-STRAT data does include both total convective and large scale precipitation reaching the surface. We use this data to partition the entire column of condensation rates into convective and large scale components. This model then calculates the rate at which these aerosols or gases are incorporated into raindrops within the cloud.
- *large scale washout* - washout by large scale precipitation in grid boxes below cloud is computed as a first order loss process applied to the precipitating fraction (F) of the grid box (defined by the maximum value of F in the overhead grid boxes). The 3D field of large scale precipitation is calculated using the 3D condensation rate along with the 2D fields of convective and large scale precipitation reaching the surface. A washout rate constant of $0.1 \text{ (mm}^{-1}\text{)}$ normalized to the precipitation rate was used.
- *convective scavenging* (Giorgi and Chameides 1986) (Koch et al. 1996) - similar to large scale scavenging but uses the fraction of the condensation rate from convective processes as determined by the 2D fields of convective and large scale precipitation reaching the surface. Also, when calculating F (the fraction of the grid box where precipitation takes place), uses different estimates for F0 (the maximum value of F, L (the cloud liquid water content), Tc (the duration of the precipitation event), and beta_min (the minimum value for the rate of conversion of cloud water to precipitation).

IMPACT can calculate photolysis rates by two different methods. In the first method, photolytic loss rate constants integrate the product of absorption coefficient, quantum yield, and solar flux over wavelength, using temperature and pressure dependence where appropriate and available. A two-stream multiple-layer UV-visible model uses 126 wavelength bins to capture the spectral detail needed for photodissociation calculations. The scattering of energy from the direct solar beam uses the delta-Eddington algorithm (Joseph et al., 1976) while the scattering of diffuse radiation is modeled using the (Sagan-Pollack 1967) algorithm. The second method available to IMPACT for calculating photolysis rates is by a fast clear-sky lookup table in which the rates are a function of cross section (a function of temperature, species, and wavelength), pressure, solar zenith angle, and column ozone. Michael Prather at the University of California, Irvine has also agreed to provide us with his upcoming tropospheric and stratospheric techniques, in which the frequency bands are optimized for minimum band usage with maximum accuracy.

IMPACT has been developed and implemented on massively parallel distributed memory super-computers such as the Cray T3E and the IBM SP2 (it also runs on Cray C and J90's, workstations and a series of other massively parallel computers). The ability to compute on parallel machines has greatly advanced our throughput capabilities and has made possible global high resolution tropospheric stratospheric atmospheric chemistry simulations.

For this COSAM exercise, only the Rn/Pb test problem was run with assimilated meteorological fields for 1997 from NASA's GEOS-STRAT product. Vertical profiles of ^{222}Rn are shown in figure 1. Similar figures will be included in the COSAM final report. Figure 2 shows predicted ^{210}Pb deposition to the surface by both wet and dry deposition. Deposition fluxes over land are predicted to vary by nearly an order of magnitude depending on local meteorology and surface type. Deposition fluxes to the ocean are substantially less.

We are presently developing a chemistry model which will treat gas phase sulfur reactions using prognostic O_3 , NO_3 , and OH . We will also include models for heterogeneous stratospheric sulfur reactions as well as aqueous sulfur reactions in the troposphere.

References

- Balkanski, Y.J., D.J. Jacob, G.M. Gardner, W.C. Graustein, and K.K. Turekian, 1993: Transport and residence times of tropospheric aerosols inferred from a global three-dimensional simulation of ^{210}Pb , *J. Geophys. Res.*, **98**, 20,573-20,586.
- DeMore, W. B., S. P. Sander, D. M. Golden, R. F. Hampson, M.J. Kurylo, C.J. Howard, A.R. Ravishankara, C.E. Kolb, and M.J. Molina, Chemical Kinetics and Photochemical Data for Use in Stratospheric Modeling, Eval. 12, JPL Publication 97-4, 1997.
- Gear, C.W., 1971: Numerical initial value problems in ordinary differential equations. Prentice-Hall, Englewood Cliffs, NJ.
- Giorgi, F. and W. L. Chameides, 1986: Rainout lifetimes of highly soluble aerosols and gases as inferred from simulations with a general circulation model, *J. Geophys. Res.*, **91**, 14,367-14,376.
- Jacob, D.J. and S.C. Wofsy, 1988: Photochemistry of biogenic emissions over the Amazon Forest, *J. Geophys. Res.*, **93**, 1477-1486.
- Jacob, D.J., J.A. Logan, R.M. Yevich, G.M. Gardner, C.M. Spivakovsky, S.C. Wofsy, J.W. Munger, S. Sillman, M.J. Prather, M.O. Rodgers, H. Westberg, and P.R. Zimmerman, 1993: Simulation of summertime ozone over North America, *J. Geophys. Res.*, **98**, 14,797-14,816.
- Jacobson, M.A., 1995: Computation of global photochemistry with SMVGEAR II, *Atmos. Environ.*, **29A**, 2541-2546.
- Joseph, J. H., W. J. Wiscombe, and J. A. Weinman, 1976: The Delta-Eddington approximation for radiative flux transfer, *J Atmos Sci*, **33**, 2452-2459.
- Kirchner, F. and W.R. Stockwell, 1996: The effect of peroxy radical reactions on the predicted concentrations of ozone, nitrogenous compounds and radicals, *J. Geophys. Res.*, **101**, 21,007-21,022.
- Koch, D.M., D.J. Jacob, W.C. Graustein, 1996: Vertical transport of tropospheric aerosols as indicated by ^7Be and ^{210}Pb in a chemical tracer model, *J. Geophys. Res.*, **101**, 18,651-18,666.
- Lin, S.J. and R.B. Rood, 1996: A fast flux form semi-Lagrangian transport scheme on the sphere, *Mon. Wea. Rev.*, **124**, 2046-2070.
- Lurmann, F.W., A.C. Lloyd, and R. Atkinson, 1986: A chemical mechanism for use in long-range transport/acid deposition computer modeling, *J. Geophys. Res.*, **91**, 10,095-10,936.

- Paulson, S.E. and J. H. Seinfeld, 1992: Development and evaluation of a photooxidation mechanism for isoprene, *J. Geophys. Res.*, **97**, 20,703-20,715.
- Penner, J.E., D. Bergmann, J.J. Walton, D. Kinnison, M.J. Prather, D. Rotman, C. Price, K.E. Pickering, and S.L. Baughcum, 1998: An evaluation of upper troposphere NO_x with two models, *J. Geophys. Res.*, **103**, 22097-22113.
- Rotman, D.A., D.J. Wuebbles, and J.E. Penner, 1993: Atmospheric Chemistry using Massively Parallel Computer, 1994 AMS Fifth Annual Symposium on Global Change Studies.
- Sagan, C., and J. B. Pollack, 1967: An isotropic nonconservative scattering and the clouds of Venus, *J. Geophys. Res.*, **72**, 469-477.
- Schneider, E.K. and R.S. Lindzen (1976) A discussion of the parameterization of momentum exchange by cumulus convection, *J. Geophys. Res.*, **81**, 3158 - 3161.
- Walton, J.J., M.C. MacCracken, and S.J. Ghan, 1988: A global-scale Lagrangian trace species model of transport, transformation, and removal processes, *J. Geophys. Res.*, **93**, 8339-8354.
- Wang, Y., D. J. Jacob, and J. A. Logan, Global simulation of tropospheric O₃-NO_x-hydrocarbon chemistry, 1. Model formulation, *J. Geophys. Res.*, **103**, 10,713-10,726, 1998a.
- Wang, Y., J. A. Logan, and D. J. Jacob, Global simulation of tropospheric O₃-NO_x-hydrocarbon chemistry, 2. Model evaluation and global ozone budget, *J. Geophys. Res.*, **103**, 10,727-10,756, 1998b.
- Wang, Y., D. J. Jacob, and J. A. Logan, Global simulation of tropospheric O₃-NO_x-hydrocarbon chemistry, 3. Origin of tropospheric ozone and effects of non-methane hydrocarbons, *J. Geophys. Res.*, **103**, 10,757-10,768, 1998c.
- Wesely, M.L., D.R. Book, R.L. Hart, and R.E. Speer, 1985: Measurements and parameterization of particulate sulfur dry deposition over grass, *J. Geophys. Res.*, **90**, 2131-2143.

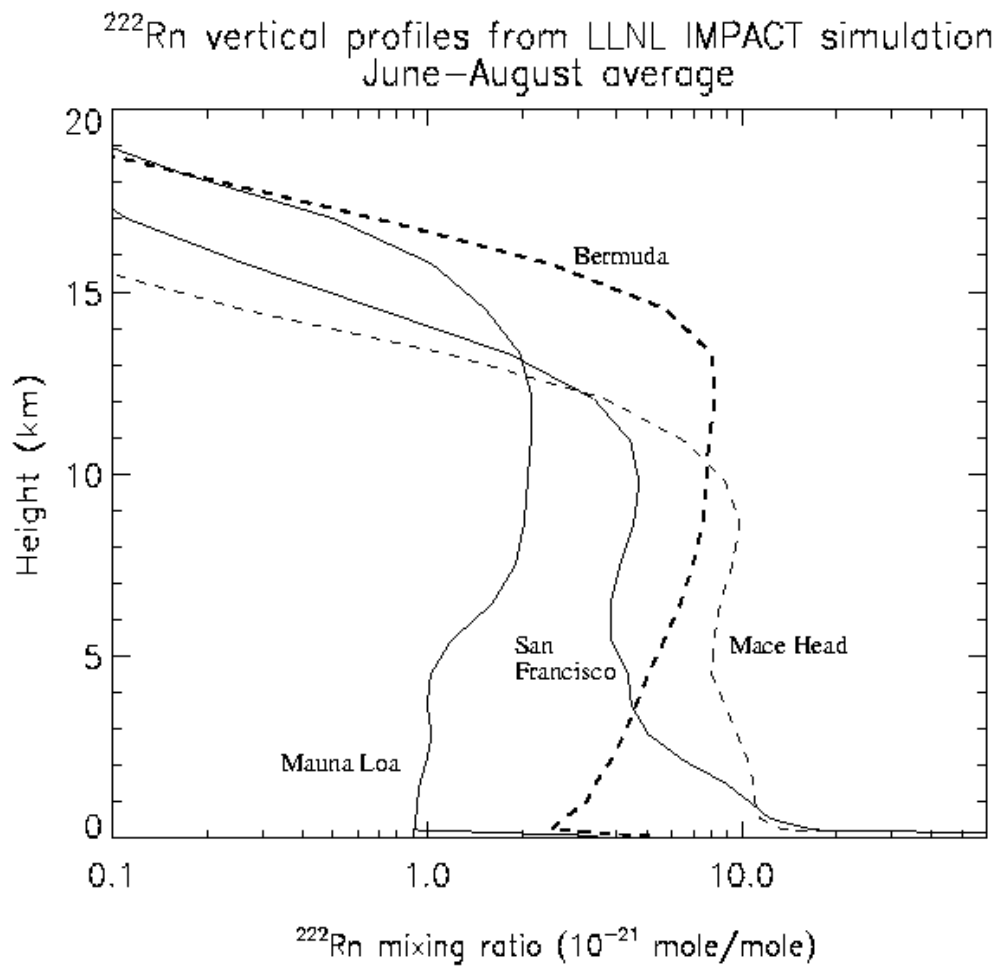


Figure 1 Vertical profile of ^{222}Rn at four sites from the LLNL IMPACT simulation.

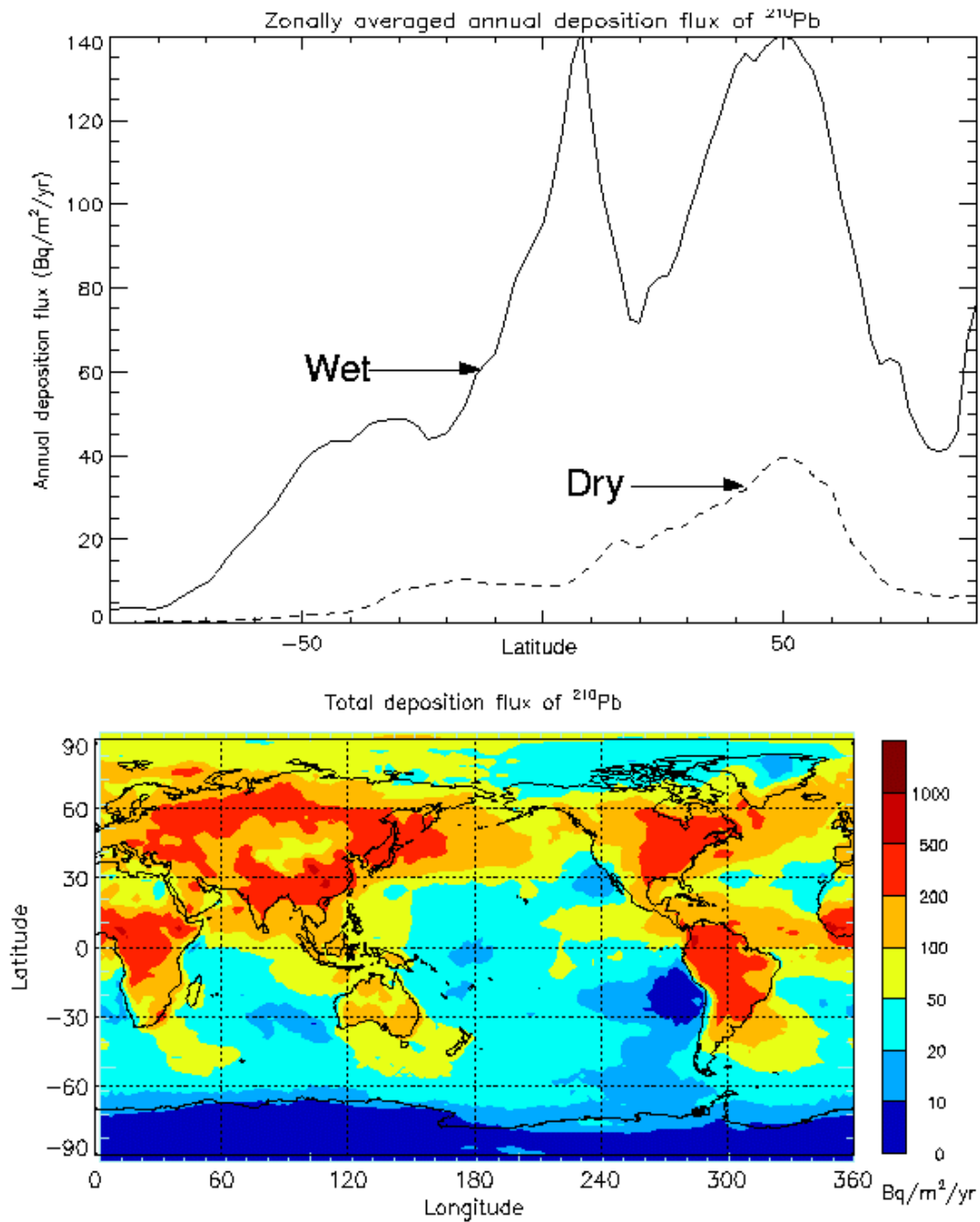


Figure 2 LLNL IMPACT model simulation of annual deposition flux of ^{210}Pb to the surface, both as wet and dry zonal averages (top) and as total deposition (bottom).

Tropospheric Sulfur Simulation with a Global 3D Model (GOCART)

Mian Chin

ABSTRACT

We present at the COSAM workshop the results of concentrations, distributions, and budgets of DMS, SO₂, sulfate, and MSA from the Georgia Tech/Goddard Global Ozone Chemistry Aerosol Radiation and Transport (GOCART) model (Chin et al., 2000). This model is driven by assimilated meteorological fields generated in the Goddard Earth Observing System Data Assimilation System (GEOS DAS). The horizontal resolution is 2 deg latitude by 2.5 deg longitude, and 20 sigma vertical levels.

Emission of SO_x from fossil fuel combustion and industrial activities are from GEIA inventory for 1985, with 64.9 TgS/yr of SO₂ and 2.1 TgS/yr of sulfate. Continuously erupting volcanic emission of SO₂ is taken from GEIA with a strength of 4.8 TgS/yr. As required by the workshop, biomass burning and aircraft emissions are not included in the results presented here. Monthly averaged biogenic emission of DMS from the ocean is provide in the COSAM exercise, with an annual flux of 19.0 TgS/yr.

The model uses a semi-lagrangian flux-form advection scheme (Lin and Rood, 1996). Boundary layer turbulent mixing is calculated using the turbulent diffusion coefficient, which is formulated in the GEOS DAS based on a 2.5 closure scheme (Helfand and Labraga, 1988). Cloud convection is parameterized using cloud mass flux from GEOS DAS (Allen et al., 1996).

Chemical reactions in the model include oxidation of DMS by OH and NO₃, and oxidation of SO₂ by OH in the air and by H₂O₂ in clouds. The monthly averaged concentrations of OH, NO₃, and H₂O₂ are prescribed using the output from the IMAGES model (Müller and Brasseur, 1995). Dry deposition velocities for SO₂, sulfate, and MSA are computed using a resistance-in-series scheme (Wesely and Hicks, 1977). Wet deposition includes scavenging of soluble species by rainout and washout parameterized with a first-order loss rate (Giorgi and Chameides, 1986), and by convective cloud updraft process (Balkanski et al., 1992) with a scavenging efficiency of 30%/km.

We present the results of 1-year simulation from July 1993 to June 1994. The model generally captures the geographical and seasonal variations of sulfate concentrations observed at the surface and mountaintop sites, even though the SO₂ concentrations are generally over predicted by the model especially in the winter at high latitudes. It is more difficult to reproduce the vertical structure for both SO₂ and sulfate observed in some short-term aircraft measurements.

References

Allen, D. J., P. Kasibhatla, A. M. Thompson, R. B. Rood, B. G. Doddridge, K. E. Pickering, R. D. Hudson, and S.-J. Lin, Transport-induced interannual variability of carbon monoxide determined using a chemistry and transport model, *J. Geophys. Res.*, 101, 28,655-28,669, 1996.

- Balkanski, Y. J., D. J. Jacob, G. M. Gardner, W. C. Graustein, and K. K. Turekian, Transport and residence times of tropospheric aerosols inferred from a global three-dimensional simulation of ^{210}Pb , *J. Geophys. Res.*, 98, 20,573-20,586, 1992.
- Chin, M., R. B. Rood, S.-J. Lin, J.-F. Müller, and A. M. Thompson, Atmospheric sulfur cycle simulated in the global model GOCART: Model description and global properties, *J. Geophys. Res.*, 105, 24,671-24,687, 2000.
- Giorgi, F., and W. L. Chameides, Rainout lifetimes of highly soluble aerosols and gases as inferred from simulations with a general circulation model, *J. Geophys. Res.*, 91, 14,367-14,376, 1986.
- Helfand, M., and J. C. Labraga, Design of a non-singular level 2.5 second-order closure model for the prediction of atmospheric turbulence, *J. Atmos. Sci.*, 45, 113-132, 1988.
- Lin, S.-J., and R. B. Rood, Multidimensional flux-form semi-Lagrangian transport schemes, *Mon. Weather Rev.*, 124, 2046-2070, 1996.
- Müller, J.-F., and G. Brasseur, IMAGES: A three-dimensional chemical transport model of the global troposphere, *J. Geophys. Res.*, 100, 16,445-16,490, 1995.
- Wesely, M. L., and B. B. Hicks, Some factors that affect the deposition rates of sulfur dioxide and similar gases on vegetation, *J. Air. Pollut. Control Assoc.*, 27, 1110-1116, 1977.

Global Modeling of Sulfate Aerosols at NCAR

Phil Rasch, Mary Barth and Jeff Kiehl

I will outline the sulfate aerosol modeling effort made by the Climate and Global Dynamics and Atmospheric Chemistry Division at NCAR. Two complementary models are used: an offline transport model MATCH (Model of Atmospheric Transport and Chemistry; Mahowald et al., JGR, 1997) and a general circulation model CCM3 (see J. Climate special issue on the CCM3, June, 1998 for the GCM description and Barth et. al and Rasch et. al, JGR, 1999 for the description of the aerosol simulation). The models share many common modules for advection, convection, cloud physics, aerosol physics, etc. The former model uses NCEP analyses to specify the meteorological fields. The later model determines its own meteorology dynamically. The two models can be used to understand the aerosol distribution both in an event based mode (where comparisons are made directly to a observation at a particular time and place) and in a climatological mode (where comparisons are made in a statistical sense). CCM3 simulations are made at approximately a 3x3 degree resolution. MATCH simulation are made at a 2x2 degree resolution. Both models predict the evolution DMS, SO₂, SO₄, and H₂O₂. Climatological distributions of (OH, O₃, NO₃) and the precursor to peroxide (HO₂) are taken from the IMAGES model (Mueller et al, 1995). An unusual feature of both models is the prediction of H₂O₂, which is produced and scavenged dynamically. MATCH also has a complete calculation of the hydrologic cycle, which is an unusual feature in an offline transport model, but provides significant addition information on the 3 dimensional distribution of cloud water, cloud fraction, and the conversion of condensate to precipitation, which helps in the construction of gas and aerosol scavenging schemes.

After a brief comparison with observations, we examine the balance between processes that contribute to the global and regional distributions of sulfate aerosol in the Earth's atmosphere. The analysis suggests that the seasonal cycle of SO₂ and SO₄²⁻ are controlled by a complex interplay between transport, chemistry and deposition processes. The seasonal cycle of these species are not strongly controlled by temporal variations in emissions, but by seasonal variations in volume of air processed by clouds, mass of liquid water serving as a site for aqueous chemistry, amount of oxidant available for the conversion from SO₂ to SO₄²⁻, vertical transport processes, and deposition. A tagging of the sulfate by emission region (Europe, N. America, Asia, and rest of world [ROW]), chemical pathway (gaseous vs. in-cloud), and type of emissions (anthropogenic vs. biogenic) is used to differentiate the balance of processes controlling the production and loading from this material. Significant differences exist in the destiny of SO₂ molecules emitted from the several regions. An SO₂ molecule emitted from the ROW source region has a much greater potential to form sulfate than one emitted from, for example, Europe. A greater fraction of the SO₂ molecules are oxidized that originate from ROW compared with other areas, and once formed, the sulfate has a longer residence time (that is, it is not readily scavenged). The yield of sulfate from ROW sources of SO₂ is a factor of four higher than that of Europe. A substantially higher fraction of the SO₂ emitted over Europe is oxidized to sulfate through the ozone pathway compared to other regions. The analysis suggests that there are significant differences in the vertical distribution, and horizontal extent, of the propagation of

sulfate emitted from the several source regions. Sulfate from Asian source regions reaches the farthest from its point of origin, and makes a significant contribution to burdens in both hemispheres, primarily from plumes reaching out in the upper troposphere. Sulfate from other source regions tend to remain trapped in their hemisphere of origin.

References

- Barth, M. C., Rasch, P. J., Kiehl, J. T., Benkovitz, C. M., Schwartz, S. E. Sulfur chemistry in the NCAR CCM: Description, evaluation, features and sensitivity to aqueous chemistry. *J. Geophys. Res.*, *105*, D1, 1387-1415, 2000.
- Mahowald NM, Rasch PJ, Eaton BE, et al. Transport of (²²²) radon to the remote troposphere using the model of atmospheric transport and chemistry and assimilated winds from ECMWF and the National Centers for Environmental Prediction, *J. Geophys. Res.*, *102*, D23, 28139-28151, 1997
- Müller, J.F and G. Brasseur, IMAGES: A three-dimensional chemical transport model of the global troposphere, *J. Geophys. Res.*, *100*, 16445-16490, 1995.
- Rasch, P. J., Barth, M. C., Kiehl, J. T., Schwartz, S. E., Benkovitz, C. M. A description of the global sulfur cycle and its controlling processes in the National Center for Atmospheric Research Community Climate Model, Version 3, *J. Geophys. Res.*, *105*, D1, 1367-1385, 2000.

THE DANISH EULERIAN HEMISPHERIC MODEL

Jesper Christensen

*National Environmental Research Institute
Frederiksborgvej 399, 4000 Roskilde, Denmark*

INTRODUCTION

Three dimensional Eulerian hemispheric air pollution model is in process of development at the National Environmental Research Institute (NERI). The model has been used to study long-range transport of pollution on the Northern Hemisphere. The present version of the model includes the long-range transport of sulphur di-oxide (SO_2) and particulate sulphate (SO_4^{2-}). The chemistry in the model is described by a simple linear oxidation of SO_2 to SO_4^{2-} , and the wet deposition of SO_2 and SO_4^{2-} is estimated by using the amount of precipitation, which is calculated from the contents of liquid cloud water.

The model has been used to study the air pollution in the Arctic for a period of 6½ years from October 1990 to May 1997. A detailed description of the model and results from the model is given in Christensen (1995) and (1997).

DESCRIPTION OF THE MODEL

The model is based on set of coupled full three dimensional advection-diffusion equations. In the present version there are four species: SO_2 , SO_4^{2-} , humidity and cloud water. The equations are coupled through chemistry, condensation and evaporation of cloud water, and the release of precipitation.

The horizontal space of the model is defined on a regular 96x96 grid that covers most of the Northern Hemisphere with a grid-distant of 150 km at 60°N, and the vertical space is defined on an irregular grid with 12 grid-points up to » 7km. Meteorological parameters are from the European Centre for Medium-range Weather Forecasts (ECMWF) on a 2.5°x2.5° grid with a time resolution of 6 and 12 hour.

The vertical diffusion is parameterized by using a K_z profile based on the Monin - Obukhov similarity theory coupled to either observations or computationally generated data for the surface layer, and this K_z profile for the surface layer is extended to the whole boundary layer by using a simple extrapolation (see Christensen, 1995, 1997).

The height of the boundary layer in the model is calculated by a simple parameterization. This parameterization is based on a simplified energy balance equation for the internal boundary-layer, where the change of the advected height of the boundary layer depends on the mechanically and convectively generated energy and the dissipation of the energy (see Christensen, 1995, 1997).

Two parts of the condensation scheme described in Sundqvist et al. (1989), the stratiform precipitation and a simple parameterization of convective precipitation, are included in the hemispheric model to give a crude estimate of the precipitation (see Christensen, 1995, 1997).

In the basic version the emissions of anthropogenic sulphur are based on the global GEIA inventory of sulphur emissions, version 1A.1, for 1985 on a 1°x1° grid (see Benkowitz et al., 1996) . These emissions are redistributed to the grid used in the model. The EMEP emissions (for Europe) for 1990 are used for

the part of grid, which is equal the EMEP grid. Natural emissions of dimethyl sulphide (DMS) from the open oceans and shelf waters are also included in the model, and they depend on the concentrations of DMS in the oceans and the wind speed in 10m (see Christensen, 1995, 1997). In the COSAM version of the model GEIA inventory of sulphur emissions, version 1B for 1985, gridded monthly DMS emission on $1^\circ \times 1^\circ$ grid from Kettle, and the volcanic emissions on $3.75^\circ \times 3.75^\circ$ grid by U. Lohmann, where all emissions are redistributed to the grid used in the model.

The chemistry is simple linear, where the oxidation rate of SO_2 to SO_4^{2-} depends on the latitude and the time in the year. This spatial and temporal variation of the oxidation rate simulates the variations of OH in the gas phase and H_2O_2 and O_3 in the liquid phase, which all are depending on the solar radiation. The maximal oxidation rate is about $5.6 \cdot 10^{-6} \text{ s}^{-1}$, and the minimal rate is $0.3 \cdot 10^{-6} \text{ s}^{-1}$ in the Arctic night.

The dry deposition velocity of SO_2 is based on the resistance method as e.g. given in Voldner et al. (1986). For snow or ice covered surface there is added an extra surface resistance, which ensures that the deposition is very low, if the surface temperature is below -2°C (Wesely, 1989).

The dry deposition velocity for SO_4^{2-} over land is given in Walcek et al., 1986. The dry deposition for SO_4^{2-} over open water is based on the work by Slinn and Slinn (1980).

The wet deposition is parameterized by using a simple scavenging ratio formulation with different in-cloud and below-cloud scavenging ratios (see Tarrasón and Iversen, 1992; Christensen, 1995, 1997).

NUMERICAL RESULTS

The basic version of the model has been run from October 1990 to May 1997. In figure 1 the annual mean concentrations of SO_2 and SO_4^{2-} for the surface level are shown. The COSAM version have been run for the period from December 1992 to December 1995.

The calculated concentrations of SO_2 and SO_4^{2-} have been compared with the European measurements of EMEP. These comparisons show that there is as good agreement between the calculated and measured concentrations, both on seasonally, monthly and even daily basis for many EMEP stations. (see Christensen, 1995, 1997); for the wet depositions and precipitation the agreement is not so good as for the air concentrations, mainly because it is very difficult to calculate the right amount of precipitation at the right time.

For the Arctic areas the model has been compared with measurements from three sites: Station Nord in north-eastern Greenland ($81^\circ 36' \text{ N}$, $16^\circ 40' \text{ W}$) for the whole period, Ny-Ålesund at Spitzbergen ($78^\circ 54' \text{ N}$, $11^\circ 53' \text{ E}$) from October 1990 to December 1993, and Alert in Northwest Territories, Canada, ($82^\circ 50' \text{ N}$, $62^\circ 30' \text{ W}$) for the period from October 1990 to June 1993 and only of SO_4^{2-} . For all three stations there is a rather good agreement between the calculated and observed concentrations of SO_2 and especially for SO_4^{2-} , see Christensen (1997).

PLANS FOR THE FUTURE

Ongoing plans about improvement of the parameterization of physical processes will continue in the future. This will be done by using mesoscale model MM5 as a preprocessor for the meteorological data. Preliminary tests for the period from October 1990 to May 1991 have shown that the performance of DEHM will be improved by using MM5.

It is also planned to get the new re-analysis from ECMWF for the period from 1979 to 1993, and use this data set to study the interannual variability of the large scale air pollution transport in the Northern Hemisphere, especially to the Arctic, e.g. the North-Atlantic oscillations importance for this transport.

It is also planned to extend the model for other species to improve the chemistry, both the gas-phase and the aqueous-phase, where one important issue is the coupling between Ozone and elemental Mercury in the Arctic during the polar sunrise.

The model development is a contribution to the Danish part of the International Arctic Monitoring and Assessment Programme, AMAP.

REFERENCES

- Benkowitz, C. M., T. Scholtz, J. Pacyna, L. Tarrasón, J. Dignon, E. Voldner, P. A. Spiro and T. E. Graedel (1996): Global Gridded Inventories of Anthropogenic Emissions of Sulphur and Nitrogen. *J. Geophys. Res.*, **101**, 29239-29253.
- Christensen, J. (1995): Transport of Air Pollution in the Troposphere to the Arctic. PhD thesis. National Environmental Research Institute, DK-4000 Roskilde, Denmark, 377 pp.
- Christensen, J. (1997): The Danish Eulerian Hemispheric Model - Three Dimensional Air Pollution Model Used for the Arctic. *Atm. Env.*, **31**, 4169-4191.
- Slinn, A. A. and W. G. N. Slinn (1980): Predictions for Particle Deposition on Natural Waters. *Atm. Env.*, **14**, 1013-1016.
- Sundqvist, H., E. Berge and J. E. Kristjansson (1989): Condensation and Cloud Parametrization Studies with a Mesoscale Numerical Weather Prediction Model. *Mon. Wea. Rev.*, **117**, 1641-1657.
- Tarrasón, L. and T. Iversen (1992): The Influence of North American Anthropogenic Sulphur Emissions over Western Europe. *Tellus*, **44B**, 114-132.
- Voldner, E. C., L. A. Barrie and A. Sirois (1986): A Literature Review of Dry Deposition of Oxides of Sulphur and Nitrogen with Emphasis on Long-Range Transport Modelling in North America. *Atm. Env.*, **20**, 2101-2123.
- Walcek, C. J., R. A. Brost, J. S. Chang and M. L. Wesely (1986): SO₂, Sulfate and HNO₃ Deposition Velocities Computed using regional Landuse and Meteorological Data. *Atmos. Env.*, **20**, 949-964.
- Wesely, M. L. (1989): Parameterization of Surface Resistances to Gaseous Dry Deposition in Regional-Scale Numerical Models. *Atm. Env.*, **23**, 1293-1304.

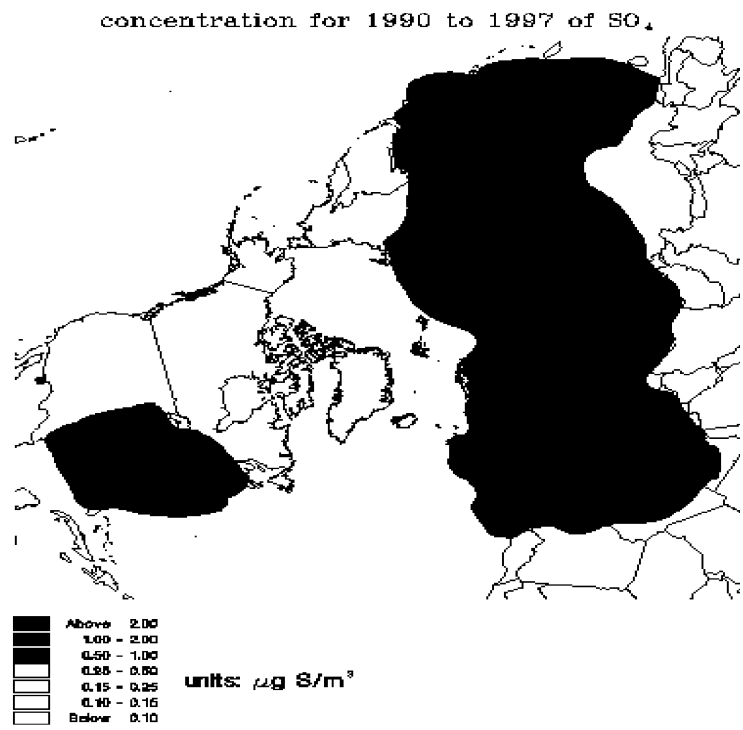
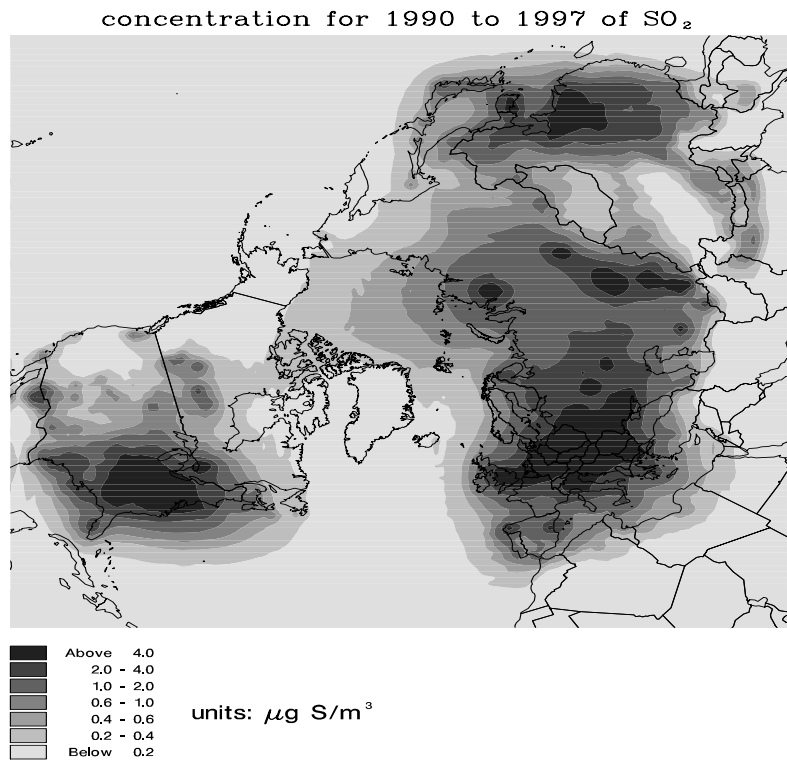


Figure 1. The mean distribution from October 1990 to May 1997 of SO₂ (top) and SO₄²⁻ (bottom) for the surface level

FIELD OBSERVATIONS USED IN THE COSAM PROJECT

F. McGovern¹ and J. Wilson²

1. Department of Experimental Physics, University College Dublin, Ireland

2. Environment Institute, EC Joint Research Centre, Ispra (VA), Italy

1 Introduction

An import part of the COSAM project is to assess the ability of the participating models to predict sulfate levels at global sites. Five geographical regions were selected for this task. These were:

- (i) On the edge of major source regions, i.e., Europe North America
- (ii) Along a North Atlantic latitudinal transect
- (iii) Along a transect from China into the Pacific Ocean
- (iv) At southern hemispheric sites
- (v) High Altitude free troposphere (FT) sites

The modelling period would be from 1993 to 1995, with the model results being compared with seasonal average values. Field observations of sulfate and related aerosol and trace gases from measurement sites in these regions were collated. Here we give details on the selected sites and summarise sulfate data collected at these sites.

2 Data Sources

In order to utilise consistent data, where similar collection, handling and analysis techniques were used; data from large-scale networks were preferred. However, the nature of scientific research means that a number of sites are operated on a single site basis. The following large-scale networks and single site operations agreed to supply data for the project

Networks

Air Ocean Chemistry Experiment (AEROCE), University of Miami (UM).

Canadian Air and Precipitation Monitoring Network (CAPMON), Canadian national networks.

US Department of the Energy network, (DOE), University of Miami.

Co-operative Programme for Monitoring and Evaluation of the Long-Range Transport of Air Pollutants in Europe (EMEP), Norwegian Institute for Air Research (NILU).

Interagency Monitoring of Protected Visual Environments (IMPROVE) USA,

Single Sites

Mauna Loa Observatory, University of Hawaii (UH), USA.

Summit, Greenland, Universite Joseph Fourier (UJF), Grenoble France

Alert, Atmospheric Environment Service (AES) Canada

Nord, Greenland, Danmarks Miljundersogelsers (DMU)

Data for the IMPROVE and CAPMON networks were obtained via the Canadian, National Atmospheric Chemistry Database (NAtChem) group (<http://airquality.tor.ee.gc.ca/natchem/particles/>)

3 COSAM Sites

A list of sites for which sulfate data were potentially available was established from these networks and single site. From this list the COSAM sites were selected which fulfilled the modelling criteria established at the Duke University planning meeting and also based on data availability and data quality. Workload was also a consideration two COSAM site lists were compiled, a full list and a short list. The full list is listed here in which the short list sites are highlighted by an *. The sites are categorised under the under the group heading outlined in Section 2.

The site ID used is consistent with that used by the original site-operating group. No COSAM site ID format has been designed for this part of the project. While sites are placed into the COSAM groups there are geographical links between sites in separate groups particularly between Group I and Group II and between Group III and Group IV sites.

(I) Boundary of Source Regions

Site	Country	ID	Lat.	Long	Alt. (m)	MSA	SO ₂	Group
Jergul*	Norway	N030	69.4	24.6	255		x	EMEP
Skreaadalen*	Norway	N08	58.82	6.72	475		x	EMEP
Bredkaelen	Sweden	SE5	63.85	15.33	404		x	EMEP
Eskdalemuir	UK	GB2	55.32	-3.2	243		x	EMEP
La Crouzille	France	FR3	45.83	1.27	497		x	EMEP
La Cartuga	Spain	ES2	37.2	-3.6	720		x	EMEP
Denali NP *	USA	DEN	63.72	-148.97	658		x	IMPROVE
Ester	Canada	EST	51.67	-110.2	707		x	CAPMON
Exp Lakes	Canada	ELA	49.65	-93.72	369		x	CAPMON
Algoma*	Canada	ALG	47.03	-84.37	411		x	CAPMON
Chapais	Canada	CPS	49.82	-74.97	381		x	CAPMON
Brigantine	USA	BRG	39.45	-74.43	5			IMPROVE
Okefenokee	USA	OKE	30.73	-82.12	38		x	IMPROVE
Pinnacles	USA	PIN	36.48	-121.15	317		x	IMPROVE
Redwood	USA	RED	41.55	-124.07	232		x	IMPROVE
Saturna	Canada	SAT	48.78	-123.13	178		x	CAPMON

(II) North Atlantic Latitudinal Transect

Site	Country	ID	Lat.	Long	Alt.(m)	MSA	SO ₂	Group
Alert	Canada	Alert	82.47	-62.5	210	x		AES
Nord*	Greenland	Nord	81.43	-17.5	???		x	DRC
Spitzbergen*	Norway	N042	78.9	11.88	474		x	EMEP
Heimaey*	Iceland	HEI	63.25	-20.15	100	x		U.Miami
Mace Head*	Ireland	IE3	53.33	-9.9	20	x		U.Miami
Kejimkujik*	Canada	KEJ	44.43	-65.2	127		x	U.Miami
Bermuda*	UK	BER	32.32	-65.27	30	x		U.Miami
Barbados*	UK	BAR	13.17	-59.43	3	x		U.Miami

(III) Transect from China into the Pacific Ocean

Site	Country	ID	Lat.	Long	Alt(m)	MSA	SO ₂	Group
Cheju*	Korea	CHE	33.52	126.48	20	x		U.Miami
Okinawa*	Japan	OKI	26.92	128.25	23	x		U.Miami
Norfolk*	Australia	NOR	-29.08	167.98	20	x		U.Miami
Midway*	USA	MID	28.22	-177.35	15	x		U.Miami
A. Samoa*	USA	SAM	-14.25	-170.58	25	x		U.Miami
Hawaii*	USA	OAH	21.33	-157.7	17	x		U.Miami

(IV) Southern Hemisphere Sites

Site	Country	ID	Lat.	Long	Alt.(m)	MSA	SO ₂	Group
Cape Grim*	Australia	CGR	-40.68	144.68	94			U.Miami
Chatham Is.*	New Zealand	CHA	-43.92	-176.5	20			U.Miami
Invercargill	New Zealand	INV	-46.43	168.35	30			U.Miami
Reunioon*	France	REU	-21.17	55.83	60	x		U.Miami
Cape Town*	S.Africa	CPT	-33.8	18.47	50			U.Miami
Palmer Station*	Antarctica	PAL	-64.92	-64.05	20	x		U.Miami
Mawson*	Antarctica	MAS	-67.6	62.5	20	x		U.Miami
Mt.Pleasant	UK	MTP	-51.75	-60.0	100	x		U.Miami

(V) Elevated Sites

Site	Country	ID	Lat.	Long	Alt(m)	MSA	SO ₂	Group
Izana*	Spain	IZO	28.3	-16.48	2367			U.Miami
Jungfrauoch*	Switzerland	CH1	46.55	7.98	3573		x	EMEP
Mauna Loa*	USA	MLO	19.53	-155.58	3397			U.Hawaii
Summit*	Greenland	SMT	73.3	-38.8	3190			C.Mellon U

* COSAM short list sites

4 Summary of COSAM Sulfate Data

A summary of sulfate data used in the COSAM project is presented here. This consists of a basic statistical analysis of the original data charts of monthly and seasonal average time series of the data. The data are presented in units of $\mu\text{g m}^{-3}$ as this was most commonly used concentration unit. The data are presented as non sea-salt sulfate (nssSO₄) or sulfate (SO₄) depending on whether the correction for sea salt sulfate was carried out or not. This correction is not considered necessary at sites, which are not greatly impacted by sea-salt aerosols, e.g., free troposphere sites. The correction was not possible for EMEP sites, as the chemical analysis does not measure the sea salt aerosol components. The data are presented in the site list order.

A scatter plot of the mean sulfate levels plotted against site latitude shows that sulfate levels at Southern Hemisphere (SH) sites were significantly lower than those measured at Northern Hemisphere (NH) sites. The average SH levels were less than $0.6 \mu\text{g m}^{-3}$. The NH levels were typically higher than this value generally ranging from $1\text{--}4 \mu\text{g m}^{-3}$. The highest average sulfate concentrations were measured at the Cheju site. It is expected that NH sulfate levels would be higher than SH levels as most of the global population lives in the NH and most industrial activities take place there.

5 Conclusion

This project brings together aerosol data from global sites. However, the issue of data compatibility has not been considered, although some problems have been noted. There is a requirement for cross comparison of sample handling and analysis methodologies between these networks and sites so that greater confidence can be had in the validity of using such combined data sets. It has been noted that the EMEP sulfate data could not be corrected for the sea-salt contribution at coastal or near coastal sites. It is recommended that aerosol sodium or other seasalt chemical species should be measured at sites, which are likely to be impacted by sea-salt aerosols.

There are strengths and weakness in all of the networks. Some of which have been mentioned here. It is at best unfortunate that many of the UM, Doe sites are no longer operational. This is due to lack of funding. Many of these sites were in the Southern Hemisphere where such data are rare. Such long-term aerosol chemical measurements are essential to develop our understanding of natural and anthropogenic influences on the global atmosphere. Outside of Antarctica the Southern Hemisphere is particularly lacking in such measurements. Other important areas have sparse coverage including the equatorial region and the developing Pacific regions. There are also few FT sites and none were found in the Southern Hemisphere. Remedial steps are required to deal with this.

The data collected for this project will be invaluable in validation of COSAM model outputs and will no doubt be of benefit to further studies of the aerosol impact on global climate. The substantial effort required to carry out these measurements, sometimes in very difficult

conditions requires recognition. Considerable credit is due to all involved in carrying out the measurements and analysis, which provide these results.

ACKNOWLEDGEMENTS

The successful completion of this part of the COSAM project has been possible due to the contribution of many groups and individual. These include Anne Hjellbrekke and J Schaug for access to the EMEP data. J. Prospero, D. Savoie H. Maring of the University of Miami for access to the AEROCE and US DOE site data. B. Vet and colleagues of NatChem who provided the Capmon and Improve data sets, Davis University, National Park Service and US Department of Interior for providing the original Improve data and the Canadian AES for access to the CapMon data. B. Hubert University of Hawaii for the Mauna Loa data. L. Barrie for access to the Alert data. Jean Luc Jaffrezo for the Summit data and N. Heidam for the Nord data, J. Wilson of the EI JRC for discussion and consultation. The WMO for provision of travel fund necessary for completion of this project. The EI JRC Ispra who provided the main funds for this project under contact NO. 13642-98-02 F1 EDISP IE.

Sulfate and MSA at Mauna Loa Observatory: How Well can Observations at a Point Represent a Model Grid Box?

Barry Huebert
University of Hawaii

Observations are made at a point in space, while models compute an average concentration for a grid cell that is hundreds of km on a side and hundreds of meters in depth. Because of this fundamental difference, a (hypothetical) perfectly realistic model might still not agree with observations within its domain. At least three factors can cause such disagreements.

The first is that the measurements may be biased in some way. A prominent example of this is the well-established losses in airborne aerosol intakes that use conical diffusers and inlet tubes [Huebert *et al.*, 1990][Sheridan and Norton, 1998]. Because of such losses, much of the published aerosol data at high altitudes is actually an under-estimate of ambient concentrations. For supermicron aerosols the reported airborne concentrations may be only 5 to 20% of ambient, while for accumulation mode particles the inlets may pass between 30 and 80% of ambient particles to a filter or impactor for collection and later analysis. According to two different intercomparisons, this tendency to underestimate ambient concentrations is particularly acute with NASA-GTE data collected from the DC-8, probably due to its high airspeed. Surface samplers also have cutoff sizes that need to be considered if the species of interest is contained in large particles.

The second consideration is that there may be significant vertical gradients within a model box, so that the surface measurements may not represent the box well. One obvious example of this is surface samplers that in winter are virtually always beneath a strong, low-level inversion. It is not surprising that winter SO₂ measurements in North America and Europe are usually much smaller than model estimates, since power plant stacks are by design releasing SO₂ well above the inversion. Thus the models will have high SO₂ concentrations in their lowest layers, but the measurements will not show it unless the bottom of the real atmosphere is mixed from the surface to the height of the lowest model grid cell. Even in the free troposphere, strong layering is observed that does not appear in model output.

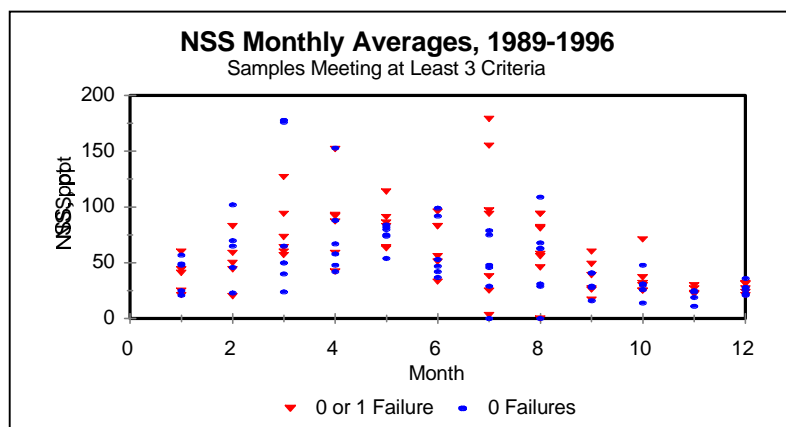
Horizontal heterogeneity within a grid square can also prevent agreement with measurements. One good example of this is Mace Head, where the grid square will contain numerous sulfur sources, although the data is dominated by clean marine air. Obviously there are large concentration gradients within this grid square, and no single measurement could be expected to represent the average. A similar situation exists at Mauna Loa, which has the active Kilauea volcano in its square. Even though the observations can be sorted to eliminate the local volcanic influence, the volcanic source will appear in model output; only the downwind side of the real atmosphere's grid square will experience those elevated concentrations. This heterogeneity is likely to cause a mismatch between models and measurements in any grid square with strong local sources.

In many ways, though, MLO data is ideal for model testing, because it is in the free troposphere (where very little time-series data exists) and it is more than 3500 km from the nearest continental sources. On nightly Teflon filter samples (exposed from 8 PM to 8 AM local time) we have analyzed NSS since 1989 and MSA since 1995. Our record includes some gaps (including the first half of 1993) that are due to instrumental failure or unresolvable questions about calibrations.

However, the sampling site is located on an active volcano, so this local influence must be removed to leave data that fairly represents the state of the free troposphere. Since the magnitude of the volcanic influence on our measured concentrations is obviously a strong function of our proximity to the source, we cannot consider our contaminated data to represent the average of the entire grid cell with volcanic its influence. To cull out a data set representative of the clean free troposphere, we used four criteria to sort out locally-influenced samples from our nightly (12 hour) filter samples. These criteria are :

Wind direction	90 to 279 degrees	(downslope)
Dew point	<-5 C	(excludes MBL air)
Condensation nuclei	<500/cc	(excludes nearby combustion and volcanoes)
Sigma CO ₂	<0.30 ppm	(excludes Mauna Loa vents above MLO)

We created two sets of sorted data: one in which every criterion was met during every hour of each 12 hour sample, and another in which a failure of any one criterion was allowed. Figure 1 shows the variability from one year to the next in the monthly averages of NSS at MLO. Some of the extreme values result from months in which only a few points remained after sorting.



The samples that met three or four criteria were averaged in two ways. In the first, the monthly values from Figure 1 were averaged (excluding any months with only 1 or 2 samples), thus weighting the average by month in each year. The second method applied no weighting, and simply averaged all the January samples in every year together, etc. The results of this averaging (Figure 2) show that all four methods agree quite well except in the month of July. Here the monthly average is a strong function of whether samples failing one criterion are included or not.

If a single failure is allowed, there appears to be a peak in July of 80 to 90 ppt, but if no failures are allowed the average is 50 to 60 ppt. All the averaging methods produce a springtime maximum in MAM of about 80 ppt and a late fall minimum of 20 to 30 ppt. It is possible that the 80 to 90 ppt peak is real, that is, it may not be local influences. If there were instances of long range transport of continental (from North American, Lee et al., 1994) aerosols in the late summer, a high CN count could cause us to mistake them for locally-influenced samples. We

thus leave the July peak as something that may or may not be representative of the FT upwind of MLO.

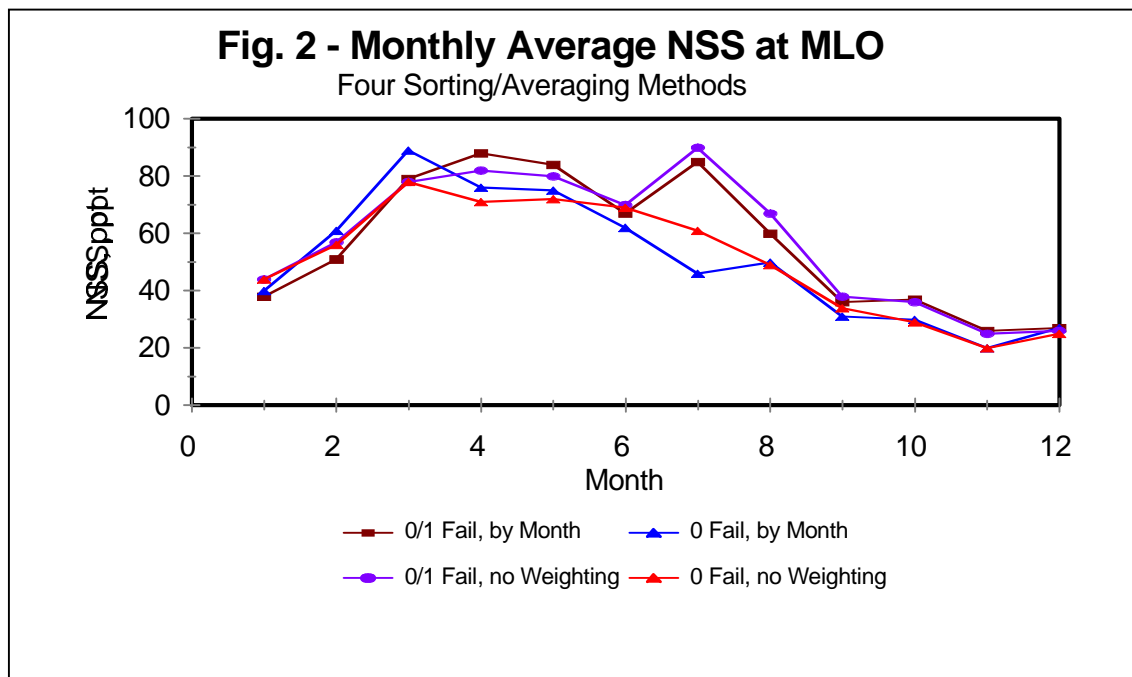
We have also measured MSA at MLO for several years now. The gross average, with no sorting, is about 0.7 ppt MSA. There does not appear to be a seasonal variation in MSA at MLO.

References

Huebert, B.J., G. Lee, and W. Warren, Airborne Aerosol Inlet Passing Efficiency Measurement, *J. Geophys. Res.*, 95 (D10), 16369-16381, 1990.

Lee, G., J.T. Merrill, and B.J. Huebert, Variation of free tropospheric total nitrate at Mauna Loa Observatory, Hawaii, *Journal of Geophysical Research*, 99, D6 (12821-12831), 1994.

Sheridan, P.J., and R.B. Norton, Determination of the passing efficiency for aerosol chemical species through a typical aircraft-mounted diffuser-type aerosol inlet system, *J. Geophys. Res.*, 103, 8215-8226, 1998.



Vertical S Profiles From Aircraft Used in COSAM

W. Richard Leitch
Cloud Physics Research Division
Atmospheric Environment Service
4905 Dufferin Street
Downsview, Ontario M3H 5T4, Canada

1 North Atlantic Regional Experiment (NARE)

One set of observational data is taken from the 1993 NARE intensive. The data were collected from the National Research Council of Canada (NRCC) DHC-6 Twin Otter aircraft from August 9 to September 8, 1993. Profiles were made between points about 50 km south of Yarmouth, Nova Scotia (about 43.3°N, 66°W) and inland over Kejimikujik National Park, Nova Scotia (about 44.3°N, 65.5°W). The flights were conducted at least 6 days a week and the air back trajectories indicate the air arrived at the region from a variety of areas (e.g. Merrill and Moody, 1996).

Details of the instrumentation and observations, as well as other analyses of the NARE data, are described in a number of papers in a section of the Journal of Geophysical Research (e.g. Fehsenfeld et al., 1996). A few aspects of the instrumentation are repeated here in brief.

All trace gas measurements were recorded at 1 s intervals. Sulfur dioxide (SO₂) was measured with a TECO 43S pulsed fluorescence monitor. The detection limit for SO₂ for a 1 s measurement is 0.2 ppbv and the uncertainty is $\pm(0.1 \text{ ppbv} + 30\% \text{ of measurement})$. Ozone was measured with a TECO 49 UV absorption analyzer. The uncertainty is $\pm(5 \text{ ppbv} + 10\% \text{ of measurement})$. H₂O₂ was measured using the Kok method and Fenton reagent chemistry. The detection limit is about 0.1 ppbv and the uncertainty is about 5%. For more details concerning these measurements, please refer to Banic et al. (1996) and Weinstein-Lloyd et al. (1996).

Mass concentrations of sulphate were measured using ion chromatography on aerosol samples collected on Teflon filters. Continuous measurements of the mass concentration of sulfate are not available directly from the measurements. Banic et al. (1996) showed that the mass concentrations of particulate sulfate (pSO₄⁻), measured from the exposed filter samples, exhibited a high linear correlation with the number concentrations of particles in the 7th channel of the Particle Measuring Systems PCASP-100X that was mounted under a wing of the aircraft. Channel 7 of this PCASP corresponds to particles of about $0.38 \mu\text{m} \pm 0.05 \mu\text{m}$ diameter. A fourth order polynomial fit constrained through the origin was fit to the data. This level of detail in the fit, shown in Figure 3.1, was used to ensure an adequate representation of the data at lower concentrations. The polynomial fit of Figure 1 was used to derive 1 s values of pSO₄⁻ mass concentration.

The effect of cloud was removed from the dataset by excluding data when the corresponding number concentration of particles measured with the FSSP-100 (2-35 μm) was

greater than 5 cm^{-3} . It is implicitly assumed that such concentrations do not occur outside of cloud. This is valid for the area of study except in extreme circumstances.

The profile data for O_3 , H_2O_2 , SO_2 and pSO_4^- for 31 profiles to approximately 3 km over 23 days and 15 profiles to 5 km over 14 days are shown in Figure 2. For each 5 km profile there are approximately 1500 data points. The average profile in each plot was derived by ordering all the 1 s data from the profiles by altitude and then taking the average of all points within selected altitude intervals. The intervals were taken from the pressure intervals used in the Canadian Regional Climate Model.

The impact of setting the below detection limit values for SO_2 to zero before computing averages, as opposed to using the indicated values, is small. The total column SO_2 for the 5-km profiles computed by leaving the BDL values as measured is <1% higher than that derived from setting the BDL values to zero.

Both the 3-km and 5-km profiles are used in the model comparisons. It is assumed that the combination of the 3-km and 5-km profiles, which cover all most of the measurement days, represent the average characteristics of the entire period, as has been discussed by Banic et al. (1996).

2 Second Eulerian Model Evaluation Field Study (EMEFS II)

A second set of observational data is taken from the Canadian component of the EMEFS II. The study was conducted from March 20 to April 29, 1990 using the NRCC DHC-6 Twin Otter aircraft. The aircraft was based out of North Bay, Ontario and profiles were made over two ground-based observation sites at Egbert, Ontario (44.2°N , 79.8°W) and Lake Traverse, Ontario (45.9°N , 78.1°W).

Details of the study and instrumentation can be found from Isaac et al. (1998). As above for the NARE study, a few aspects of the instrumentation are briefly repeated.

All trace gas measurements were recorded at 1 s intervals. Sulfur dioxide was measured with a TECO 43S pulsed fluorescence monitor. The detection limit for SO_2 for a 1 s measurement was 0.3 ppbv and the uncertainty is $\pm(0.1 \text{ ppbv} + 30\% \text{ of measurement})$. Ozone was measured with a modified Unisearch LMA-3 using EOSIN-Y. The detection limit was 3 ppbv and the uncertainty is estimated at $\pm(2 \text{ ppbv} + 30\% \text{ of measurement})$. H_2O_2 was measured using the Kok fluorometric technique with peroxidase. The detection limit is 0.1 ppbv and the uncertainty is estimated at $\pm 20\%$.

Again, because continuous measurements of the mass concentration of sulfate were not available directly from the measurements, high-resolution sulphate concentrations were derived using the PCASP number concentrations as a surrogate. A good relationship between the mass concentrations of sulphate, measured using ion chromatography on aerosol samples collected on Teflon filters, and channel 6 of the PCASP was found for flights during the period April 8-April

15, 1990 inclusive. The constrained time period is due to problems with the PCASP operation. The data and fitted curve are also shown in Figure 1.

As with the NARE data, the effect of cloud was removed from the dataset by excluding data when the corresponding number concentration of particles measured with the FSSP-100 (2-35 μm) was greater than 5 cm^{-3} .

The O_3 , H_2O_2 and SO_2 data are taken from 34 profiles over Egbert and 30 profiles over Lake Traverse on 24 days. Because of the above-mentioned PCASP problems, the pSO_4^- data are from 14 profiles over Egbert and 10 profiles over Lake Traverse on 7 days. Compilations of the profiles for each constituent are shown in Figure 3 for Egbert and Lake Traverse. The data were processed as for NARE, with the exception that instead of being separated by upper profile altitude, they are separated by location. This was done because there is about 230 km separating Egbert and Lake Traverse. For air traffic reasons, about 80% of the profiles over Egbert were restricted to about 3 km, whereas 90% of the profiles made over Lake Traverse profiles were to 5 km or higher. The average profiles for both the Egbert and Lake Traverse measurements are used in the comparisons.

Acknowledgements: We are grateful to Ms. Nicole Shantz of AES for processing the NARE and EMEFS II profile data.

REFERENCES

Banic, C.M., W.R. Leitch, G.A. Isaac, M.D. Couture, L.I. Kleinman, S.R. Springston and J.I. MacPherson, Transport of ozone and sulfur to the North Atlantic atmosphere during NARE, *J. Geophys. Res.*, 101, 29091-29104, 1996.

Isaac, G.A., C.M. Banic, W.R. Leitch, K.G. Anlauf, M.D. Couture, P.S.K. Liu, A.M. Macdonald, K.I.A. MacQuarrie, K.J. Puckett, and H.A. Wiebe, Vertical profiles and horizontal transport of atmospheric aerosols and trace gases over central Ontario, *J. Geophys. Res.*, 103, 22015-22037, 1998.

Fehsenfeld, F.C., P. Daum, W.R. Leitch, M. Trainer, D.D. Parrish, and G. Huebler, Transport and processing of O_3 and O_3 precursors over the North Atlantic: An overview of the 1993 North Atlantic Regional Experiment (NARE) summer intensive, *J. Geophys. Res.*, 28877-28891, 1996.

Merrill, J.T. and J.L. Moody, Synoptic meteorology and transport during the North Atlantic Regional Experiment (NARE) intensive, *J. Geophys. Res.*, 101, 28903-28921, 1996.

Weinstein-Lloyd, J.B., P.H. Daum, L.J. Nunnermacker, J.H. Lee, and L.I. Kleinman, Measurement of peroxides and related species in the 1993 North Atlantic Regional Experiment, *J. Geophys. Res.*, 101, 29081-29090, 1996.

Sulphate - PCASP

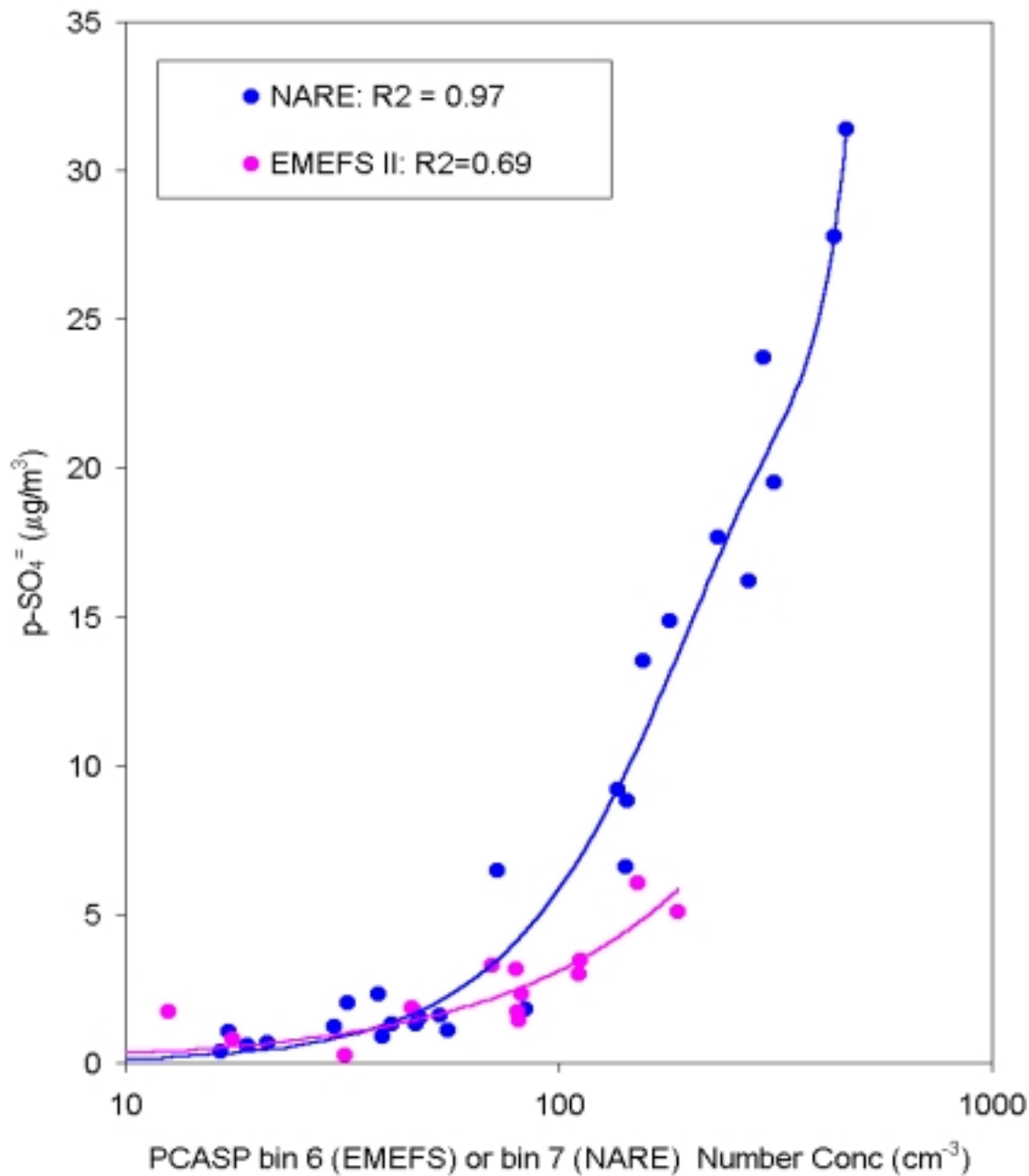


Figure 1. Plots of the measurements of particulate sulphate mass ($p\text{-SO}_4^-$) with the number concentrations of particles from channel 7 of the PCASP for NARE and with channel 6 of the PCASP for EMEFS. The number concentration data were collected at 1 s intervals and have been averaged to correspond with the filter sampling times. NARE data are for the whole study. The EMEFS data are for the period April 8-April 15, 1990 inclusive. The best polynomial fits to each dataset are also shown.

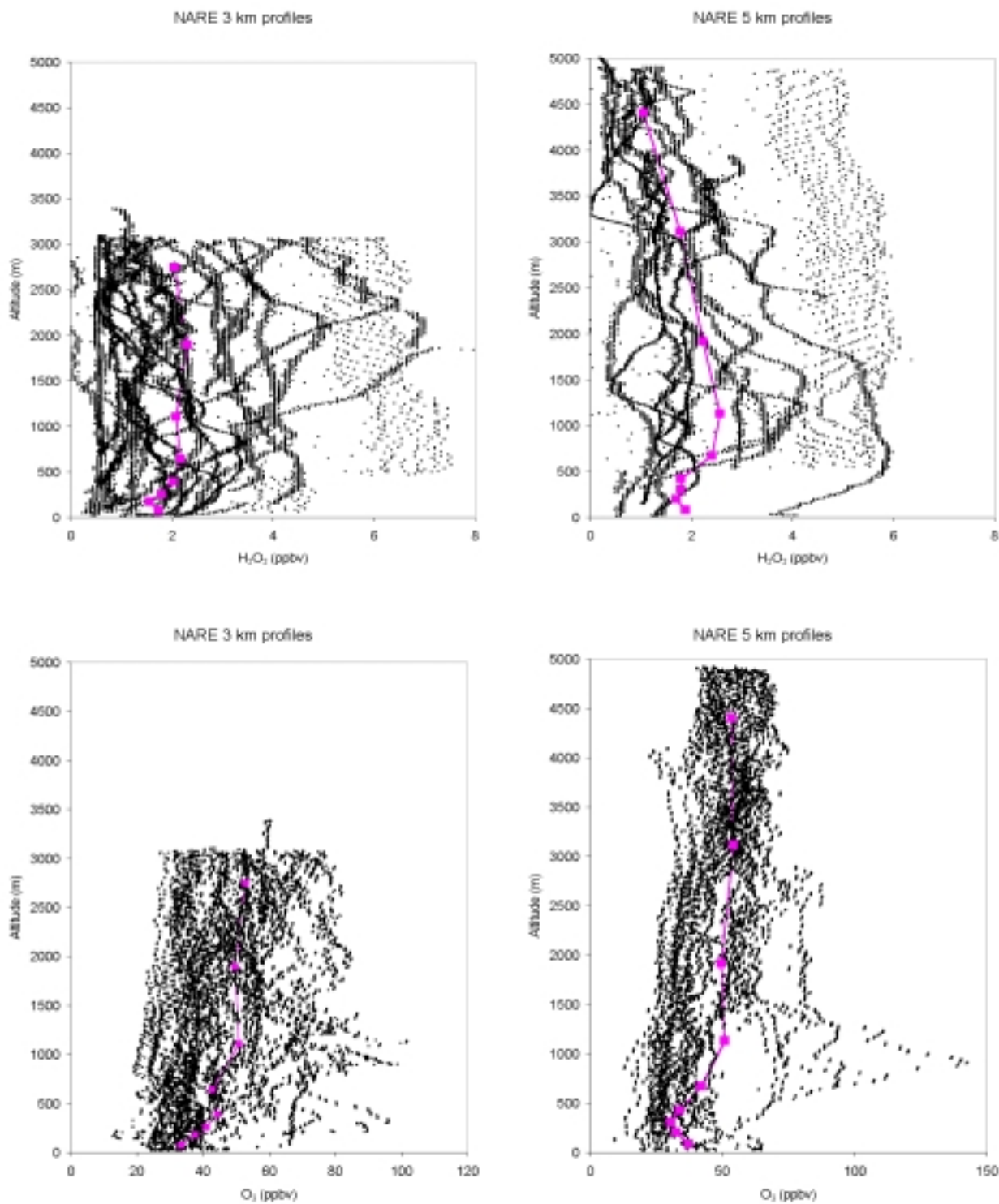


Figure 2. Profiles of H₂O₂, O₃, SO₂ and p-SO₄⁻ for the NARE study. The 3 km plots are made up of 31 profiles over 23 days. The 5 km data consist of 15 profiles over 14 days. The average profile in each plot was obtained by first ordering all the 1 s data from the profiles by altitude and then taking the average of all points within selected pressure intervals corresponding to those used in the Canadian Regional Climate Model.

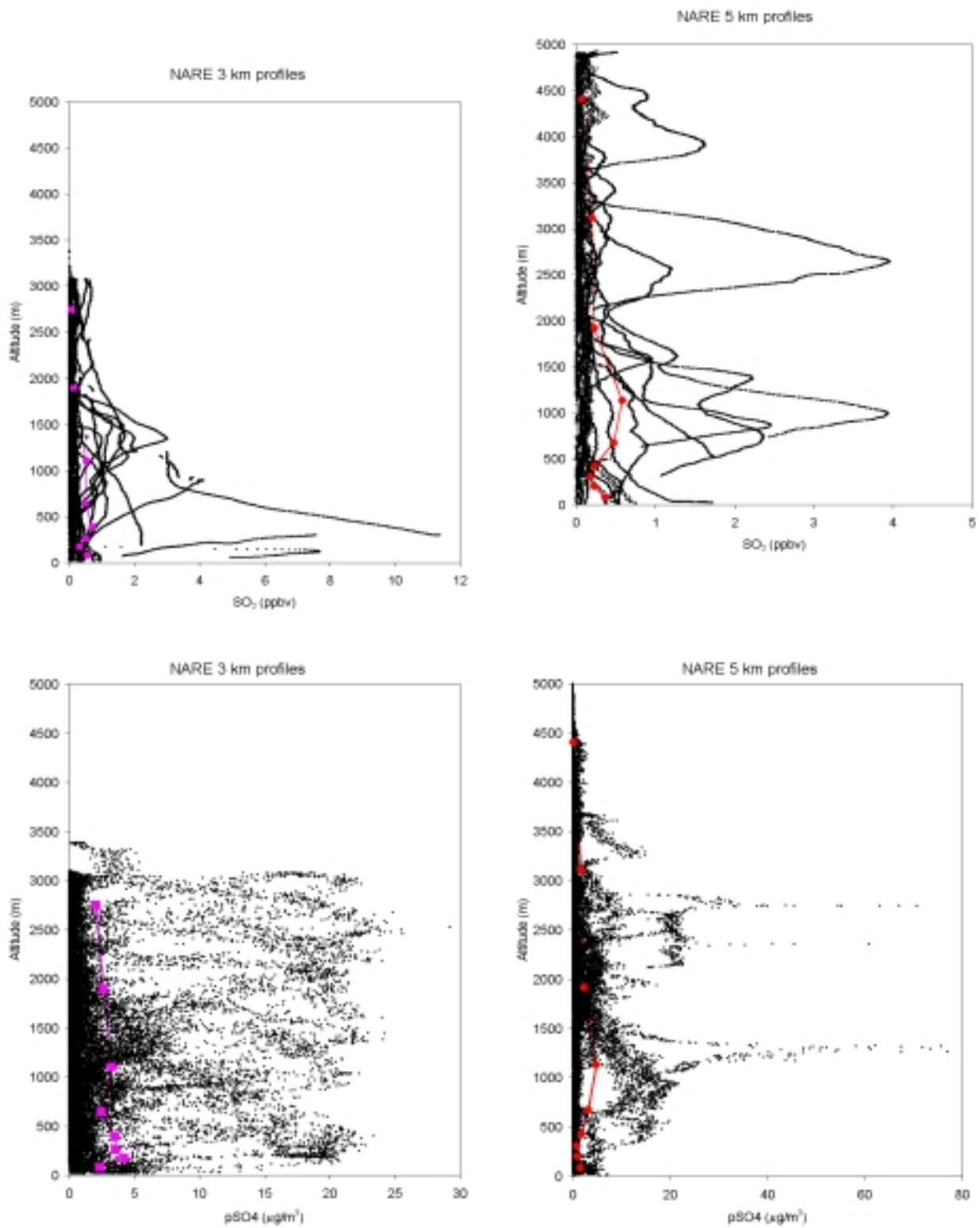


Figure 2 (cont.)

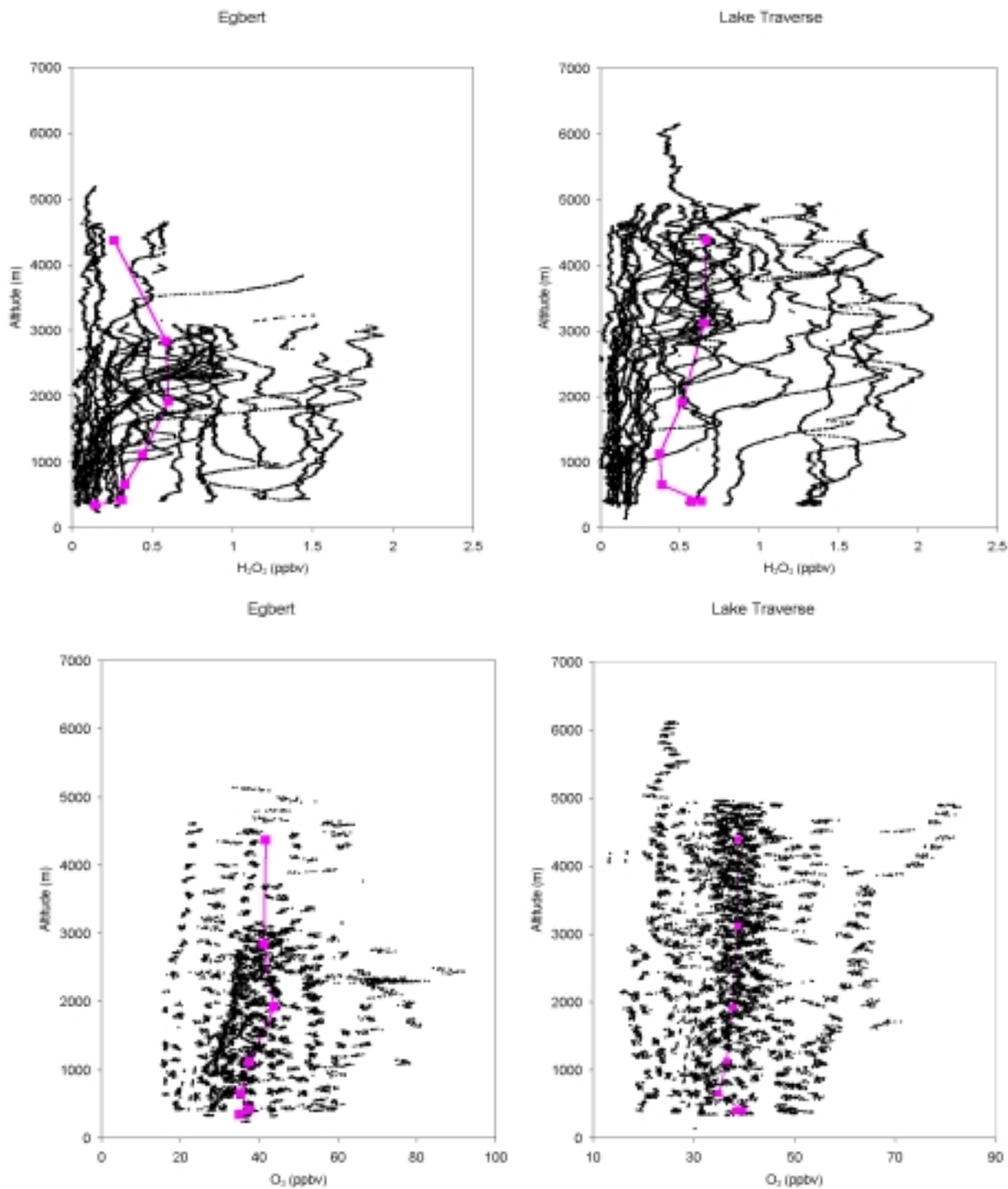


Figure 3. Profiles of H₂O₂, O₃, SO₂ and p-SO₄⁼ for the EMEFS study. The O₃, H₂O₂ and SO₂ data are taken from 34 profiles over Egbert and 30 profiles over Lake Traverse on 24 days. Because of the limitations of the PCASP operation, the pSO₄⁼ data are from 14 profiles over Egbert and 10 profiles over Lake Traverse on 7 days. The average profiles were compiled in the same way as described for figure 2.

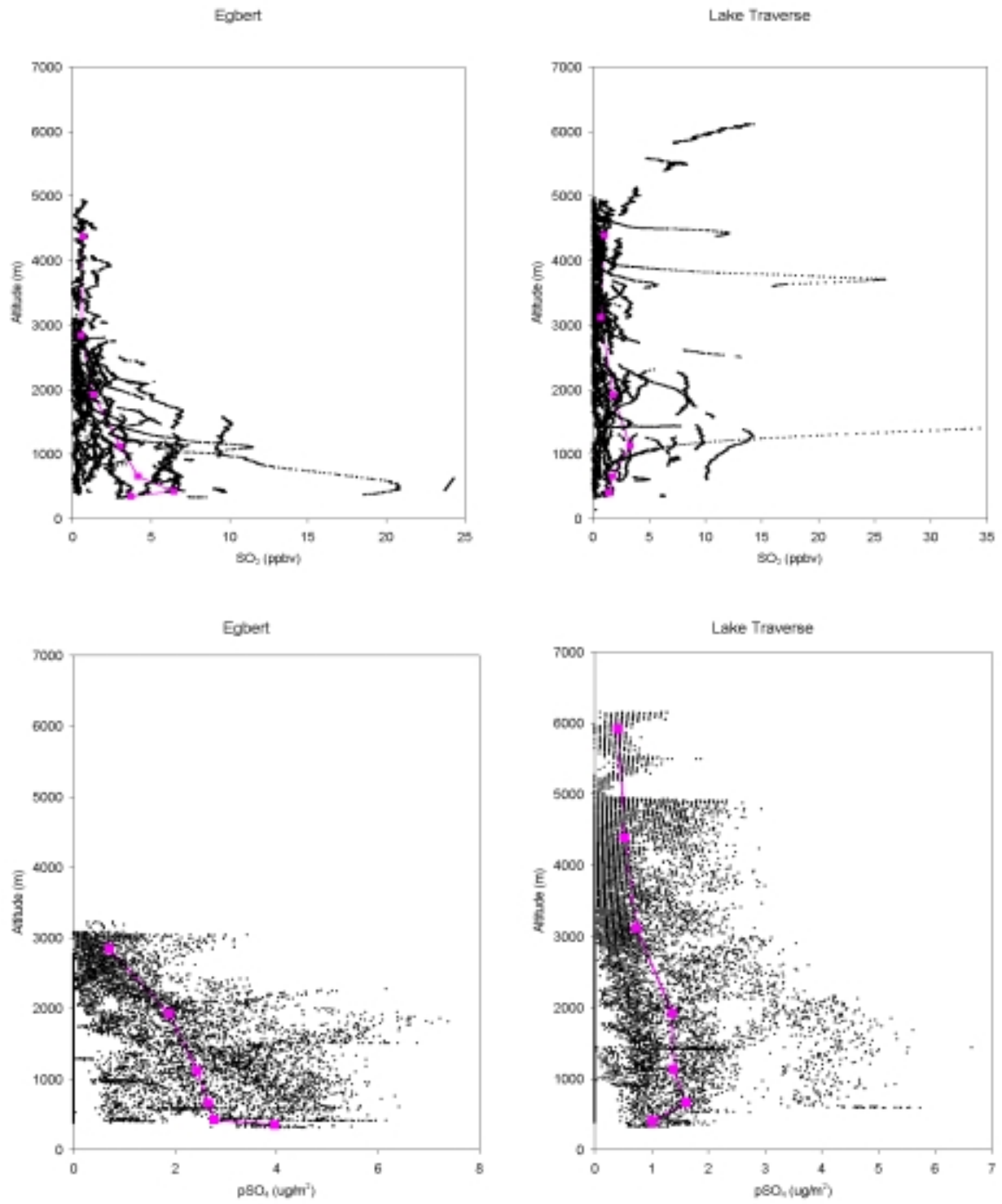


Figure 3 (cont.)

Using Airborne Radon Measurements In The Development And Validation Of Global 3-D Atmospheric Models

Mark Kritz
Atmospheric Sciences Research Center
State University of New York, Albany

Introduction

Because their chemical sources and sinks are negligible and their physical source and removal mechanisms generally well understood, natural and artificial radionuclides have in the past played a unique and valuable role in tracing and elucidating large-scale atmospheric motions and transports, particularly in the areas of intra-stratospheric movements and stratosphere-to-troposphere exchange. More recently, with the emergence of advanced global atmospheric models, there has been a growing realization of the important role these radionuclides can play in the development and validation of the transport components of such models. In this work we will confine ourselves to the application of free tropospheric radon observations for this purpose.

Radon (^{222}Rn) enters the atmosphere from the crust, where it is produced by the radioactive decay of trace quantities of its parent, ^{226}Ra . Although its rate of entry into the atmosphere is strongly dependent upon local factors such as soil depth, permeability and moisture content, as well as the local ^{226}Ra content, and can vary significantly on scales as small as a few meters (Schery et al., 1984) these differences tend to average out on regional scales and a canonical value of 1 radon atom $\text{cm}^{-2} \text{sec}^{-1}$ has been accepted as an interim working figure for global-scale analyses (Turekian et al., 1977; Jacob et al., 1997). Radon emissions from the sea are less than 1% of the land values (Wilkening and Clements, 1975). Because radon is a noble gas and relatively insoluble in water its removal from the atmosphere by precipitation is negligible, so that its only significant atmospheric sink is its own radioactive decay, which occurs with a half-life of 3.823 days. For these reasons shipboard measurements of atmospheric radon have long been used as an indicator of the transport of continental air over the oceans (e.g., Prospero and Carlson 1970; Kritz and Rancher, 1980).

The utility of comparisons between tropospheric radon observations and model-calculated results is demonstrated by a growing number of publications, by my own recent work in this area (which, for reasons of space, must be the focus of this discussion) and by the results of two prior WCRP workshops (Jacob et al., 1997; Rasch et al., in preparation.) The underlying idea in such comparisons is that if the models are handling transport correctly, the predicted free tropospheric radon distributions ought to correspond reasonably well with the observed distributions. If this can be shown to be the case one can proceed with increased confidence to use these models to address the more difficult questions relating to the distribution and effects of chemically active tropospheric trace constituents such as sulfur, odd nitrogen and ozone.

It should be noted that while the assumption of a 1 atom $\text{cm}^{-2} \text{sec}^{-1}$ global continental source strength may have been warranted for initial comparisons with model results, continuing

improvements in model performance may soon justify a more refined assessment of possible large-scale variations in the radon source function. It is also clear that these same improvements in model performance place higher demands on the quality of the radon measurements used for the purpose of model development and validation. I will pay particular attention to this latter question in the balance of this discussion.

Radon measurement techniques used in tracer applications

Because of its short radioactive lifetime and predominant continental source, shipboard radon measurements found a relatively early application as an indicator of continental air in experiments conducted in presumably remote marine areas. One such application was that of Prospero and Carlson (1970), who used dust and radon measurements to trace the progress of African plumes over the Atlantic. Another was a study of the halogen chemistry of the tropical marine boundary layer in the Equatorial Atlantic, in which it was found that the periods in which closure could be obtained in a box model analysis of the halogen species measurements had a one-to-one correspondence with the periods of the lowest ambient radon concentrations (Kritz and Rancher, 1980).

The radon measurement techniques used in these and many similar studies were based on the collection and measurement of short-lived radon daughter products, rather than a direct measurement of radon gas itself. These products, which have an effective half-life of approximately 40 minutes and are generally in radioactive equilibrium with radon, are quickly and irreversibly scavenged by particles of the ambient atmospheric aerosol and so can be collected on filters along with such particles. In practice, a typical measurement scenario consists of drawing ambient air through a filter for 15 to 30 minutes, and then moving the filter under a suitable detector and counting for 30 to 60 minutes, so that the activity of the short-lived radon daughters collected on the filter can be determined. If the volume of air sampled, the filter trapping efficiency, and the overall detector counting efficiency are known, and the ambient radon activity not too low (so that only a very few counts are obtained and counting statistics are poor) the number of counts obtained can be used to estimate the corresponding ambient radon activity with an uncertainty on the order of $\pm 20\%$ (Kritz et al., 1990). The technique is described in detail in that reference, and in the works cited therein.

Although the *radon daughter technique* offers the advantage of relatively light weight and minimal space requirements (though at the cost of a relatively long sampling time) one problem inherent in the method, particularly when used aboard aircraft, is that it is sometimes difficult in practice to meet the requirements mentioned in the preceding paragraph. Among such problems are uncontrollable variations in filter trapping efficiency, losses (in the sampling inlet) of the aerosol particles to which the radon daughters are attached, variations in the overall detector counting efficiency, and high detector background count rates. These effects cannot be discussed in detail here but a thorough discussion can be found in Kritz et al. (1990) and Kritz et al. (1993) and in the references cited in those publications.

Even so, with adequate controls and safeguards reasonable results can be obtained--particularly when it is borne in mind that the purpose of the radon measurements made in the four works cited above was not to make a quantitative determination, but rather to obtain a more or less

qualitative result which could be used as an indication of low, moderate or high ambient radon levels. But while this was entirely adequate for the purposes of those applications, some caution is needed when using measurements obtained in this manner and for that purpose in the more demanding application of model validation.

Radon measurement techniques for model development and validation

The measurements presented in Kritz et al. (1990) were obtained in the course of a study of troposphere to stratosphere exchange, with the goal of determining whether low but finite quantities of radon could be found in the lower mid-latitude stratosphere. Thus the semi-quantitative results provided by the radon daughter technique were well-matched to the goals of that experiment. Although, as it happened, we never did detect any radon in this region, we did discover the existence of much higher than expected radon abundances in the upper mid-latitude *troposphere* in the region where the measurements were made (between Hawaii and California.) Although in Kritz et al. (1990) we presented a meteorological explanation for this phenomena, soon thereafter Balkanski et al (1992) took these results one step further by demonstrating their utility in a global 3-D modeling study. This in turn helped provide the rationale for a new series of free tropospheric radon measurements intended for the specific purpose of model development and validation, and for the design and fabrication of a new, more sensitive and accurate radon measurement system capable of operation as an aircraft climbed to altitude--in other words, a system with a sampling time on the order of one minute.

The approach chosen for this task was that of *whole air sampling*, in which a large compressor was used to collect a series of individual pressurized air samples during the course of a flight. The resultant system consisted of an inlet, first stage pump, main compressor, pressure monitoring sensors and relief valves, data system, and 32 individual steel sample cylinders. These had a water volume of 2.5 L and a pressure rating of 1800 psig, so that when fully pressurized each held approximately 300 STP L of ambient air. Following each flight the sample cylinders were removed from the aircraft and taken to a ground-based laboratory, where the radon each contained was stripped out by cold-trapping and analyzed in individual counting cells. Because these samples could be counted for periods as long as twelve hours, as opposed to the hour-long counts characteristic of the filter methods, and because background count rates of the laboratory counting system were more than an order of magnitude less than those characteristic of the airborne detectors, the overall 2(σ) uncertainty of the resultant measurements was generally better than $\pm 8\%$.

Another important factor in quality control and in the assessment of system performance is the collection of duplicate in-flight samples. Several such simultaneously-collected sample pairs are obtained in the course of each of our flight campaigns, and analyzed (as are all of the samples collected) under double-blind conditions. The result spread (half of the difference in the analyzed value of the two samples, divided by their mean) of the five sample pairs collected in the 1994 flight series were $\pm 1.1\%$, $\pm 0.1\%$, $\pm 2.8\%$, $\pm 2.3\%$ and $\pm 7.1\%$. (The ambient radon concentration for this last sample pair was close to the lower limit of quantitative detection for the system.) Full details of this system and its performance are given in Kritz et al. (1998).

In its initial configuration this system weighed more than 500 kg, occupied approximately 4 m² of cabin floor space, and consumed approximately 4.5 kW of electrical power. While this did not pose a problem aboard the large aircraft on which it was originally flown, the system has since been reconfigured and in 1996 was successfully flown aboard a Lear Jet. However, while we are familiar with and have used lighter and more compact airborne radon measurement instrumentation in other applications (e.g., Kritz et al., 1990 and 1993, mentioned earlier) we know of no approach which would have provided the combination of fast sampling time, sensitivity, precision and accuracy called for by the model validation project.

Results of our 1994 campaign and its initial application to model development and validation

The system was flown on fifteen flights during the spring and summer of 1994. Whole air samples for post-flight laboratory analysis were obtained as the plane climbed to altitude following takeoff from Moffett Field, California (37.4N, 122.0W) and during the descent at the end of each flight. Collection of the first sample coincided with the start of the takeoff roll; when that cylinder was fully pressurized its inlet valve was closed, and the fill procedure repeated with successive cylinders until the plane reached cruising altitude. A similar procedure was followed for the descent. As mentioned earlier additional, duplicate, samples were sometimes collected while the plane was cruising at altitude. Thus the profiles consist of a series of samples, each spanning an altitude range of ~1 km, separated by intervals of ~100 in. The altitudes and locations corresponding to each sample were obtained from the aircraft's navigation and flight data systems and are presented, together with the results for the ascents, in Kritz et al., (1998). Comparison of model results with these individual profiles, and with their mean, is included as exercise O6D of the COSAM workshop.

Two characteristics of the resultant profiles are immediately evident: first, the high degree of day-to-day variability in both the radon column density and the shape of the profiles; and second, a characteristic increase in radon concentrations (relative to the mid-tropospheric values) in the uppermost troposphere. This latter characteristic was observed on most of the individual profiles, as well as in the mean profile.

References

- Balkanski, Y. J., D. J. Jacob, R. Arimoto and M. A. Kritz, Distribution of ²²²Rn over the north Pacific: Implications for continental influences, *J Atmos. Chem.*, 14, 353-374, 1992.
- Jacob, D. J., M. J. Prather, P. J. Rasch, R.-L. Shia, Y. J. Balkanski, S. R. Beagley, D. J. Bergmann, W. T. Blackshear, M. Brown, M. Chiba, M. P. Chipperfield, J. de Grandpre, J. E. Dignon, J. Feichter, C. Genthon, W. L. Grose, P. S. Kasibhatla, I. Kohler, M. A. Kritz, K. Law, J. E. Penner, M. Ramonet, C. E. Reeves, D. A. Rotman, D. Z. Stockwell, P. F. J. van Velthoven, G. Verver, O. Wild, H. Yang and P. Zimmerman, Evaluation and intercomparison of global atmospheric transport models using ²²²Rn and other short-lived tracers, *J. Geophys. Res.*, 102, 5953-5970, 1997.

Kritz, M. A. and J. Rancher, Circulation of Na, Br and Cl in the tropical marine atmosphere, *J. Geophys. Res.* 85, 1633-1639, 1980.

Kritz, M. A., S. W. Rosner, K. K. Kelly, M. Lowenstein and K. R. Chan, Radon measurements in the lower tropical stratosphere: Evidence for rapid vertical transport and dehydration of tropospheric air, *J. Geophys. Res.*, 98, 8725-8736, 1993.

Kritz, M. A., S. W. Rosner and D. Z. Stockwell, Validation of an off-line 3-1) chemical transport model using observed radon profiles, 1, Observations, *J. Geophys. Res.*, 103, 8425-8432, 1998.

Kritz, M. A., J.-C. Lerouilly, and E. F. Danielsen, The China Clipper: Fast advective transport of radon-rich air from the Asian boundary layer to the upper troposphere near California, *Tellus* 42B, 46-61, 1990.

Prospero, J. M. and T. N. Carlson, Radon-222 in the North Atlantic trade winds: relationship to dust transport from Africa, *Science* 167, 974-977, 1970.

Schery, S. D., D. H. Gaeddert and M. H. Wilkening, Factors affecting exhalation of radon from a gravelly sandy loam, *J. Geophys. Res.*, 89, 7299-7309, 1984.

Turekian, K. K., Y. Nozaki and L. K. Benninger, Geochemistry of atmospheric radon and radon products, *Ann. Rev. Earth Planet. Sci.* 5, 227-255, 1977.

Wilkening, M. H., and W. E. Clements, Radon 222 from the ocean surface, *J. Geophys. Res.* 80, 3828-3830, 1975.

A Global Database Of Dimethylsulfide Emissions

Geert-Jan Roelofs¹ And Jamie Kettle²

¹ Institute for Marine and Atmospheric research Utrecht (IMAU),
Princetonplein 5, 3584 CC Utrecht, The Netherlands,

² Max Planck Institute for Chemistry, Postfach 3060, 55020 Mainz, Germany

Abstract

A database of 15617 point measurements of dimethylsulfide (DMS) in surface waters has been assembled. The database was processed to create a series of climatological monthly $1^{\circ}\times 1^{\circ}$ latitude–longitude squares of data. Using a parameterization for the air-sea exchange coefficient or transfer velocity, which depends on wind speed and ocean temperature, monthly DMS emission distributions have been calculated.

Introduction

Dimethylsulfide produced by plankton may influence the radiation budget of the earth, as was first proposed by Charlson et al. (1987). According to this hypothesis (known by its acronym, CLAW, after the authors of the publication), dimethylsulfoniopropionate (DMSP) in phytoplankton cells is released into the water column where it is transformed into dimethylsulfide (DMS). DMS diffuses through the sea surface to the atmosphere where it is oxidized to SO_2 and methane sulfonic acid (MSA). SO_2 can be oxidized to H_2SO_4 , which can then form sulfate particles, that may alter the radiation budget of the earth through modification of cloud optical properties. This may cool down the temperature of the upper ocean and consequently change the metabolism and speciation of plankton (Lawrence, 1993). In turn, this may modify the emission of DMS to the atmosphere. The processes that govern each step in the hypothesis remain poorly understood and are the subject of continuing investigations (Andreae and Crutzen, 1997).

Because the rate of aerosol production from marine DMS can be influenced by climatic feedbacks (Andreae and Crutzen, 1997), there has been extensive work on the processes that control the production of DMS and its precursors, its emission and oxidation in the atmosphere, and the parameterisation of the effect of the resultant sulfate particles on the radiation budget. The parameterisation of the DMSP production and release processes within a plankton community is of particular interest, and the ultimate goal is to understand this process well enough to predict both the generation and destruction of DMS in the upper ocean as a function of latitude, longitude, and time.

DMS is a hydrolysis product of dimethylsulfoniopropionate (DMSP), a compound produced by phytoplankton possibly for cellular osmotic regulation or cryoprotection. There have been many studies which found correlations between DMS and chlorophyll *a* concentration. Other studies have observed correlations between DMSP and chlorophyll *a* concentration. These relationships

were thought to hold much promise for being able to deduce the DMS flux from satellite or airplane determinations of chlorophyll concentration.

On the other hand, there have also been studies where no correlation was found with either phytoplankton cell number or chlorophyll concentration on larger regional scales. This has several possible explanations. First, populations of phytoplankton are not homogeneous in the ocean, and second, different species of phytoplankton contain different amounts of DMSP and different concentrations and types of chlorophyll. Even though DMS is produced by phytoplankton, it is released to the water column by phytoplankton and zooplankton excretion, by phytoplankton senescence, by zooplankton grazing, and possibly by viral infection. In addition, DMS is subject to a number of removal mechanisms including bacterial and photochemical degradation, surface outgassing, and downward mixing which vary according to time, place, and meteorological conditions. One can therefore not necessarily expect a simple correlation between DMS and phytoplankton cell number or chlorophyll concentration.

Methods

The center of the project is a database of 15617 DMS measurements which were contributed by scientists or digitized from publications. This project was originally proposed at the NATO Advanced Research Workshop on Biogeochemical Ocean–Atmosphere Transfers (BOAT) held in Bermuda, 1992. For a complete list of the contributed and digitized data sets we refer to Kettle et al. (1998).

Points from the database were excluded if associated temperature or salinity values, which were also measured, fell outside certain broad threshold limits. After this, a statistical checking procedure was implemented whereby the data in the database were divided up into monthly $5^{\circ}\times 5^{\circ}$ squares. For each square, a mean and the standard deviation was calculated. Then, each point in the square was compared with the mean, and if it fell outside of 4.5 standard deviations of the mean, it was discarded. The mean and the standard deviation were then recalculated, and the selection process was repeated until no further points failed the standard deviation test. At the end, this left a database cleaned of outlying points, leaving 14980 good data points from the starting number of 15617.

The monthly average pixels (ocean data squares) were distributed among 57 biogeochemical provinces (Longhurst et al., 1995) and average monthly DMS concentrations were calculated for each province. The temporal distribution of data in some provinces was sufficient to construct an annual pattern of DMS concentrations by connecting the existing points with a spline construction. In many cases, the temporal distribution of data was not sufficient to construct a clear annual cycle, and in these cases the annual trends of DMS concentrations were taken from other provinces which had a better data set and were considered to be oceanographically similar. The discontinuities between the boundaries of the biogeochemical provinces were smoothed by the application of an 11-point filter. This became the first-guess DMS concentration field. An interpolation scheme was developed and applied to oceanic regions with little or no data coverage. Eventually, a series of 12 monthly maps of sea surface DMS concentration was

created. Uncertainties of the resulting DMS concentrations are associated with the spatial variability of DMS concentrations within a biogeochemical province. In provinces where there were no field investigations, no statement about data variability can be made, and it must be assumed that the variability in these provinces is similar to that in biogeographically similar provinces for which data are available. Additional uncertainty is associated with the extrapolation method. This was quantified by repeating the procedure for fields for which maps have already been created based on a large database of measurements, e.g., nitrate, silicate, phosphate, and oxygen from the World Ocean Atlas and from the annually averaged field of chlorophyll measured by the satellite-based Coastal Zone Color Scanner (CZCS).

The monthly DMS surface concentration distributions were used to calculate the DMS emission flux from the ocean surface. Generally, the air-sea flux F_{DMS} is expressed as

$$F_{DMS} = k_w \times \left([DMS]_{sw} - \frac{[DMS]_{BL}}{H} \right)$$

where $[DMS]_{sw}$ and $[DMS]_{BL}$ are the concentrations of DMS in ocean surface water and in the boundary layer, respectively. H is the Henry's law constant for DMS and k_w the transfer velocity. Since DMS is relatively insoluble and H is large, the second term between brackets vanishes, so:

$$F_{DMS} = k_w \times [DMS]_{sw}.$$

In this work the parameterization for k_w from Liss and Merlivat (1986) was used. Three regimes concerning the state of the ocean surface are distinguished, and the transfer velocity is parameterized in terms of wind speed and ocean temperature:

$$\begin{aligned} k_w &= a \times 0.17 \times u_{10} && \text{for } u_{10} < 3.6 \\ k_w &= b(2.85 \times u_{10}^{10.26}) + 0.612 \times a && \text{for } 3.6 < u_{10} < 13 \\ k_w &= b(5.90 \times u_{10} - 49.91) + 0.612 \times a && \text{for } u_{10} > 13 \end{aligned}$$

with u_{10} the wind speed at 10 m above the surface (m s^{-1}) and:

$$a = \left(\frac{600}{Sc} \right)^{2/3} \quad b = \left(\frac{600}{Sc} \right)^{1/2}$$

Sc is the Schmidt number, which decreases as the water temperature increases. The dependence of Sc on sea surface temperature (SST) for DMS was presented by Erickson et al. (1990) and can be expressed by means of a polynomial:

$$Sc = a_1 + a_2(SST) + a_3(SST)^2 + \dots$$

Results

Information about climatological wind speeds was obtained from the global wind stress climatology based on ECMWF (European Centre for Medium Range Weather Forecasts) analysis performed by Trenberth et al. (1989). This information is provided at $2.5^\circ \times 2.5^\circ$ latitude–

longitude resolution and is interpolated to $1^{\circ} \times 1^{\circ}$ latitude–longitude resolution for use in this work. Figures 1 and 2 display the distributions of the sea surface DMS concentrations and the derived emission fluxes for January and July, respectively. The figures clearly indicate the seasonality of the DMS concentrations and the associated emissions to the atmosphere, with relatively low values in winter and high values in summer, especially on the SH. The upwelling regions near the South American and African coasts are clearly visible. Globally integrated, the DMS emission fluxes are about 2.8 and 1.4 Tg S per month for January and July, respectively, and 28.9 Tg S yearly.

References

- A.J. Kettle, M.O. Andreae, D. Amouroux, T.W. Andreae, T.S. Bates, H. Berresheim, H. Bingemer, R. Boniforti, G. Helas, C. Leck, M. Maspero, P. Matrai, A.R. McTaggart, N. Mihalopoulos, B.C. Nguyen, A. Novo, J.P. Putaud, S. Rapsomanikis, G. Roberts, G. Schebeske, S. Sharma, R. Simó, R. Staubes, S. Turner, and G. Uher (1999), A global data base of sea surface dimethyl sulfide (DMS) measurements and a simple model to predict sea surface DMS as a function of latitude, longitude, and month. *Global Biogeochem. Cycles*, **13**, 399-444.
- Charlson, R. J., J. E. Lovelock, M. O. Andreae, and S. G. Warren, Oceanic phytoplankton, atmospheric sulphur, cloud albedo and climate, *Nature*, 326, 655–661, 1987.
- Lawrence, M. G., An empirical analysis of the strength of the phytoplankton-dimethylsulfide-cloud-climate feedback cycle, *J. Geophys. Res.*, 98, 20663–20673, 1993.
- Andreae, M. O. and P. J. Crutzen, Atmospheric aerosols: biogeochemical sources and role in atmospheric chemistry, *Science*, 276, 1052–1058, 1997.
- Longhurst, A., S. Sathyendranath, T. Platt, and C. Caverhill, An estimate of global primary production in the ocean from satellite radiometer data, *J. Plankton Res.*, 17, 1245–1271, 1995.
- Liss, P. S. and L. Merlivat, Air-sea exchange rates: introduction and synthesis, in *The Role of Air–Sea Exchange in Geochemical Cycling*, edited by P. Buat-Menard. pp. 113–127. D. Reidel Publishing Company, Berlin, 1986.
- Erickson III, D. J., S. J. Ghan, and J. E. Penner, Global ocean-to-atmosphere dimethyl sulfide flux, *J. Geophys. Res.*, 95, 7543–7552, 1990.
- Trenberth, K. E., J. G. Olson and W. G. Large, A global ocean wind stress climatology based on ECMWF analysis, NCAR/TN–338+STR, NCAR Technical Note, August, 1989.

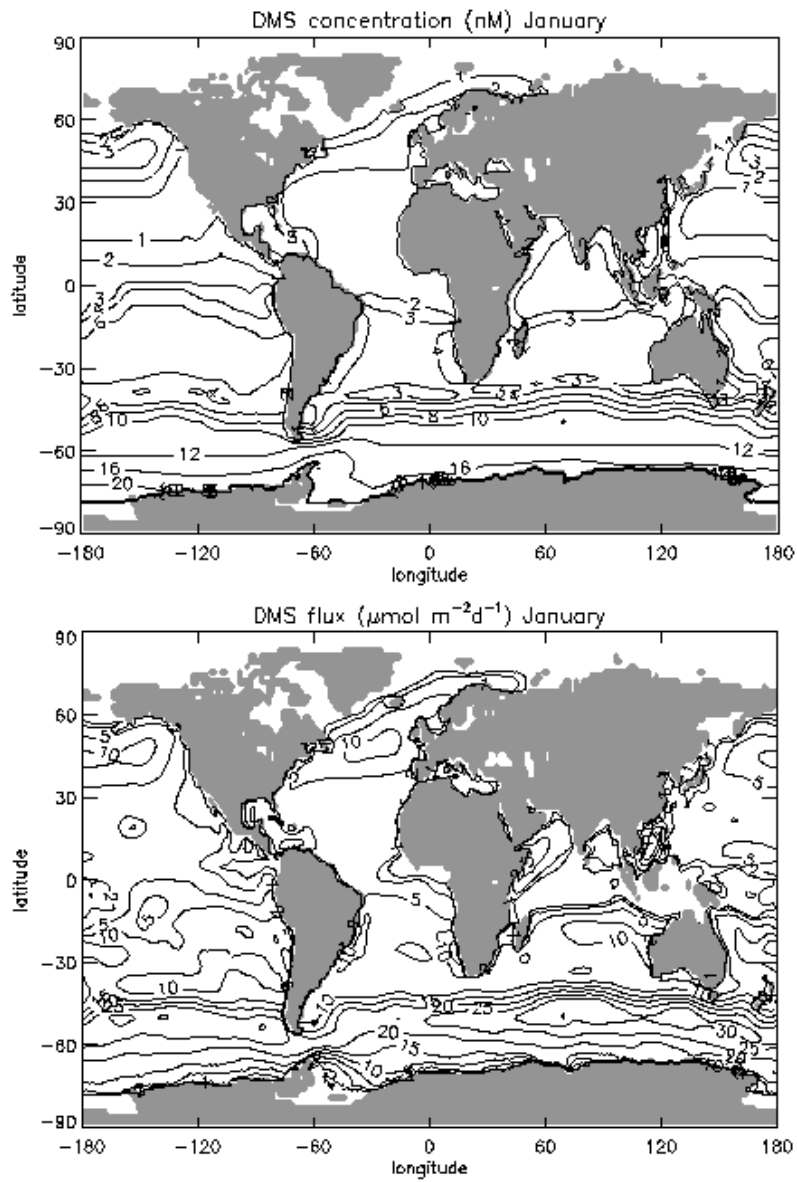


Figure 1. Interpolated sea surface DMS concentration (nM) (top panel) and DMS emission flux ($\mu\text{mol m}^{-2} \text{day}^{-1}$) (bottom panel) for January.

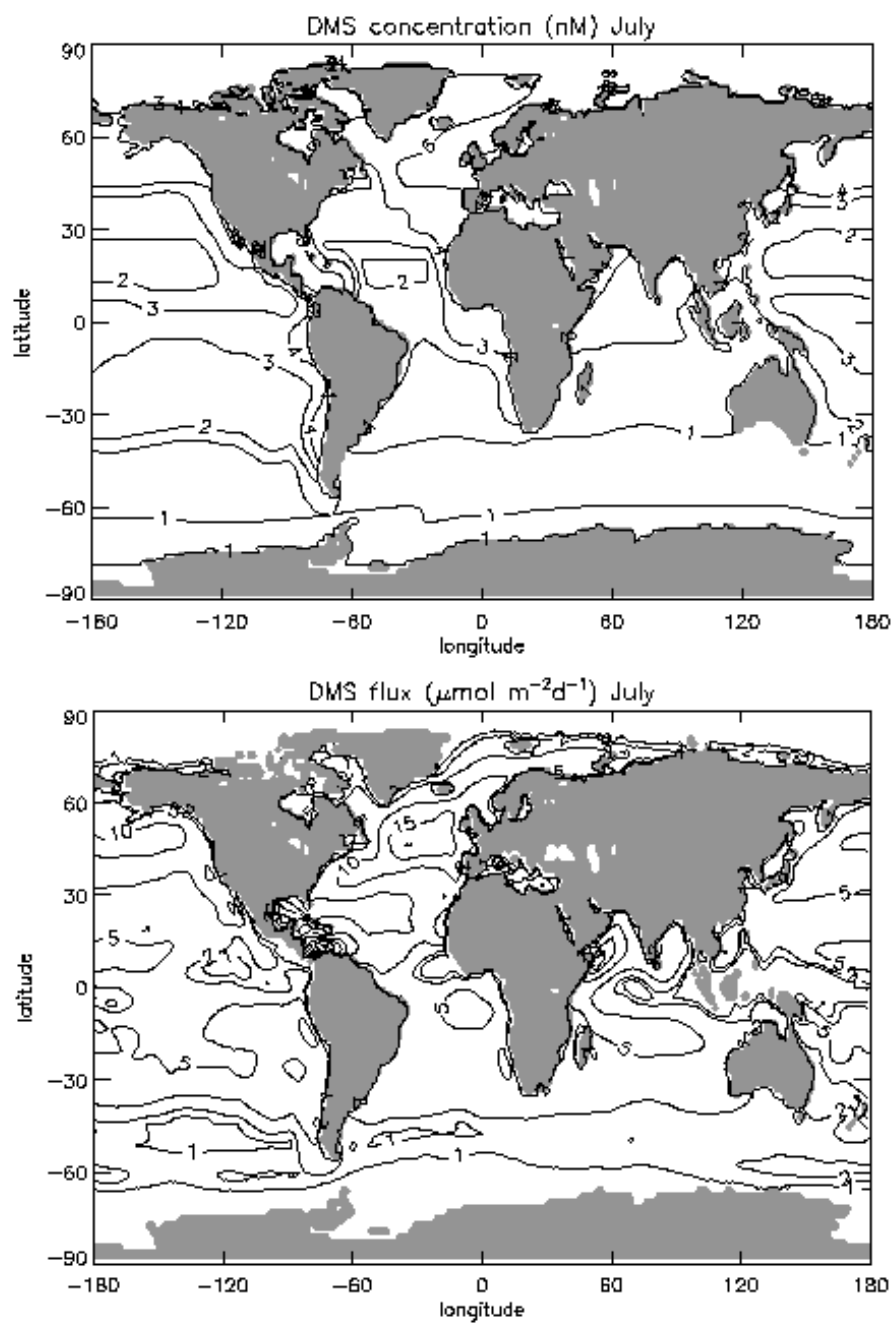


Figure 2. As Figure 1 but for July.

SOME PROBLEM POINTS IN ATMOSPHERIC SULPHUR MODELLING

Trond Iversen
Department of Geophysics
University of Oslo, Norway

Numerical model calculations of the atmospheric dispersion and deposition of sulphur compounds have been made regularly over the last 20-25 years. Early models applied so-called lumped coefficient chemistry for the purpose of calculating transboundary acid precipitation. Gradually the models have developed into tools which describe processes more explicitly and cover larger portions of the globe. Presently there are several hemispheric and global sulphur models off-line or on-line to meteorological field calculations. One purpose of running with resolved process description is the aim of estimating how sulphate concentrations influence size-distributions of particles. Based on this, estimates of optical effects and effects on cloud microphysics can be made, in an effort to evaluate possible climatic impacts.

In this presentation we discuss some problem points in sulphur modelling illustrated by some sensitivity experiments which is made in the calculations by Seland and Iversen (1998). The model is covering large parts of the Northern Hemisphere, and calculates black carbon as well as sulphur. Particulate matter is separated into different components depending on production mechanisms and assumed properties relative to radiation and cloud processes.

Unfortunately several links in the chain of processes from emission to deposition are poorly known. These processes are different aspects of in-cloud oxidation of SO_2 to sulphate, including assumptions about reductions of oxidation rates due to ice; and the efficiency of below-cloud scavenging of particulate sulphate.

Many models have problems with producing enough sulphate in air. We hypothesize that this is due to underestimated boundary layer clouds in meteorological models. A good stratocumulus parameterization scheme requires a good description of the structure of the turbulent boundary layer, in particular under windy and well mixed conditions. Frequently numerical weather prediction models have problems with this cloud type, as well as with shallow convection and fog. We have constructed a very simple scheme which is linked to a low but positive Richardson number and available humidity in the ABL. We do not claim this scheme to be sufficiently sophisticated for use in meteorological models, but use it here for the purpose of studying effects on sulphate production.

Having established the (hopefully) correct amount and frequency of non-precipitating clouds, the chemistry must be properly described. We use prescribed concentrations for oxidants from the global model by Berntsen and Isaksen (1997), in addition to a conservative estimate of catalysing metal ions which produce a minimum in-cloud oxidation rate. The oxidation by H_2O_2 is often much faster than can be described with the time-step length normally used with large-scale

models. The physical processes regulating the overall turnover to sulphate is then the time required for replenishment of SO₂ and oxidant-rich air. We use a replenishment time of 1 hour, and have tabulated the replenishment by solving a simple diffusion process.

The oxidation rate is assumed reduced in ice-dominated cloud. This part is very uncertain, and is one of the focused points here.

Amongst the deposition processes, we discuss here the washout of particles below clouds. This process also appears very uncertain from theoretical calculations, laboratory experiments and field measurements. Comparing figures synthesized by Hobbs (1993) and Seinfeld and Pandis (1998) it is seen that differences are more than an order of magnitude. Different modellers use very different parameter values. A sensitivity test reveals very large impacts on the turnover time for sulphate in the atmosphere.

The enclosed figures 1, 2 and 3 show impacts of different parameter changes on the sulphate column burden estimated over large parts of the northern hemisphere for the month of April 1988. Meteorological data are from ECMWF. Emissions are taken from Spiro et al (1992) with changes for the DMS-emissions (Tarrasón *et al.* 1995) and for anthropogenic emissions in Europe (EMEP) and North America (NAPAP).

The base case use a parameterized stratocumulus cloudiness, a reduction of the wet oxidation rate by multiplying with a factor varying linearly from 1 at 0°C to 0.1 at -10°C, and a below-cloud scavenging ratio of $6 \cdot 10^5$ for the most abundant sulphate-component produced by in-cloud oxidation (a3). The turnover time for sulphate is 3.48 days. In the first test, the stratocumulus parameterization is removed, giving a turnover time of 3.53 days, and a column burden typically reduced up to 5% over remote areas. In the second test the reduced oxidation rate due to ice is made over the temperature interval -10°C to -20°C, giving a turnover time of 3.35 days and a column burden increase of around 5% close to sources and 3-5 % reduction more remotely. Since more sulphate is produced centrally, the SO₂ -reservoir is depleted. The final test was to reduce the below-cloud scavenging-ratio for the a3-component by a factor 4. The effect of this is considerable with a turnover time increased to 5.44 days and a column burden increased by typically 50%.

In conclusion, since these parameters are inaccurately known, calculations should be regarded as uncertain, in particular in remote areas and in the free troposphere. Better knowledge on how to treat below-cloud scavenging in models is urgently needed, and the effects of ice-clouds and mixed-phase clouds on oxidation rates and wet scavenging is also of importance, as is the availability of boundary-layer clouds.

Acknowledgement. Øyvind Seland at University of Oslo has made the model calculations presented in this paper.

REFERENCES

- Berntsen, T.K. and Isaksen, I.S.A. (1997) A global three-dimensional chemical transport mode for the troposphere; 1. Model description and CO and ozone results. *J. Geoph. Res.*, **102**, 21239-21280.
- Hobbs, P.V. (1993) Aerosol-Cloud interactions. In: *Aerosol-Cloud-Climate Interactions* (P.V. Hobbs, ed.). *International Geophysics Series*, **54**, Academic Press.
- Seinfeld, J.H. and Pandis, S.N. (1998) *Atmospheric Chemistry of Air Pollution*. John Wiley & Sons. Inc. USA.
- Seland, Ø. and Iversen, T (1999) A scheme for black carbon and sulphate aerosols tested in a hemispheric scale, Eulerian dispersion model. *Atmos. Environment*, **30**, 2853-2879.
- Spiro, P.A., Jacob, D.J. and Logan, J.A. (1992) Global inventory of sulphur emissions with 1x1 resolution. *J. Geoph. Res.*, **D97**, 6023-6036.
- Tarrasón, L., Turner, S. and Fløisand, I. (1995) Estimation of seasonal dimethyl sulphide fluxes over the North Atlantic Ocean and their contribution to European pollution levels. *J. Geoph. Res.*, **100**, 11623-11639.

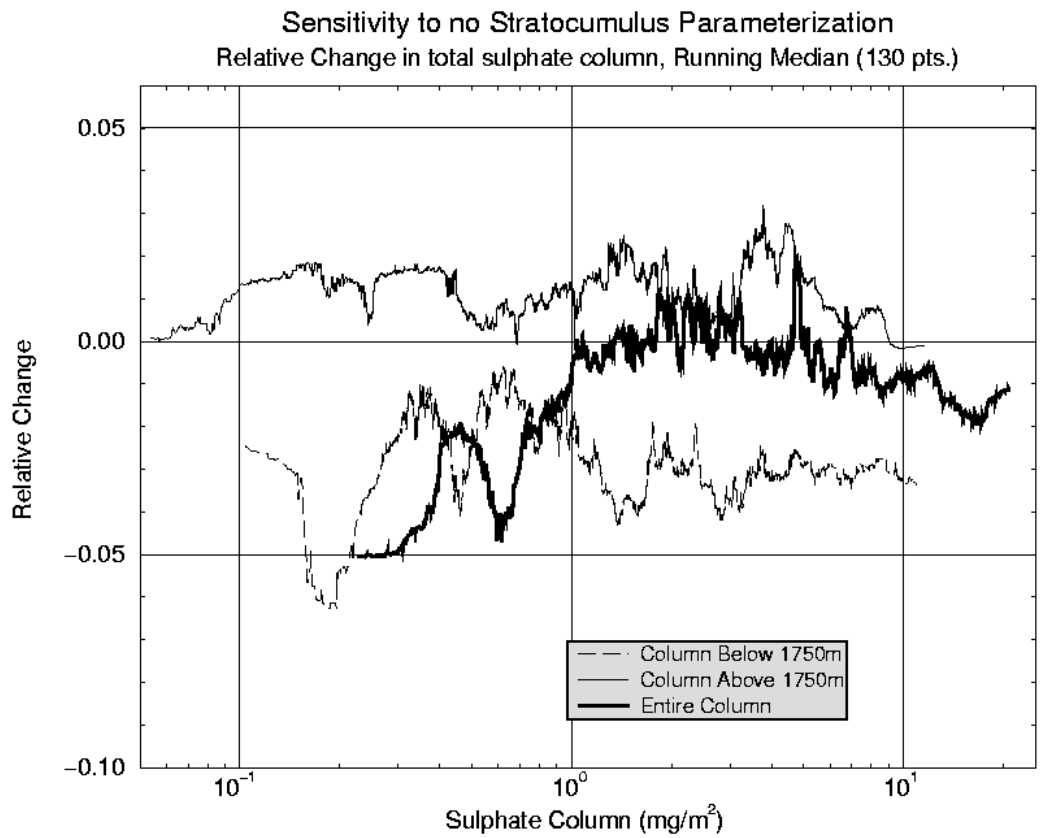


Figure 1: Effects of removing stratocumulus parameterization on sulphate column burden

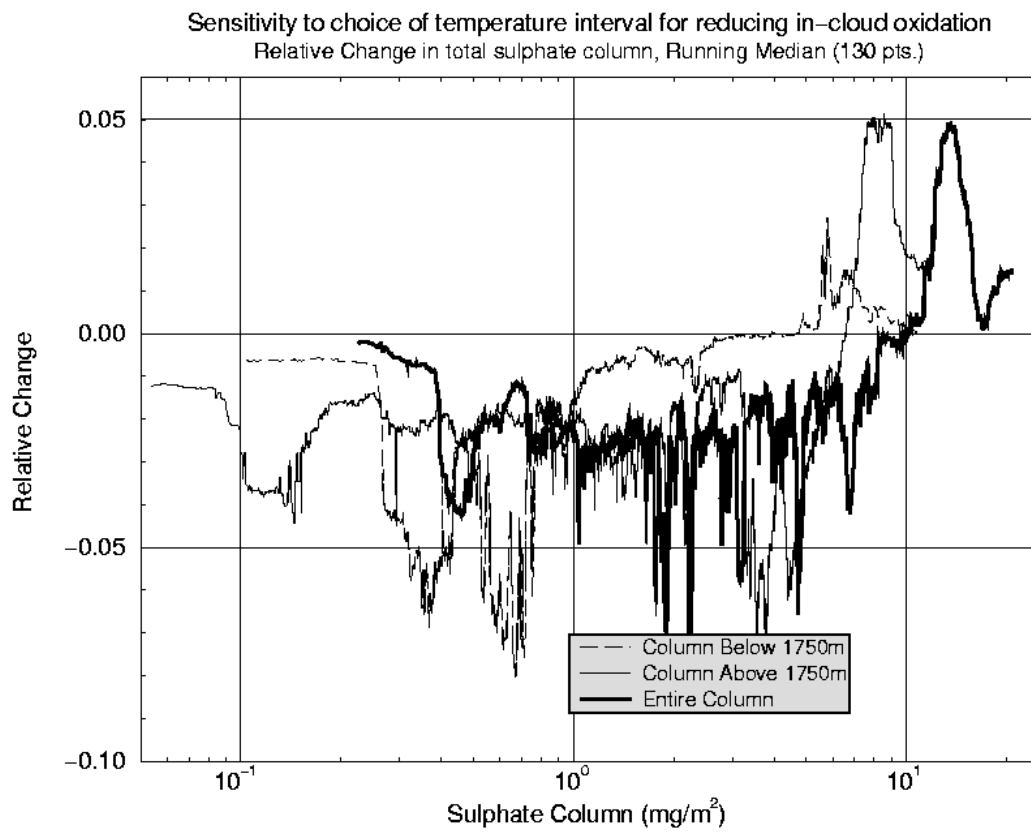


Figure 2: Effects of reducing ice-cloud oxidation-rate-reduction on sulphate column burdens

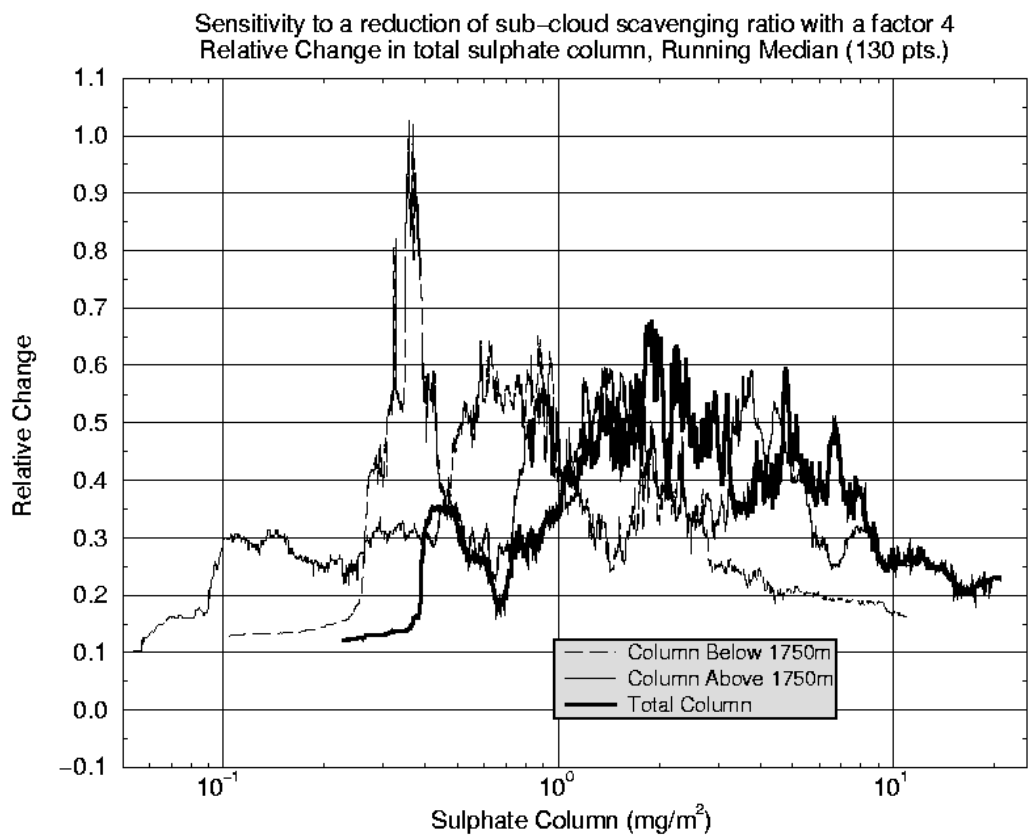


Figure 3: Effects of reducing below-cloud scavenging ratio on sulphate column burdens

Simulation of Size-Segregated Global Sea-salt and Sulphate Aerosol Mixtures Using the Canadian Global Climate Model III (GCMIII)

S.L. Gong¹, L.A. Barrie¹, N.A. McFarlane¹, M. Lazare¹
U. Lohmann³, J.-P. Blanchet² and L. Spacek²

¹Atmospheric Environment Service, 4905 Dufferin Street, Downsview, Ontario M3H 5T4, Canada

²Atmospheric Science Program, Department of Physics, Dalhousie University, Halifax, N.S. B3H 3J5, Canada

³Department of Earth Sciences, University of Quebec at Montreal, P.O.Box 8888, Stn Downtown, Montreal, QC H3C 3P8, Canada

Sea salt and sulphate are major global aerosol sources that play an important role in tropospheric chemistry and climate. The Canadian Global Climate Model (GCMiii) coupled with CAM - Canadian Aerosol Module was used to simulate the global distribution of size-segregated sea-salt and sulphate aerosols of both anthropogenic and natural origins in the atmosphere. CAM is a sectional model which carries aerosol particles as an active constituency. In current configuration, the aerosol mixtures are divided into 12 size sections [$r = 0.005-10 \mu\text{m}$] and assumed to be internally mixed. Processes simulated in CAM include production, nucleation, condensation, aerosol-cloud interaction, removal and transport in the atmosphere for each type of aerosols. The transport of aerosols in GCMiii includes a semi-Lagrangian advection, vertical diffusion and convection.

The results were obtained using the model with a linear physical transform grid of T47 [$\sim 3.75^\circ$ longitude], vertical resolution of 22 levels [from surface to 12 hPa pressure level] and 20 minute integration time step. Simulated global aerosol concentrations were compared with observations. Reasonable agreement was found in terms of absolute magnitude and seasonal variations.

The atmospheric distribution and residence time is investigated in this study for various size ranges. The relative abundance of sea-salt and sulphate is in good agreement with measurements. For example, the relative fraction of sub-micron sea-salt and sulphate in the remote marine atmosphere agrees with observations of ACE 1 and RITS 93 campaigns that indicated a dominance of sub-micron sea-salt over sulphate.

Details of the global sea-salt and sulfur budget were extracted from the simulation as a function of particle size. The simulation of mixed aerosols also showed the impact of sea-salt on the sulphate aerosols: a reduction of sulphate concentration due to the condensation of sulphuric vapour to the existing sea-salt aerosols which have a shorter residence time than sulphate aerosol. This impact is especially profound over southern oceans.

NARCM - LITE Intercomparison Study

L. Spacek¹, R. Hoff^{2,4}, A. Vandermeer²,
J. S. Fontecilla¹, J.-P. Blanchet¹, S. Gong³, L. Barrie³

- (1) Dept. of Earth Sciences, Univ. of Quebec at Montreal, QC Canada
- (2) Dept. of Phys. and Astr., York Univ., North York, ON Canada
- (3) Atmospheric Environment Service, Downsview, ON Canada
- (4) Atmospheric Environment Service, Egbert, ON Canada

1 Introduction

The Lidar In-Space Technology Experiment (LITE) provided a unique dataset of space and time distribution of aerosols and cloudiness in the atmosphere. Comparison of aerosol backscatter observation with model output can serve as a valuable tool in assessing the efficiency of the model.

2 Northern Aerosol Regional Climate Model

The NARCM is a limited-area non-hydrostatic dynamical model with physical parameterization and aerosol package. The dynamical kernel of NARCM is the same as the dynamical kernel of the CRCM (Canadian Regional Climate Model) (Laprise et al., 1997). The model equations, fully elastic and non-hydrostatic, are solved with the semi-implicit and semi-Lagrangian method that assures large flexibility of the model that performs on broad scales of space resolutions ranging from hemispheric to micro scales. Semi-Lagrangian advection treats favorably the transport of atmospheric constituents including aerosols. The horizontal discretization is done on a regular polar-stereographic grid, the Gal-Chan coordinate following terrain is used in vertical. The variables in the model are fully staggered using Arakawa's C-grid. The sponge zone is defined on the lateral boundaries and on the lid that allows a soft driving of the model. The NARCM uses physical parameterization package of the Canadian GCM (McFarlane et al., 1992) and in such a way the results of the CGCM that serve as the initial and boundary conditions are highly compatible with the NARCM internal regime. However, it does not exclude the possibility of using boundary condition originating from other models. The package contains terrestrial and solar radiation with all possible cycles, convective and stratiform clouds and precipitation parameterization, turbulent vertical fluxes of momentum, heat, water vapour and aerosols, gravity wave drag and CLASS (Canadian Land Surface Scheme) (Verseghy et al., 1991, 1993). NARCM uses 12 size-bins starting from 0.005, 0.01, 0.02, ..., 20.48 μm , for sea salt and sulphate, 4 cloud characteristics and 5 gaseous compounds that are advected separately, 33 tracers totally. CAM (Canadian Aerosol Module) assures physics and chemistry calculations. The principal processes simulated up to now are in-cloud oxidation, clear air chemistry, coagulation, nucleation, condensation, dry deposition, in-cloud and below cloud scavenging. Further parameterization are being developed. The final version of NARCM will include sulphate, black carbon, organics, soil and sea salt aerosols in a dynamic fashion.

3 Experiment

The simulation domain is centered at the North Atlantic as seen from figure below as well as the position of three LITE orbits used for comparison.

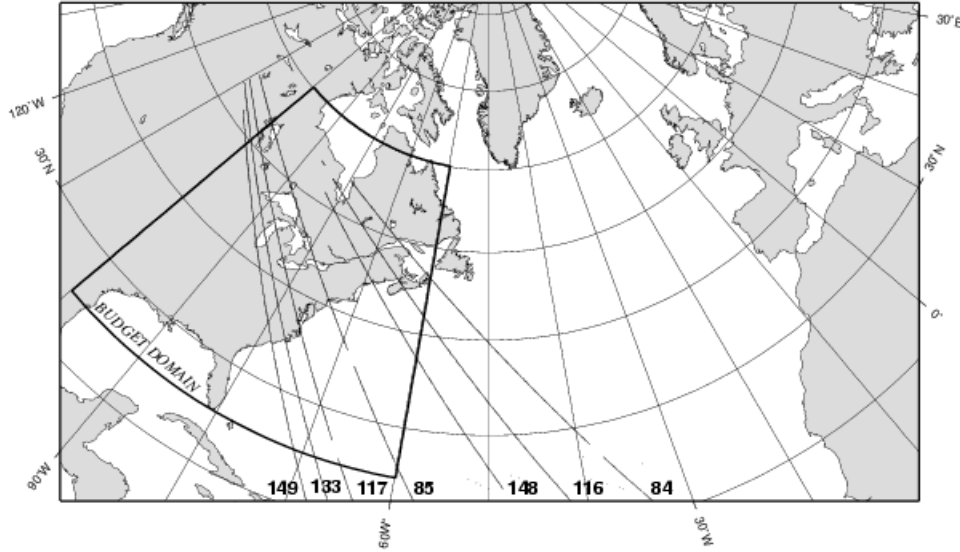


Fig.1 Experimental domain

The horizontal step is 100 km with 120x70 grid points in the domain, 22 levels with higher resolution near surface are used in vertical. Time step equals 20 minutes. The target dates are 17 Sep 1994 01Z (orbit 115), 17 Sep 1994 03Z (orbit 117) and 17 Sep 1994 04Z (orbit 117). Series of simulation has been run starting successively from 7, 8, 9, 10 September 1994 00Z and 12Z and for 11 September 1994 00Z and the results and the ensemble mean have been compared with observations. This approach allows us to find out the best starting date for future simulations. Backscattering coefficient has been found as a suitable variable for comparison. It is defined as

$$\beta_{s(r_1, r_2)} = P(180^\circ) \int_{r_2}^{r_1} Q_s(n, x) r_2 \frac{dN(r)}{dr} dr$$

where P is phase function, $Q_s(n, x)$ is diffusion efficiency, n is refractive index and $x = \frac{2\pi}{\lambda}$ where

λ is wavelength is size parameter. Phase function and diffusion efficiency are both calculated using the Mie theory for each spectral interval and each aerosol species for 11 intervals of relative humidity. Weighted mean of the sums for each species gives the backscattering coefficient for the model output.

4 Results

The results can be seen from Figure 2. The orbit 117 had almost no cloudiness. The position of the sulphate plume from North America given by NARCM agrees well with observations. Only sulphate and sea-salt were included in the present version. Other species like black carbon, organics, soil will be included in NARCM in order to improve the model performance in future.

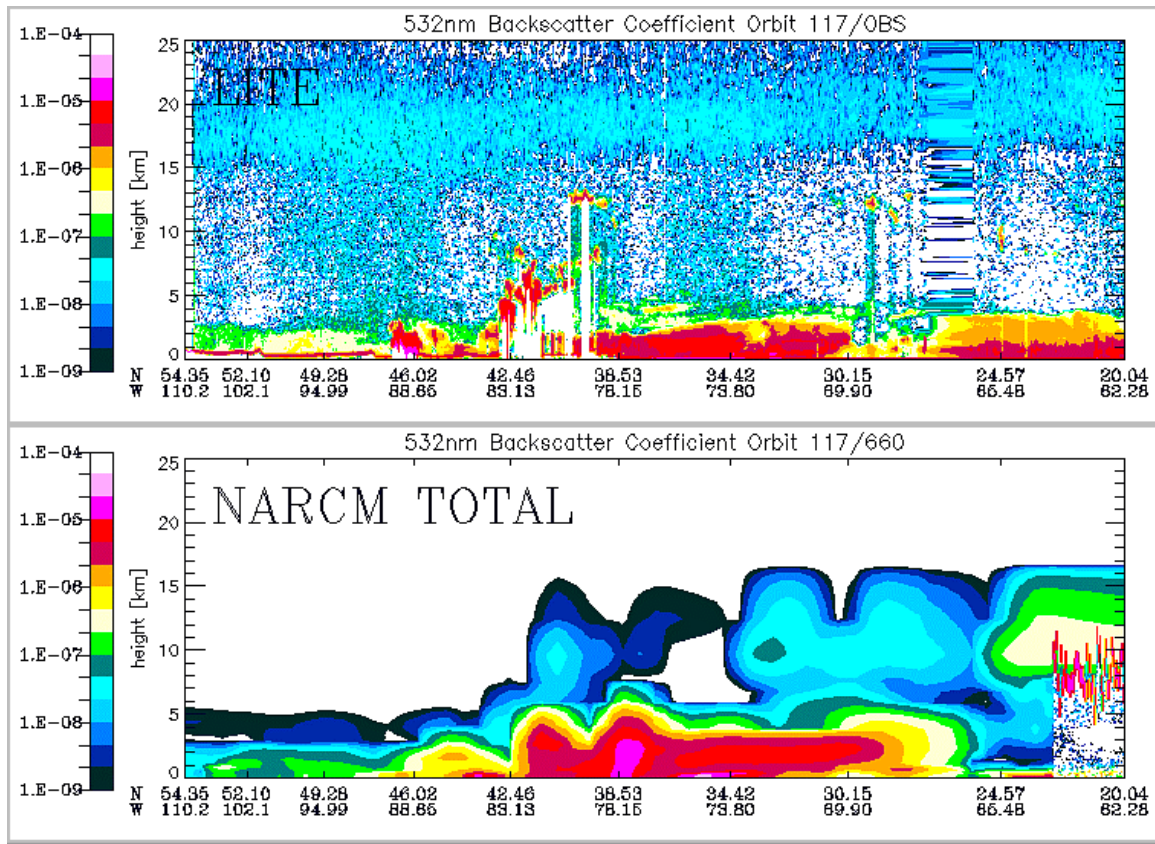


Fig.2 Backcattering coefficient observed (upper) modelled (lower)

5 References

- Hoff, R. M. and Strawbridge K. B., LITE Observations of Anthropogenically Produced Aerosols, in *Advances in Atmospheric Remote Sensing with Lidar*, A. Ansmann, R. Neuber, P. Rairoux and U. Wandinger, eds. Springer-Verlag, Berlin, 1996, pp. 141-144
- Laprise, R., Caya, D., Bergeron, G., Giguere, M. (1997) The formulation of Andre Robert MC2 (Mesoscale Compressible Community) model. *Atmosphere-Ocean*, 35(1), 195-220
- Lohmann, U., Roeckner, E., (1996), Design and performance of a new cloud microphysics scheme developed for the ECHAM general circulation model, *Clim. Dyn.*, 12, 557-572
- McFarlane, N. A., Boer, G. J., Blanchet, J.-P. and Lazare, M. (1992), The Canadian Climate Centre second generation general circulation model and its equilibrium climate, *J. Climate*, 5, 1013-1044
- Verseghy, D. L. (1991) CLASS - a Canadian land surface scheme for GCMs, I. Soil model. *Int. J. Climatol.*, 11, 111-133
- Verseghy, D. L., McFarlane N. A., Lazare, M. (1993) CLASS - a Canadian land surface scheme for GCMs, II. Vegetation model and coupled runs, *Int. J. Climatol.*, 13, 347-370

The ^{210}Pb Data Bank : An Overview

Marie-Antoinette Melieres
Laboratoire de glaciologie et geophysic de l'environnement
BP 96 - 38330 Saint Martin d'Herès cedex France

A ^{210}Pb database (see reference 1) has recently been constructed and is now available. This base includes approximately 1000 ^{210}Pb measurements (with references) of concentration in air at the Earth's surface (yearly averaged and/or seasonal), together with deposition flux both at the atmosphere-Earth and water-sediment interfaces. We consider here only the atmosphere concentration and deposition flux.

An overview of the geographical distribution of the sites of measurement was first presented. The database points out the complete lack of information in some large areas of the planet. This concerns mainly three continents: Africa, Asia (except India and Japan) and South America (except the West Coast). As models are predicting high values (concentration or fluxes) in central Asia and central Africa, it is pointed out how interesting it would be to have some estimation in the center of those continents for testing transport and deposition simulated by models (whose predictions largely differ from one to another).

The data are analyzed and summarized (see reference 2). The atmospheric data (concentration and deposition flux) are synthesized for the different geographical areas when sufficient measurements are available. The trends are discussed in terms of mechanisms (sources, atmospheric circulation, and climate).

The spatial coverage, largely incomplete, is broad enough to allow a first attempt at an analysis in terms of source, transport, and deposition mechanism over a large part of the globe. Illustration of three different mechanism interacting in the ^{210}Pb transport and deposit are summarized below.

Influence of zonal atmospheric circulation:

When annual averages are considered, the zonal character of the atmospheric circulation is one of the driving mechanisms that explain ^{210}Pb distribution. The measured latitudinal distribution (concentration and flux) reflects, to a large extent, the source proportion on the zonal band: in a latitudinal band average the proportion of ice-free continental areas (source of ^{222}Rn) compared with the oceanic or ice-covered areas (absence of source) will govern air enrichment in ^{210}Pb .

The longitudinal distribution results mainly from the air mass origin (enriched continental or depleted oceanic), resulting in turn from the direction of the zonal circulation (westerlies, trade winds, etc.). Illustration of this mechanism is presented relative to the latitudinal gradient over India, where the concentration increase from South to North - Another consequence is the resulting difference between the west and the East Side of continents. Over continents, the origin of the dominant air mass is a determining factor for the annual concentration of ^{210}Pb in air, depending on its continental or oceanic origin (i.e., enriched or depleted in ^{210}Pb). Asymmetry is therefore to be expected in the ^{210}Pb concentration in surface air between eastern and western parts of the continents. The zonal

circulation is from west to east (westerlies) in the temperate latitude bands (30°-60°). This is illustrated by the longitudinal gradient observed over the USA and Europe (30°-60°N). It also appears to exist in the seasonal atmospheric circulation illustrated by the distribution in Japan where the highest values are recorded: the air masses originate from central Asia and are presumably very much enriched in ^{210}Pb .

Influence of vertical atmospheric exchanges:

The vertical transport of ^{210}Pb is determined by vertical atmospheric exchange between the boundary layer and the free troposphere. In ice-free continental areas, where the air in the boundary layer is enriched in ^{210}Pb , compared to the free troposphere, the vertical transport results in lowering in the surface concentration of ^{210}Pb in air. On the other hand, when the air mass is stable, ^{222}Rn and its daughters accumulate in the boundary layer leading to high surface concentration of ^{210}Pb . A consequence is that, when seasonal anticyclones occur over a continental area, air masses become enriched in ^{210}Pb (possibility of high concentration over central Asia: no measurements). Thus continental regions with frequent anticyclonic conditions can experience higher annual ^{210}Pb concentrations (and vice versa for the low-pressure zones). In regions with negligible ^{222}Rn sources (oceanic and polar areas), atmospheric vertical exchange induces an increase in the ^{210}Pb concentration in surface air. This relative enrichment results from ^{210}Pb originating in continental source and brought through the free troposphere by long range transport. (example of Mauna Loa).

Deposition processes and the role of precipitation:

Lead 210 has a long half-life (22.3 years) compared to its atmospheric residence time due to deposition processes (dry and wet deposition). Therefore these processes are to be the main mechanisms in removal processes from the atmosphere. Wet deposition is caused by precipitation scavenging and, in most cases, is more efficient than dry deposition. As precipitation acts as a pump for atmospheric constituents, both concentration in air and deposition flux are influenced by precipitation. In regions with comparable concentrations of ^{210}Pb in the air, it is expected that concentration decrease when rainfall increases. However, considering air masses transport time together with different seasonal distributions of precipitation, no systematic relationship exists between the mean annual ^{210}Pb concentration in air and the mean annual amount of precipitation. The role of the precipitation is well illustrated in Antarctica, where the concentration in surface air is homogeneous and where a strong gradient of precipitation exists from the coast toward the center. There the flux deposition is linearly dependent on precipitation. A consequence of those mechanisms is the difference between northern and southern hemisphere latitudinal distributions in terms of ^{210}Pb concentration as well as in terms of flux deposition. This results from the asymmetry in the distribution in ice-free continents. This is particularly visible in the polar zones where concentration in Antarctica is a factor of 10 lower than in Arctic regions. However, although the concentration distribution seems to be fairly well understood, flux deposition in the northern polar zone, which undergoes large changes, involves a less straightforward interpretation, notably when compared with Antarctica.

As a conclusion, despite the lack of global coverage, the data bank can provide some transects where different mechanisms are well illustrated and where model simulations can be tested by data. It is nevertheless very important for future to develop data collection in

Central Asia and Central Africa where no data exist and where a maximum of concentration is predicted.

References

1). The lead 210 data bank:

<http://glaciog.ujf-grenoble.fr/glaciers/data/bd-preis.html>

2). A compilation of data on lead 210 concentration in surface air and fluxes at the air-surface and water sediment interfaces

Preiss, N., M.-A. Mélières, M. Pourchet, J. of Geophys. Research, 101, 28,847 - 28,862; 1996

APPENDIX A

COSAM WORKSHOP PARTICIPANTS LIST

<p>Victor Savtchenko JPS WCRP c/o WMO Giuseppe-Motta C.P. 2300, CH-1211 Geneva 2 Switzerland Tel: (41-22)73-08-486 Fax: (41-22)73-08-036 email: Savtchenko_V@gateway.WMO.ch</p>	<p>Julian Wilson Environment Institute Joint Research Centre 1-21020 Ispra (VA) Italy Tel: +39-0332-785204 Fax: +39-0332-789793 email: julian.weilson@jrc.it</p>
<p>Francis McGovern Department of Experimental Physics UCD, Belfield Dublin 4, Ireland email: francis.mcgovern@ucd.ir</p>	<p>Sunling Gong Atmospheric Environment Service 4905 Dufferin Street Downsview, Ontario M3H 5T4 Tel: (416) 739-5749 Fax: (416) 739-5704 email: sunling.gong@ec.gc.ca</p>
<p>Xuexi Tie NCAR ACD P.O. Box 3000, Boulder CO 80307 Tel: (303) 497-1470 email: xxtie@ucar.edu</p>	<p>Phil Rasch NCAR CMD P.O. Box 3000, Boulder CO 80307 email: pjr@ucar.edu Tel: (303) 497-1368 Fax: (303) 497-1324 email: pjr@ucar.edu</p>
<p>Carmen Benkovitz BNL, Bldg. 815E, ECD 75 Rutherford Dr., PO Box 5000 Upton, NY 11973-5000, USA Tel: (516) 344-4135 Fax: (516) 344-2887 email: cmb@bnl.gov</p>	<p>Mark Kritz ASRC/Suny Box 468 Moffett Field, LA 94035 U.S.A. Tel: (650) 604-5493 email: mkritz@asrc.cestm.albany.edu</p>
<p>Trond Iversen Department of Geophysics University of Oslo P.O. Box 1022 Blinden, N-0315 Oslo Norway Tel: 47-22-855-821 Fax: 47-22-855-269 email: trond.iversen@geofysikk.uio.no</p>	<p>Jane Dignon Atmospheric Science Division Lawrence Livermore National Lab P.O. Box 808, L-103 Livermore, CA 94550 U.S.A. Tel: (925) 423-2570 Fax: (925) 423-4908 email: dignon@llnl.gov</p>

<p>Dan Bergmann Atmospheric Science Division Lawrence Livermore National Lab P.O. box 808 L-103 Livermore, CA 94550 U.S.A. Tel: (925) 423-6765 Fax: (925) 423-4908 email: dbergmann@llnl.gov</p>	<p>Billie L. Beattie & David Wanh Atmospheric Science Division Environment Canada 45 Alderney Dr. Dartmouth, N.S. Tel: (902) 426-9137 (BB) (902) 426-9136 (DW) Fax: (902) 426-9158 email: Billie.Beattie@ec.gc.ca David.Wanh@ec.gc.ca</p>
<p>Mian Chin Georgia Tech NASA Goddard Space Flight Center Code 916 Greenbelt, MD 20771 U.S.A. Tel: (301) 286-5488 Fax: (301) 286-1754 email: Chin@rondo.gsfc.nasa.gov</p>	<p>Yuhong Yi Atmospheric Environment Service 4905 Dufferin Street Downsview, Ontario M3H 5T4 CANADA Tel: (416) 739-4193 email: yuhong.yi@ec.gc.ca</p>
<p>Jianping Huang Atmospheric Environment Service 4905 Dufferin Street Downsview, Ontario M3H 5T4 Tel: (416) 739-4442 email: jianping.huang@ec.gc.ca</p>	<p>Lubos Spacek University of quebec at Montreal Earth Sciences Department Email: spacek@sca.ugam.ca</p>
<p>Peter Adams Chemical Eng. 210-41 California Inst. of Tech. Pasadena, CA 91125 U.S.A. Tel: (626) 395-4130 email: Ptera@cco.caltech.edu</p>	<p>Jesper Christensen Dept. of Atmospheric Environment National Environmental Research Inst. Frederik Griegvei 399 DK-4000 Roskild Denmark Tel: +45 46-301-175 email: lugc@sun1.dmu.dk</p>
<p>Richard C. Easter MSIN K9-30 Pacific Northwest National Lab P.O. Box 999 Richland WA 99352 U.S.A. Tel: (509) 372-6175 email: richard.easter@pnl.gov</p>	<p>Joyce E. Penner University of michigan 2455 Hayward Ann Arbor, MI 48105-2143 U.S.A. Tel: (734) 936-0519 Fax: (734) 764-5137 email: penner@umich.edu</p>

<p>Erik Kjellstrom MIT, Bldg. 57-1726 Cambridge, MA 02139 U.S.A. Tel: (617) 253-7609 email: erik@misu.su.se</p>	<p>Jean-Luc Jaffrezo Laboratoire de Glaciologie et Geophysique de l'Environnement, BP 96, 38 402 Saint Martin d'Hères Cedex, France. e-mail: jlj@glaciog.ujf-grenoble.fr</p>
<p>Cate Bridgman Chemistry Department Cambridge University Lensfield Road Cambridge, England email: Cate.Bridgman@atm.ch.cam.ac.uk</p>	<p>Kathy Law Centre for Atmospheric Science Department of Chemistry University of Cambridge Lensfield Road Cambridge, CB2 1EW, UK Tel: 44 1223 336518 Fax: 44 1223 336362</p>
<p>Tore Flatlandsmo Dept. of Geophysics University of Oslo P.O. 1022 Blindern N-0315 Oslo NORWAY Tel: +47-22-85-58-19 email: torefl@geofysikk.unio.no</p>	<p>Christine Land Max-Planck-Institut für Meteorologie Bundesstr. 55 20146 Hamburg Germany Tel: +49 (0)40 41173 110 Fax: +49 (0)40 41173 298 email: land@dkrz.de</p>
<p>Marie-Antoniette Melieres Lab. Glaciologie 2 geophysique de l'environnement (L.G.G.E) BP.96-3840, St. Martin D'heres France Tel: 33-4-76-82-42-11 Fax: 33-4-76-82-42-01 email: melieres@glaciog.ujfn.grenoble.fr</p>	<p>Dorothy Koch GISS 2880 Broadway New York, NY 1002 U.S.A. Tel: 212-678-5561 Fax: 212-678-5552 email: Koch@thebes.giss.nasa.gov</p>
<p>Barry J. Huebert Department of Oceanography University of Hawaii 1000 Pope Road, MSB 407 Honolulu, HI 96822 USA Tel: 1-808-956-6896 Fax: 1-808-956-9165 email: huebert@soest.hawaii.edu</p>	<p>Ulrike Lohmann Dalhousie University Dept. of Physics Halifax, N.S. Canada B3H 3J5 Tel: 1-902-494-2324 Fax: 1-902-494-5191 email: Ulrike.Lohmann@Dal.Ca</p>
<p>Ad Jeuken KNMI Postbus201, 3730AE DeBilt The Netherlands Tel: 131-302206650 Fax: 131-30-2210407</p>	

Appendix B:

Final Agenda For COSAM Halifax Workshop

MONDAY 19 OCTOBER 1998 DAY 1		
08:45 - 09:00	Welcome and Introductory Remarks	U. Lohmann for L.A. Barrie
09:00 -09:15	Summary of the Last WCRP Workshop on Modeling Aerosols in Cambridge UK	P. Rasch
09:15 - 09:30	Summary Of Model Experiment: Design, The Models and Summary Results	R. Leaitch for L.A. Barrie and Y. Yi
09:30-09:45	Sulfur in the GISS GCM	Dorothy Koch
09:30 - 10:00	Modeling of the coupled tropospheric chemistry - sulfur cycle in ECHAM	G.J. Roelofs
10:00 - 10:30	Break	
10:30 - 10:45	Sensitivity of The Vertical Sulfur Profiles In The CCCMA GCM To Treatment Of Aqueous Phase Chemistry	U. Lohmann
10:45 - 11:00	Tracer Modeling with ECHAM4: Nudging And Transport	E. Kjellstrom
11:00 - 11:15	The TOMCAT Off-Line Chemical Transport Model	C. Bridgeman
11:15 - 11:30	Global Sulfate Modeling With The Tracer Transport TM3	A. Jeuken
11:30 -11:45	MIRAGE - Model for Integrated Research on Atmospheric Global Exchanges	R. C. Easter
11:45 -12:00	LLNL's Impact Model. A 3D Global Tropospheric/ Stratospheric Chemical Transport Model Designed For Massively Parallel Computers	Dan Bergmann
12:00 - 13:30	Lunch	
13:30 - 13:45	Tropospheric Sulfur Simulation with a Global 3-D Model GEOS CTM.	M. Chin
13:45 - 14:00	Global Modeling Of Sulfate Aerosols at NCAR	P. Rasch
14:00 - 14:15	The Danish Eulerian Hemispheric Model	J. Christensen
14:15 - 14:45	Observations Used In COSAM	F. McGovern , J. Wilson
14:45 - 15:00	Overview of aerosol sampling in the Univ. of Miami ocean network	J. Prospero
15:00 - 15:30	Break	
15.30 - 15:45	Heterogeneous chemistry in OsloCTM2.	T. Flatlandsmo
15:45 - 16:00	Sulfate on the Greenland Ice Sheet: Seasonal Cycle And Size Distribution	J.L Jaffrezo
16:00 - 16:15	Observations of NSS at MLO: Can Measurements at a Point Represent an Entire Grid Square?	B. Huebert
16:15 - 16:30	Vertical S Profiles From Aircraft Used in COSAM	R. Leaitch
16:30 - 16:45	Using Airborne Radon Measurements In Model Development And Validation	M. Kritz
16:45 - 17:00	How Much Have The 1985 GEIA Anthropogenic S Emissions Changed?	C. Benkovitz.
17:00 - 17:15	DMS Emissions Used In The COSAM Exercise	G.J. Roelofs

<i>TUESDAY 20 OCTOBER 1998: DAY 2 WORKING GROUPS</i>		
09:00 - 09:15	Some Problem Points in Atmospheric Sulphur Modeling	T. Iversen
09:15 - 09:30	Simulation of Size-segregated Sea-salt and Sulphate in the Canadian GCM	S.L. Gong
09:30 - 09:45	NARCM-LITE Intercomparison Study	L. Spacek
09:45 - 10:00	Modeling the composition of the sulfate aerosol	P. Adams
10:00 - 10:15	The 210 Pb data bank : an overview	M.-A. Melieres
Break 10:15 -10:45		

SUMMARY INTRODUCTION OF RESULTS BY WORKING GROUP CHAIRS		
10:45 - 11:05	Regional and Global Sulphur Budgets:	P. Kasibhatla/Roelofs
11:05 - 11:25	Vertical Profiles	U. Lohmann/Leitch
11:25 - 11:45	Remote Region Ground Level Distributions	J. Wilson/McGovern

THE PURPOSE OF THE WORKING GROUPS IS: "TO PRODUCE DRAFT SECTIONS FOR THE RESULTS AND DISCUSSION SECTION OF A COSAM REPORT/PUBLICATION"

TOPIC	BUDGETS	VERTICAL PROFILES	REMOTE REGION GROUND LEVEL DISTRIBUTIONS
12:00 - 13:30	LUNCH		
13:30 - 15:00	WORKING GROUP I SESSION	WORKING GROUP II SESSION	WORKING GROUP III SESSION
15:00 - 15:30	BREAK		
15:30 - 17:00	PLENARY SESSION		
19:00	BANQUET		

<i>WEDNESDAY 21 OCTOBER 1998: DAY 3: WORKING GROUPS</i>			
WORKING GROUP WRITING SESSIONS FOR COSAM REPORT AND PUBLICATION			
I	Regional and Global Sulphur Budgets:	P. Kasibhatla	
II	Vertical Profiles:	U. Lohmann	
III	Remote Region Ground Level Distributions	L. Barrie	
BREAK			
TOPIC	BUDGETS	VERTICAL PROFILES	REMOTE REGION GROUND LEVEL DISTRIBUTIONS
09:00 - 12:00	WORKING GROUP I SESSION	WORKING GROUP II SESSION	WORKING GROUP III SESSION
12:00 - 13:30	LUNCH		
13:30 - 15:00	WORKING GROUP I SESSION	WORKING GROUP II SESSION	WORKING GROUP III SESSION
15:00 - 15:30	BREAK		
15:30 - 17:00	PLENARY SESSION: 1. Overview of working group highlights 2. Future directions		

DAY 4 Thursday Morning 09-12:00 October 22 1998 COSAM Committee Meeting

APPENDIX C

Reports of the Working Groups

Annex 1: Global and Regional Sulphur budgets

Prepared by Geert-Jan Roelofs and Prasad Kasibhatla

O2: GLOBAL BUDGETS

SO₂

Table 1. *SO₂* sources (1e12 moles/yr), sinks (%), content (1e12 moles) and lifetime (days)

	GA	GB	GC	GD	CA	CB	CC	CE	CF	HA
SO₂ sources										
Emission	2.27	2.28	2.37	2.35	2.29	2.28	2.37	2.18	2.30	1.87
From DMS	0.51	0.59	0.50	0.59	0.48	0.53	0.53	0.53	0.60	0.00
Total (=100%)	2.78	2.87	2.87	2.94	2.78	2.80	2.90	2.71	2.90	1.87
SO₂ sinks (%)										
dry deposition	40.8	35.2	40.3	46.4	40.4	44.6	34.8	38.0	31.5	25.2
wet deposition	1.8	0.1	0.6	3.5	1.7	0.0	5.3	15.5	2.1	25.9
SO ₂ +OH	17.1	14.2	13.6	11.8	18.5	14.4	4.8	21.7	9.3	44.9
Aqueous ph chem	41.3	53.0	44.7	38.9	39.5	38.8	54.5	23.0	55.3	0.0
Strat-trop exch	0.0	0.0	0.0	0.0	0.0	0.1	0.0	0.0	0.0	2.4
SO ₂ content	0.020	0.015	0.016	0.012	0.013	0.024	0.010	0.022	0.014	0.008
SO ₂ lifetime	2.6	1.9	2.1	1.5	1.7	3.2	1.2	2.9	1.8	1.7

Table 1 shows the submitted data for the global *SO₂* budgets. We note that HA covers only the Northern Hemisphere. We have included budgets for HA in the table, but we will not discuss it in this section. Generally, sources and sinks balance within about 3%. Discrepancies may be connected to the definition of the domain (e.g., troposphere vs. whole model domain), and not all models submitted a budget for stratosphere-troposphere exchange of *SO₂*. We have listed the gas phase source of *SO₂* from DMS and the gas phase sink of *SO₂* through reaction with OH separately. Differences between simulated *SO₂* yields from DMS are associated with the simulation of MSA.

The global source of *SO₂* consists of direct emissions and chemical production from DMS reaction with OH. The total source is about 2.8e12 mole/yr (~100 Tg S/yr), which is simulated consistently between models. Models are also quite consistent concerning the dominant sink for *SO₂*, which is dry deposition (about 1e12 mole/yr, or 35-45%). Next in importance is aqueous phase chemistry, i.e., oxidation of *SO₂* to sulfate in cloud and rain water. This sink is also of the order of 1e12 mole/yr, but it displays a somewhat larger range between models (generally 40-55%). Third in importance, and more or less negatively correlated to the aqueous phase

chemistry, is the gas phase oxidation of SO₂ by OH (5-20%). Note that direct wet deposition is relatively large in HA, and also contributes somewhat in various other models. Differences may be related to the definition of wet deposition. After SO₂ dissolves in cloud water, it is for the largest part oxidized to sulfate and can be wet deposited in precipitation from the same cloud. Some models regard this as aqueous phase chemistry, others as wet deposition of SO₂.

The simulated SO₂ content ranges between about 1e10 moles (0.35 Tg, associated with a lifetime of 1-2 days, CA, CC, GD), and 2e10 moles (0.7 Tg, lifetime 2.5-3.5 days, GA, CB, CE). A longer lifetime and larger SO₂ content may be associated with a less efficient aqueous oxidation to sulfate.

Sulfate

Table 2. Sulfate sources (1e12 moles/yr), sinks (%), content (1e12 moles) and lifetime (days)

	GA	GB	GC	GD	CA	CB	CC	CE	CF	HA
sulfate source										
emission	0.06	0.10	0.00	0.00	0.05	0.07	0.04	0.07	0.04	0.09
SO ₂ +OH	0.48	0.41	0.39	0.35	0.51	0.40	0.14	0.59	0.27	0.84
aqueous ph chem	1.15	1.52	1.28	1.14	1.10	1.09	1.58	0.62	1.60	0.00
total (=100%)	1.68	2.03	1.67	1.49	1.66	1.56	1.76	1.28	1.91	0.93
sulfate sinks										
(%)										
dry deposition	19	18	17	13	14	11	22	10	6	28
wet deposition	81	83	85	104	86	88	79	90	94	52
strat.-trop. exch.	0.0	0.0	0.0	0.0	0.2	0.2	0.0	0.0	0.0	7.0
Sulfate content	0.025	0.029	0.033	0.021	0.025	0.023	0.025	0.017	0.019	0.010
sulfate lifetime	5.4	5.3	7.1	5.1	5.4	5.4	5.2	4.9	3.6	3.7

Table 2 shows the submitted data for the global sulfate budgets. Sources and sinks balance within a few percent for sulfate. In GD, sources and sinks are not in balance, which may be a result of budgeting errors. Direct emissions of sulfate are relatively small and the source of sulfate is dominated by the gaseous and aqueous phase oxidation of SO₂, which is estimated between 1.3e12 and 2e12 mole/yr. The contribution of the gas phase production is between 15 and 50%. Largest contributions of the aqueous phase production are simulated by GB, CC and CF, and the smallest contributions by CE. Models with a large contribution by aqueous phase oxidation generally tend to simulate a small contribution by gas phase oxidation (CC, CF), and vice versa (GA, CA, CE). However, different definitions regarding SO₂ wet deposition and aqueous phase oxidation may play a role, as explained earlier. It should be noted that the definition directly affects the calculated sulfate lifetime.

Sulfate is removed from the atmosphere by wet and dry deposition (>80% and <20%, respectively). The data suggest an inverse correlation between the relative importance of sulfate wet deposition (smaller in GC and GB and larger in CF and CE) and the sulfate content. In the next section this will be examined further.

The sulfate content ranges with a factor of two between 1.7×10^{10} mole and 3.3×10^{10} mole (equivalent to 0.6 and 1.1 Tg S). Similarly, the sulfate lifetime ranges between 3.5 and 7 days. We note that the submitted budgets for Pb^{210} , which is attached to aerosols and whose sinks are therefore similar as sulfate, are consistent with these findings.

O4: REGIONAL BUDGETS

a) EMEP

SO_2

Figures 1a and 1b show diagrams of the submitted emission and sink budgets for SO_2 in DJF and JJA for the EMEP region (Europe). Here we present data for the total column, although data are available for two layers, i.e. below and above 2.5 km altitude. We note that the submitted transport budgets were not always consistent. Therefore, we recalculated the transport budgets as the residual of the sources and other sinks.

Emissions of SO_2 in the EMEP region are consistent between models, about 1.7×10^{12} moles in DJF and 1.1×10^{12} moles in JJA. We do not separate the DMS source, which contributes relatively little in EMEP. In DJF, the dominant SO_2 sink is dry deposition, with a contribution of about 50% in all models. The remainder is removed from the region by transport (20-50%) and aqueous phase oxidation (5-30%). We remark that in DJF all models show that more than 80% of the SO_2 column resides below 2.5 km altitude (further referred to as L1; the region above 2.5 km will be referred to as L2). However, the total column budget ranges between 2×10^9 and 5×10^9 moles (not shown here). The SO_2 oxidation efficiency in the aqueous phase appears to be negatively correlated with the SO_2 burden in DJF. Dry deposition appears rather low for HA. Furthermore, HA does not distinguish between gas and aqueous phase chemistry processes.

In JJA, the contribution of dry deposition is somewhat smaller (25-40%) than in DJF, whereas the contribution by gas phase oxidation of SO_2 is more significant (10-25%). This is due to summer convection, which efficiently transports SO_2 out of the boundary layer, and to enhanced photochemical activity in summer compared to winter. We note that the impact of convection on the relative distribution between L1 and L2 is more evident in the budget of Rn, whose lifetime is seasonally independent. Table 3 shows that large differences occur between the simulated convective transport efficiencies, with relatively large effects in GB, CE and CF, and moderate effects in GC, GD, CA, and HA. For HA, the total emission of Rn appears to be scaled incorrectly.

Table 3. Rn budgets (1×10^{18} mole/mole) and fraction in L1 (%) in EMEP.

	GA	GB	GC	GD	CA	CB	CC	CE	CF	HA
total column DJF		31.4	28.2	35.1	37.6	41.2	34.5	34.2	31.0	18.1
in L2 (%) DJF		29	9	20	26	30	23	19	20	34
total column JJA		34.7	26.8	34.6	36.8	38.2	32.7	31.8	30.0	20.4
in L2 (%) JJA		47	13	24	27	38	32	36	41	37

Direct wet deposition of SO_2 removes less than 10% of the emitted SO_2 . The remainder (between 30 and 55%) is removed by transport and by aqueous phase oxidation, but their relative

importance differs between models. Nevertheless, in all models more SO₂ is transported out of the region in DJF than in JJA, associated with the shorter chemical lifetime in JJA. Some models predict a somewhat larger fraction of SO₂ in L2 in JJA compared to DJF, most notably CE (not shown). Absolutely, however, the column amount of SO₂ is smaller by a factor of 2 to 3 in JJA due to the larger abundance of oxidants.

Sulfate

Figures 2a and 2b show diagrams of the source and sinks of sulfate in DJF and JJA. Additionally, Figure 3 displays the sulfate burdens in L1, L2, and the total column for DJF and JJA.

In DJF, the main sources of sulfate in the EMEP region are aqueous phase oxidation of SO₂ and direct emissions of sulfate. The prescribed emission scenarios are not applied consistently in the models, which is reflected in different direct sulfate emission budgets ranging between 0 and 1e10 moles. Furthermore, large differences exist for the simulated SO₂ aqueous phase oxidation budget, so that the simulated total sulfate source ranges between 2e10 and 5.5e10 moles. Smaller sulfate production rates are directly related to relatively inefficient SO₂ aqueous phase chemistry (e.g., GA, GB, CB and CE), and vice versa (CA, CC). Sulfate sinks are dry deposition (below 15% in all models), wet deposition (50-70%), and transport out of the region (25-40%). A very efficient wet deposition (upto 90% in winter) and consequently a small transport contribution is simulated by CF, and a relatively large transport efficiency of about 60% and smaller wet deposition contributions by CA and GC. These models are also characterized by the smallest (about 3e8 moles) and largest sulfate column contents (12e8 moles) in DJF, respectively. The sulfate fraction above 2.5 km is in some models more than 50% (GB, CF) and in others below 30% (GC, HA), which is consistent with the relative convective transport strength discussed earlier.

Due to enhanced photochemical activity, the gas phase oxidation of SO₂ contributes about 50% to the sulfate source in JJA, but much smaller and larger contributions are simulated by CC and CE, respectively. The total chemical sulfate source is somewhat more consistent in JJA than in DJF, between 4e10 and 6e10 moles. So, whereas aqueous phase oxidation appears to dominate sulfate production in DJF, gas phase oxidation also plays a role in JJA. In fact, differences in the aqueous phase chemistry rate between models are somewhat compensated by the gas phase chemistry in JJA.

The relative importance of sulfate transport out of the region in JJA is somewhat enhanced compared to DJF, most notably in the models with relatively strong convection (GB, CE, CF). Convection transports pollutants into the free troposphere, where wind velocities are larger than in the lower troposphere while the sulfate lifetime is longer. These models also simulate a less efficient wet sulfate deposition in JJA, most notably in GB and CE. On the other hand, in GC and CA, characterized by smaller convection efficiency, the fraction of sulfate transported out of the region is smaller in JJA than in DJF.

Due to enhanced photochemical activity, the sulfate burden in EMEP is larger in summer than in winter. Due to the compensating effect between gas phase and aqueous phase chemistry

efficiencies, the relative scatter between simulated sulfate burdens is smaller in JJA than in DJF. However, simulated seasonalities of the sulfate burden differ strongly between models, with burdens that are larger in summer than winter by between 20% (GC,CA, HA) and 150% (GB, CB, CF). The models that show a moderate increase of sulfate in summer compared to winter (GC, CA and HA) also display a moderate impact of convective transports on the Rn vertical distributions (Table 3). Nevertheless, the relative distribution of sulfate between L1 and L2 is not very different from that in DJF for all models. During winter the SO₂ oxidation rate is relatively small causing long SO₂ lifetimes and significant detrainment of SO₂ out of the boundary layer into the free troposphere where it reacts further. On the other hand, during summer the SO₂ oxidation is efficient and convection carries the sulfate produced into the free troposphere.

SO_x

Most models simulate dry deposition as the largest sulfur sink (as SO₂) in the EMEP region, followed by transport out of the region in winter, and both transport and wet deposition (as sulfate) in summer. As a result of the seasonal dependence of the SO₂ oxidation rate, sulfur transports are mainly as SO₂ in DJF and as sulfate in JJA. However, large differences exist between models in the efficiencies of aqueous phase oxidation of SO₂ and wet deposition of sulfate, which are both cloud-related processes. Therefore, the simulated sulfur transports from the EMEP region vary with more than a factor of two, i.e. between about 3e10 to 7e10 moles. For SO₂ and sulfate separately, the range easily spans a factor of 5, especially in DJF.

b) ENA.

Qualitatively, the models display similar results for ENA as for EMEP. However, due to differences in terrain and/or wind direction, the relative importance of dry deposition as a sink for SO₂ is somewhat larger for ENA. Further, part of ENA is located more southward than EMEP. This is expressed in a more efficient gas and aqueous phase oxidation of SO₂ to sulfate, convective transports, and sulfate wet deposition. As a result, sulfur transports for ENA are smaller than for EMEP, although emissions are of the same order of magnitude, especially in winter. However, relatively large differences in transport budgets are found between the models also for ENA.

c) SEA

It is noted that some models simulate relatively large SO₂ emissions above 2.5 km altitude, probably from volcanoes. The absolute strength of these emissions varies strongly between models. The relative strength, however, is below 5% and inconsistencies in the simulation of this source do not seriously hamper the comparison. SEA is located even more southward than EMEP and ENA. Hence, chemical oxidation of SO₂ to sulfate is faster, both in the gas and aqueous phase, throughout the year. The SO₂ oxidation source of sulfate is more consistent between the models for this region than for the other regions. Also, sulfate burdens in DJF and JJA are of the same order of magnitude, although some models simulate larger columns in JJA by a factor of 2 (GA, GB), whereas others simulate smaller columns down to a factor of 0.5 (GC). Probably the convection efficiency plays a role here.

CONCLUDING REMARKS

The models are consistent in the simulation of emissions and of dry deposition of species. Models display large differences in the processes that are cloud-related. These are firstly the in-cloud oxidation of SO₂ to sulfate which acts as a source of sulfate, secondly wet deposition of sulfate which determines the sulfate lifetime and tropospheric content, and thirdly convection which “pumps” pollutants from the lower into the free troposphere. We note that also for Pb²¹⁰, for which only wet deposition and convection are relevant cloud-related processes, large differences are found in the simulated lifetime and (regional) burden.

From comparison of the summer and winter regional sulfate budgets, different ways of model behavior can be deduced. A few models consistently simulate large sulfate loading in summer (compared to the other models) and small sulfate loading in winter. These are GA, GB, and CB. These models display a large seasonal dependence of the convective transport efficiency combined with a rather small aerosol wet deposition efficiency. It may be that these models represent relatively inefficient uptake of soluble species in convective updrafts. However, examination of the Rn data suggests that strong convective updrafts transport the pollutants out of reach of precipitating clouds. This leads to a relatively large sulfate loading in the upper troposphere. GD simulates a similar sulfate burden seasonality, but it does not display a large seasonal dependence of convective transports. As GA, GB, and CB clearly simulate an enhanced burden in L2 in summer as a result of convection, GD simulates an enhanced burden in L1. Apparently a large part of the emitted SO₂ remains in the lower troposphere due to the relatively inefficient convective transports, where it reacts further. GD simulates a significantly weaker efficiency of convective transport in all regions than GB, although they both use the climate model ECHAM. However, they treat convective transports of pollutants differently.

GC, CA, and to a smaller extent HA are characterized by relatively high sulfate loading in winter compared to the other models, and small sulfate loading in summer. GC and CA simulate efficient SO₂ oxidation in the aqueous phase during winter, and in all three models the sulfate wet deposition is relatively inefficient in winter. In summer, however, they behave more in line with the other models. In GC, inefficient convective transports in summer keep sulfate mostly in the lower troposphere where lifetimes are relatively low. The remaining models, CE and CF have relatively low sulfate loading in both seasons. For CF, this is directly related to the very efficient sulfate wet deposition, especially in winter, when compared to other models. CE, on the other hand, simulates relatively inefficient SO₂ oxidation and subsequently more efficient transport of SO₂ out of polluted regions when compared to the other models.

Some of the models consider full chemistry or calculate hydrogen peroxide concentrations from HO₂, in order to simulate the oxidant limitation which is important particularly in winter. Significant differences between these models (GA, GB, CA, CB, CC) and those that use monthly averaged oxidant concentrations can not be detected in the data, although they simulate somewhat smaller sulfate columns in EMEP in DJF. Apparently, the oxidant limiting effect is small compared to differences in the representation of cloud-related processes.

We note that differences between models may not only arise from the way certain processes are represented (e.g., all models calculate aqueous phase sulfate formation and wet deposition of sulfate) but also from which processes are represented (e.g., uptake of SO₂ on liquid films on ice particles, below cloud scavenging by ice particles, sedimentation of aerosols in the free troposphere). A relatively new subject in global aerosol modeling is representation of different sizes. Considering the fact that modeling of size-resolved aerosol physics and chemistry, including multiphase processes and considering internal and external mixing of several chemical species, is an extremely complex task with many uncertainties, we do not expect that global sulfur simulations from different models will converge considerably in the near future.

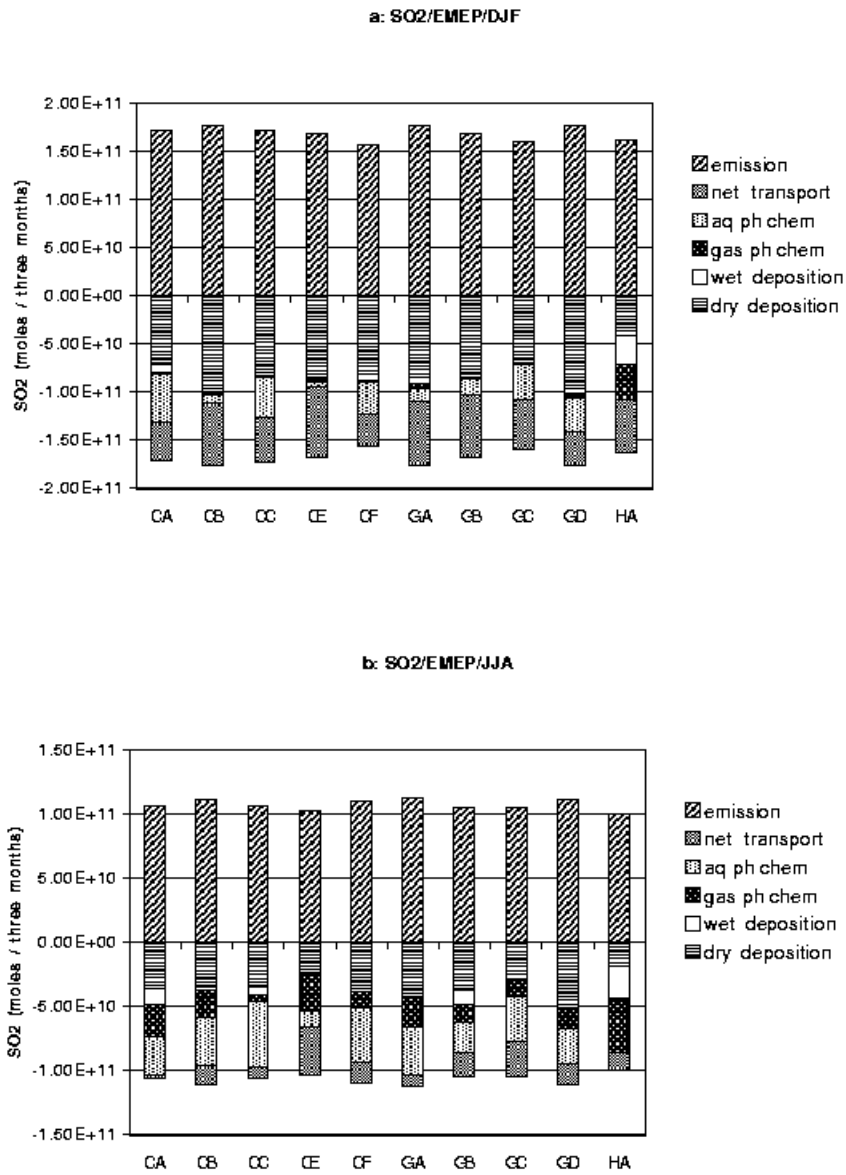


Figure 1. Simulated SO₂ budgets for EMEP. a) DJF and b) JJA. Sources have positive values, sinks have negative values.

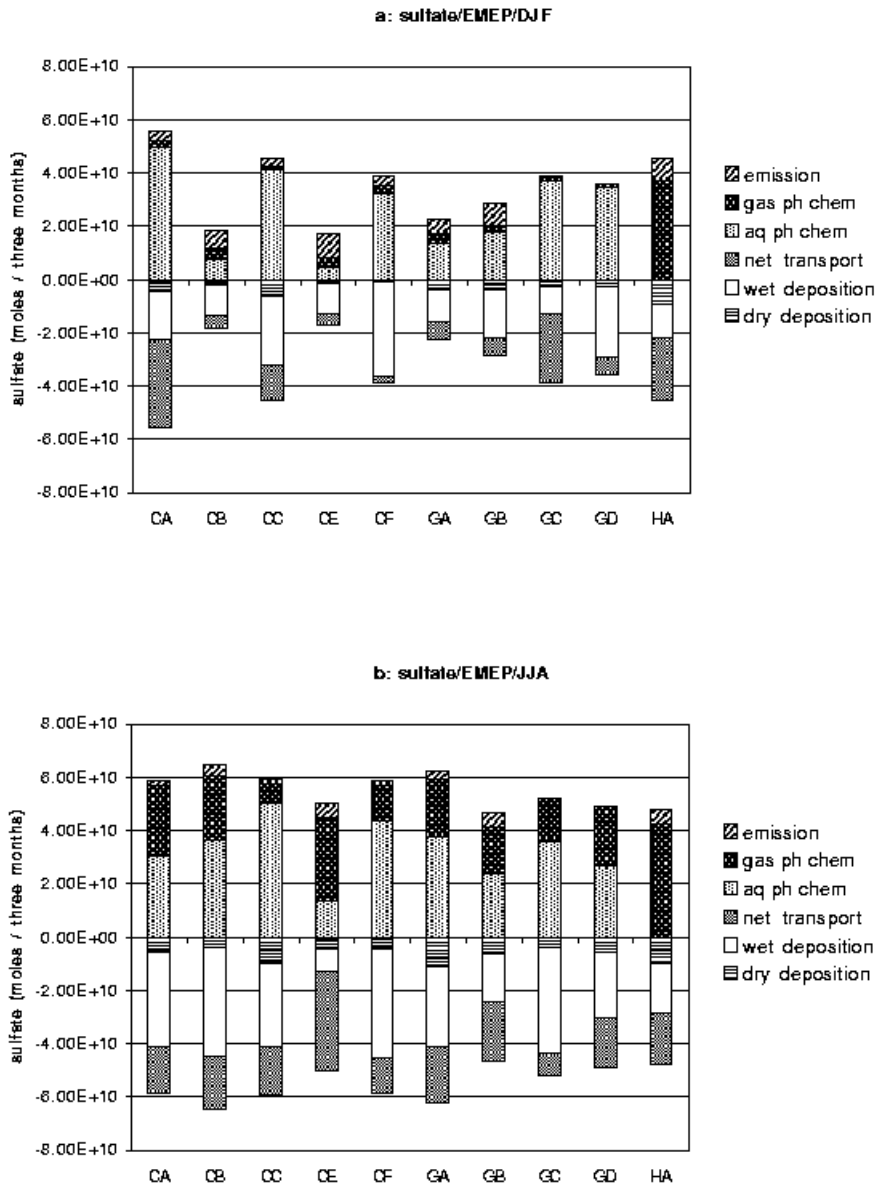


Figure 2. Simulated sulfate budgets for EMEP. a) DJF and b) JJA. Sources have positive values, sinks have negative values.

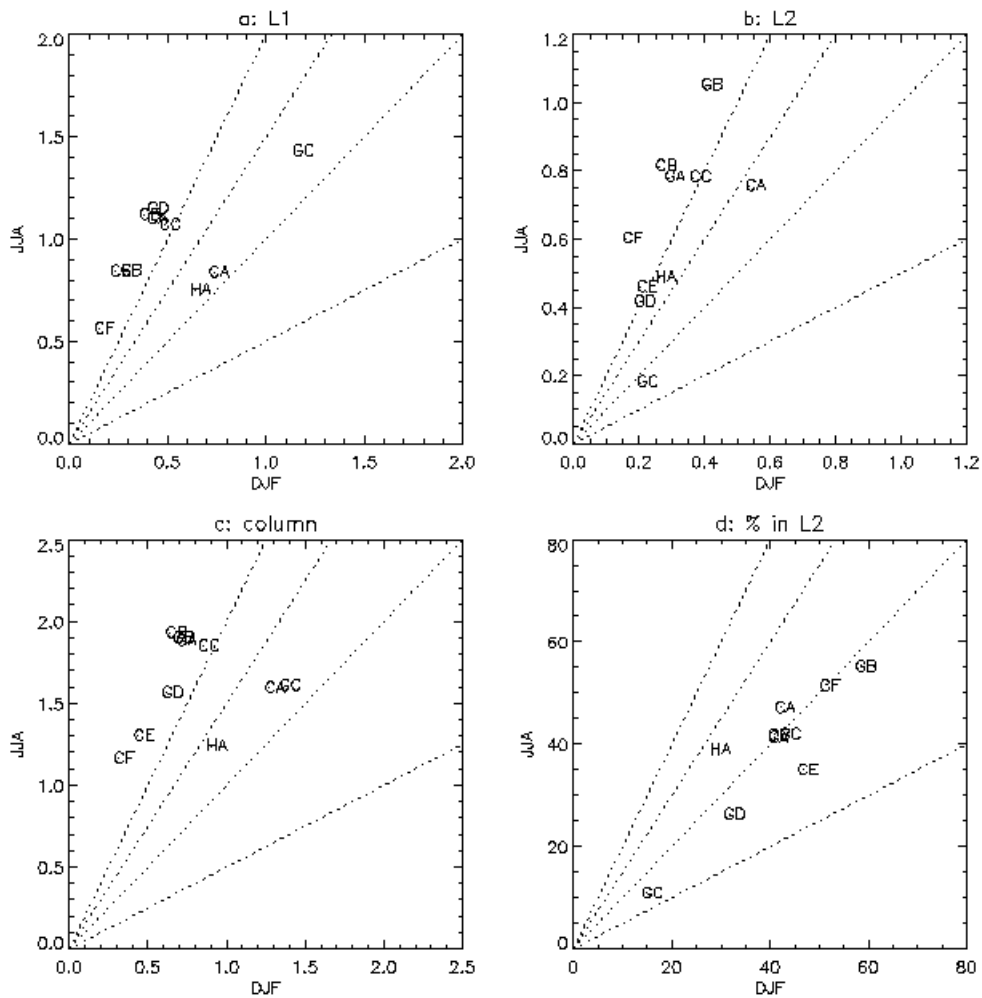


Figure 3. Scatter diagrams for EMEP of (a) sulfate burden below 2.5 km altitude, (b) sulfate burden above 2.5 km altitude, (c) total column burden of sulfate, and (d) percentage of the column burden that resides above 2.5 km altitude. Units are 10^9 mole (a, b, c) and percent (d). Horizontal and vertical axes represent simulated values for winter and summer, respectively; dotted lines represent winter to summer ratios of 2:1, 3:2, 1:1, and 1:2.

Annex 2: Vertical Profiles

Prepared by Ulrike Lohmann

Participants: Richard Leitch, Kathy Law, Ulrike Lohmann, Carmen Benkovitz,
Dan Bergman, Mark Kritz, Phil Rasch, Dorothy Koch,
Ad Jeuken, Trond Iversen, Mian Chin, Berry Huebert

We compared simulated vertical profiles of SO₂ and SO₄ at NARE for August/September and North Bay for March/April with observations. Observed vertical profiles of radon are available during June-August at San Francisco. Additionally they were simulated during this time at Mauna Loa, Bermuda and Mace Head. Meridional transects of simulated DMS, SO₂, SO₄ and MSA were obtained during winter and summer in the Atlantic along 30W and during spring and fall in the Pacific along 160°W.

Summary of sulfur vertical profiles:

Both observed sites have some problems, NARE is close to the coast and North Bay close to emission centers, so depending on the grid box size of the models, different emissions enter the grid boxes.

The vertical profiles of SO₂ and SO₄ at NARE from models running with full chemistry tend to agree best with observations. The secondary maximum at 10 km at NARE and North Bay in some models is also seen in the meridional transects, but so far no common feature of the models showing this secondary maximum could be identified. It might be oxidant limitation.

A comparison of the simulated near surface concentrations of SO₂ and SO₄ with free tropospheric SO₂ and SO₄ from North Bay and NARE yields that realistic surface values of SO₂ and SO₄ do not guarantee an agreement aloft. This conclusion was further complicated by the fact that some models seem to be too high at the NARE site, but good or too low at North Bay.

Summary on radon vertical profiles:

Modeled values at 10 km altitude were examined. Values were particularly sensitive to the influence of nearby continents. Concentrations in all models are lowest at Mauna Loa (Hawaii) and largest at Mace Head which experiences the greatest continental influence.

A comparison with observed vertical profiles is only possible at San Francisco. There the agreement between modeled and observed radon concentration is generally good, though only one model captures the observed upper tropospheric increase in radon.

A strong correlation between high levels of sulfate at 6 km at the NARE site with high levels of radon at 6 km at Mace Head is found. This suggests that the model to model differences in higher altitude sulfate may be due to transport differences rather than chemistry.

Summary of meridional transects:

The seasonal cycle in all models of DMS and MSA appears to be opposite the intuitively expected with a maximum in fall.

The tropical DMS plume is much weaker in model GD as compared to GB, which is indicative of different oxidation of convective transport, more likely due to differences in oxidation.

3 out of 7 models show unrealistically high MSA in the free troposphere.

Most models produce a reasonable seasonal cycle of SO₂ and SO₄ in the Arctic.

Models with coarse vertical resolution have high levels of SO₂ in the upper troposphere and lower stratosphere and do not have a well defined tropopause. Some models are very diffusive in the vertical.

Annex 3: Remote region ground level distribution / Comparison of the models with surface observations

Prepared by J. Wilson and F. McGovern

1. The working group wished to acknowledge the scientists who provided the observational data used in the comparison. It also reiterated its belief in the need for long term support for the development of a global network of regionally representative ground based observational sites.

The working group also stressed the value of an inter-comparison between models and observational data and recommended more feedback between the sites and modelers. For example the Mauna Loa data set is filtered by B. Hubert to remove local volcanic contamination, but the models do not necessarily account for this in their volcanic emissions. In general the site people have a better idea what influences their data and the modelers know what is driving their models. Such contacts would be of mutual benefit to the modelers in improving their models and the site operators to improve their measurements with respect to modeling needs.

On a related note the exercise was valuable in identifying potential problems with using data from different sources for example the Iceland AEROCE and Iceland EMEP sites, or EMEP data from coastal locations, which the modelers are not always aware of.

2. The preliminary comparisons between the models and the observations were as a whole encouraging, with the mean deviation of each of the models from the entire set of sulfate observations not exceeding a factor of two (this will change with the revised model runs and diagnostics). However this overall picture hides significant variations in the models behavior at the individual sites. A preliminary classification of the sites into those that should be easier for the models, and those that should be difficult (sites in areas with strong concentration gradients, variable annual cycles etc) was attempted and will be developed for the final analysis.

As has been observed in individual studies the models do not represent the observed seasonal SO₂ and MSA distributions as well as they do sulfate.

3. There was conflicting evidence as to the performance of the off-line models using analyzed wind fields, or GCMs nudged to analyzed data, in comparison with the climatological GCM runs. This will be addressed in the final analysis.

4. The working group recommended that while conducting sulphur simulations the models, data for the high altitude sites is extracted from the model grid element at the altitude of the site, that in turn has been corrected for the surface altitude assumed in the model. For Mauna Loa, the surface altitude of the models is sea level, and the models will need to go up to 3397 m to obtain the data for comparison with the observations, whereas for Jungfrauoch, the model surface will be several hundred meters depending on the model resolution, and the models will need to go to 3573 m – model surface to obtain the data.

5. Model comparisons also identified a limitation in the use of seasonal average observations, in the comparison, at several of the sites close to the source regions. In some cases, the seasonal average was either not representative of the annual cycle in observations, or there was inter-annual variation in the observations (Mace Head was a typical example). In order to get comparable data on the cycles and irregularities in the observations from the models, the working group requested that monthly average observations be used for the final comparison studies. The working group recognized that this increased workload required an extra commitment. However, this was considered to be worthwhile as it will allow for a more quantified approach to the inter-comparison. The increased knowledge, of the performance of the models, can be used to develop appropriate tools and reference points for future similar work.

APPENDIX D

Summary Of Models Summary of Sulfur Models for COSAM Exercise

Model Code	Full Name	Simulation Interval	Horizontal Resolution	Vertical Resolution	Meteorology	Clouds
GA	GISS GCM	3 years	4 ⁰ H 5 ⁰	9 levels (10hPa)	Generated	Prognostic
GB	ECHAM/IMAU	2 years	3.75 ⁰ H 3.75 ⁰	19 levels (10 hPa)	Generated	Prognostic
GC	CCC GCM	15 months	3.75 ⁰ H 3.75 ⁰	22 (10 hPa)	Generated	Prognostic
GD	ECHAM4	7/93 to 6/94	2.81 ⁰ H 2.81 ⁰	19 levels (10 hPa)	Generated/Nudged	Prognostic
CA	CTM/Cambridge	6/93 to 12/94	5.6 ⁰ H 5.6 ⁰	31 levels		No
CB	KNMI/IMAU	1/93 to 12/93	3.75 ⁰ H 5 ⁰	19 levels	from ECMWF	ECMWF
CC	MIRAGE	7/93 to 6/94	2.81 ⁰ H 2.81 ⁰	24 levels	Generated/Nudged	Prognostic
CD	IMPACT/LLNL	3/97 to 2/98	2 ⁰ H 2.5 ⁰	46 levels		NASA/DAO
CE	GEOS CTM	7/93 to 6/94	2 ⁰ H 2.5 ⁰	20 levels	Assimilated GEOS/DAS	GEOS/DAS
CF	NCAR	9/92 to 12/95			Assimilated NASA- DAO GEOS-STRAT	Prognostic
HA	Hemispheric CTM	6/93 to				

(Continues....)

Model Code	Oxidant Chemistry			Transport	Dry Deposition	Wet Deposition
	H ₂ O ₂	OH	O ₃			
GA	Prognostic	Imported	Imported	2 nd order moments	Resistance in series ³	Coupled to cloud parameterization
GB	Full Chem	Full Chem	Full Chem	Semi-Lagrangian	Resistance in series ²	Coupled to cloud parameterization
GC	Imported	Imported	Imported	Semi-Lagrangian	Resistance in series ⁹	Giogi & Chameides ⁵
GD	Imported			SPITFIRE ¹⁰	Resistance in series ⁹	Giogi & Chameides ⁵
CA	Full Chem	Full Chem	Full Chem			
CB	Full Chem	Full Chem	Full Chem	Advection ⁶ Convection ⁷ Vertical diff ⁸	Resistance in series ⁹	Adapted Balkanski ⁴
CC	Prognostic ¹¹	Prognostic ¹¹	Prescribed	Finite difference ¹²	Const dep vel	Below and in-cloud
CD	Full Chem	Full Chem	Full Chem	Flux form, semi-Lagrangian ¹	Resistance in series ³	Convective updraft ⁴ Large scale ⁵
CE	Monthly avg	Monthly avg	No	Flux form, semi-Lagrangian ¹	Resistance in series ²	Rainout/washout. Scavenging in cloud updraft
CF						

Full Chem = full oxidant chemistry.

Imported = imported from other model.

¹ Lin and Rood, 1996.

² Wesely, 1989.

³ Jacob, Wang, Wesely

⁴ Balkanski et al. JGR 1993

⁵ Giogi and Chameides

⁶ Russell & Lerner

⁷ Tiedke

⁸ Louis

⁹ Ganzeveld et al. JGR 1998

¹⁰ Rasch & Lawrence, 1998

¹¹ CO-CH₄ chem with prescribed O₃ and NO_x

¹² Bott, 1989

Summary of Sulfur Models Submitted for COSAM Exercise

(Continued..)

Model Code	Contact	Remarks
GA	Koch, GISS/Columbia, USA	
GB	Roelofs, The Netherlands	Transport out of BL may be too low. Nucleation scavenging of aerosols in convective clouds appears too low. Cloud pH is prognostic but does not include influence of NH ₃ . No chem in ice particles, below-cloud scavenging of particles and gases.
GC	Lohmann, Canada	
GD	Kjellstrom, Sweden	The Rn emissions are too low - they are not scaled to give a global sum of 72 moles yr ⁻¹ .
CA	Bridgeman, UK	
CB	Jeuken, The Netherlands	Cloud pH not fixed but calculated from dissolved acids and bases including influence of NH ₃ /NH ₄ which are tracers in the model. BL exchange may be too low in winter due to too simple BL-scheme, wet removal of aerosol is too low.
CC	Easter, PNNL, USA	Aqueous chemistry includes CH ₃ O ₂ H and uses pH=4.5 for O ₃ .
CD	Bergmann, LLNL, USA	Only Rn/Pb calculations submitted. Full sulfur chemistry simulations in near future.
CE	Chin, NASA, USA	
CF	Rasch, NCAR, USA	
HA	Christensen, Denmark	